Submerged Gravel Shorelines of the Inner to Mid-Shelf Offshore Hottentot's Bay, Namibia

by

T. Heeralal (BSc. Hons)

Submitted in fulfilment of the academic requirements for the degree of Master of Science in the

Discipline of Geological Sciences

School of Agriculture, Engineering and Sciences

University of KwaZulu-Natal

July 2024

Supervised by Prof. A.N. Green

As the candidate's supervisor I have/have not approved this dissertation for submission.

Signed: [redacted] Name: Prof. A.N. Green Date: 17/07/2024

Acknowledgements

First and foremost, I would like to thank God for His guidance and strength throughout this journey. As it is written in Psalm 121:2 “My help comes from the Lord, the Maker of heaven and earth.” This work would not have been possible without His blessings.

I would like to express my deepest gratitude to my Supervisor, Prof. Andrew Green. Your relentless support, dedication, and guidance, especially during these challenging last six months, have been invaluable. I am truly honoured to be a student of yours. Your patience especially during my moments of doubt, your willingness to listen, and your readiness to offer support have been a beacon of hope. I am deeply grateful for the countless hours you have invested in refining my ideas and improving my research. Your passion for geology and dedication to your students are truly inspiring.

To my mum and dad. Your unwavering belief in me has been my constant source of strength. You have always pushed me to follow my dreams and have molded me into the woman I am today. I am deeply grateful for all your sacrifices throughout the years. It was not easy but you both made sure you gave me everything I needed. Thank you for your consistent love and support which have been the bedrock of this journey. I am extremely lucky to have you both as my parents.

To my partner Daniel Chuang. Thank you for being my rock, my IT support specialist, my private chef, my problem solver and my best friend. You effortlessly ensured my comfort throughout this journey, whether it was providing me the best workspace and environment or simply putting my mind at ease by being the present and most loving fur dad to our babies Astro, and Radhika. Thank you for making me smile on my most down days and caring for me and being the best partner, anyone could ever ask for. You are a blessing!

I wish to thank Marinja Bester for all the valuable input and guidance over all the delicious hot chocolates and grilled cheese sandwiches. Thank you for your support and guidance as well as always being ever ready to listen to my crack theories and answering the phone at odd hours when I panicked. I have learned so much from you and consider myself lucky to have you as my friend. As they say, ‘iron sharpens iron” I can firmly say that our friendship can attest to this.

Declaration 1

COLLEGE OF AGRICULTURE, ENGINEERING AND SCIENCE

DECLARATION 1 - PLAGIARISM

I, Tamera Heeralal, declare that.

1. The research reported in this thesis, except where otherwise indicated, is my original research.

2. This thesis has not been submitted for any degree or examination at any other university.

3. This thesis does not contain other persons' data, pictures, graphs, or other information, unless specifically acknowledged as being sourced from other persons.

4. This thesis does not contain other persons' writing, unless specifically acknowledged as being sourced from other researchers. Where other written sources have been quoted, then:
   a. Their words have been re-written, but the general information attributed to them has been referenced.
   b. Where their exact words have been used, then their writing has been placed in italics and inside quotation marks and referenced.

5. This thesis does not contain text, graphics or tables copied and pasted from the Internet, unless specifically acknowledged, and the source being detailed in the thesis and in the References sections.

6. This thesis comprises portions of published material, or material in review where the candidate was an author who contributed substantially to the manuscripts. **Appendix 1** refers to a recently published paper where the digitising, core logging and core data management were performed by the candidate: Green, A.N., Senna, W., Cooper, J.A.G., Heeralal, T. and Labuschagne, H., 2024. Antecedent bedrock control on the sediment-starved continental shelf of south/central Namibia. Marine Geology, 469, 107242. **Appendix 2** refers to a paper in review where the candidate helped digitise the sub bottom profiles and collated and

managed all core data for the area: Green, A.N., Meltzer, L., Cooper, J.A.G., Heeralal, T., Labuschagne, H., in press. Anatomy and stratigraphic evolution of a shelf bypass valley system. Geomorphology.

Signed [redacted]

....

Declaration 2 Publications

Publication 1

Green, A. N., Senna, W., Cooper, J. A. G., Heeralal, T., & Labuschagne, H. (2024). Antecedent bedrock control on the sediment-starved continental shelf of south/central Namibia. Marine Geology, 469, 107242.

A.N Green: Formal analysis, Funding acquisition, Investigation, Methodology, Project administration, Resources, Software, Supervision, Writing – original draft.

W. Senna**:** Formal analysis, Writing – original draft.

J.A.G. Cooper: Formal analysis, Writing – original draft.

T. Heeralal: Formal analysis, Investigation, Methodology, Writing – original draft, Writing – review & editing.

H. Labuschagne: Data curation, Funding acquisition, Project administration, Resources, Supervision, Writing – review & editing.

Publication 2

Green, A.N., Meltzer, L., Cooper, J.A.G., Heeralal, T., Labuschagne, H. (in review). Anatomy and stratigraphic evolution of a shelf bypass valley system. GSA Bulletin.

A.N Green: Formal analysis, Funding acquisition, Investigation, Methodology, Project administration, Resources, Software, Supervision, Writing – original draft.

L. Meltzer**:** Formal analysis, Writing – original draft.

J.A.G. Cooper: Formal analysis, Writing – original draft.

T. Heeralal: Formal analysis, Investigation, Methodology, Writing – original draft, Writing – review & editing.

H. Labuschagne: Data curation, Funding acquisition, Project administration, Resources, Supervision, Writing – review & editing.

Signed: _[redacted]________________________

Abstract

The western margin of southern Africa hosts extensive diamond placer deposits spanning from the lower Orange River to the southern Namibian coastline. These diamonds are associated with gravels deposited by surfzone processes during sea level fluctuations. During the postglacial transgression (23,000 to 6,000 BP), these diamondiferous gravels were concentrated and submerged. This study focuses on Area 4 of ML103A offshore Hottentots Bay, employing pseudo-3D seismic profiles, multibeam bathymetry, backscatter data, and over 6,400 drill cores to analyse the geomorphology and seismic stratigraphy of the inner to mid-shelf region.

With the use of a pseudo-3D grid of ultra-high-resolution sub-bottom profiles and extensive borehole data, this study reconstructs the morphology of the paleo-land surface (H1) on which the current shelf sediments lie. H1 comprises a weathered bedrock surface overlain by saprolite or clay and mantled by Eocene-age sandstones. The overlying unconsolidated sediment consists of four seismic and lithostratigraphic units (C-F), including lowermost gravel Units C and D deposited in multiple phases from late Oligocene to late Pliocene/Pleistocene. These deposits formed lowstand lags in small channels on the inner shelf edge and developed into a thickly embayed beach on the innermost shelf. The bedrock-hosted embayment provided preferential accommodation for multi-stacked gravel beaches, contrasting with barrier spit and back barrier sequences to the south, closer to the Orange River. Once accommodation in the embayment was filled, material spilled into the strait, forming linear beaches anchored by a landward bedrock high, resistant to wave reworking and preserved through overstepping during significant sea level rises, notably MWP-1B of the Holocene.

The dissertation emphasizes the need for further dating of these gravel beaches, challenging due to the polycyclic nature of their materials.

Contents

List of figures

Chapter 1: Introduction

In the context of global warming and rising sea level it has become critical to understand the way shorelines may behave in an uncertain future, a topic that has spurred much debate (e.g. Vousdoukas et al, 2020; Cooper et al., 2020). In this light, it has become increasingly important to examine shorelines, now submerged on the continental shelf, as analogues for future coastal behaviour in a changing world (Green et al., 2018).

Submerged shorelines help illuminate the relationships between rates of sea-level change, antecedent geomorphic settings (Pretorius et al., 2016), past climate changes (Green et al., 2022) and resulting coastal change. Their preservation in relation to antecedent gradient (Green et al., 2018), rates of sea-level rise (Locker et al., 1996; Green et al., 2014) and sediment supply (Mellet et al., 2012) relay valuable information on how modern shorelines will evolve through time and space with respect to climate change and post glacial sea-level rise.

Coastlines respond to rises in sea level via three different mechanisms (Carter, 1988):

(1) shorelines have the ability to migrate landward while preserving their volume, a phenomenon known as “rollover.”

(2) shorelines may be overstepped and submerged in place.

(3) shorelines may be eroded completely.

The preservation of shorelines as relict features on the seafloor is attributed to the overstepping or partial overstepping of the palaeo-shore feature. The degree to which overstepped shorelines are preserved depends on their resilience to wave ravinement processes (Pretorius et al, 2017), in addition to multiple other factors such as shoreline sediment volume, antecedent slope, system energy, diagenetic factors, climate, and rates of sea-level rise (Storms et al., 2008). Transgressive stratigraphic facets preserved alongside the palaeo-shoreline contribute to understanding the processes that facilitate or impede the preservation of recently submerged or older palaeo-shorelines (Green et al., 2018).

When compared to submerged sandy shorelines, of which relatively few documented examples exist (Cooper et al., 2016), gravel-dominated beaches and barriers are a more common facet of submerged landscapes on the continental shelves of the world (e.g. Kirkpatrick et al., 2019; Runds et al., 2019). This is because gravels have longer relaxation times, and thus the inertial constraint on their movement due to sea-level rise is large (Long et al., 2006). According to Mellett et al., (2012) continental shelves located offshore of present-day gravel-dominated coasts thus provide exceptional potential for exploring the conditions required for drowning and preservation of coastal landscapes.

The Namibian coastline of SW Africa is considered a predominantly sandy coast (Cooper and Green, 2023). However, over several millions of years, the delivery of gravel to the coast via the Orange River has built substantial accumulations of gravel along the southern shorelines (Apollus, 1995; Bluck et al., 2005), and continental shelf. It thus poses a unique laboratory for the examination of submerged gravel landscapes in a subtropical setting.

1.1 **Aims and objects.**

The main aim of this dissertation is to examine the geomorphology and seismic stratigraphy of the inner to mid shelf of Hottentot's Bay on the south-central Namibian coast (Fig. 1.1). Focus will be paid to the relationship between various gravel deposits and their influencing factors. The objectives of this study thus include:

1) To define the seismic stratigraphy of the inner continental shelf.
2) Link this to lithological data from numerous boreholes drilled in the region
3) To investigate the corresponding palaeo-depositional environments based on sequence stratigraphy principals.
4) Establish an evolutionary model, with particular focus on the gravel deposits, of the study area.

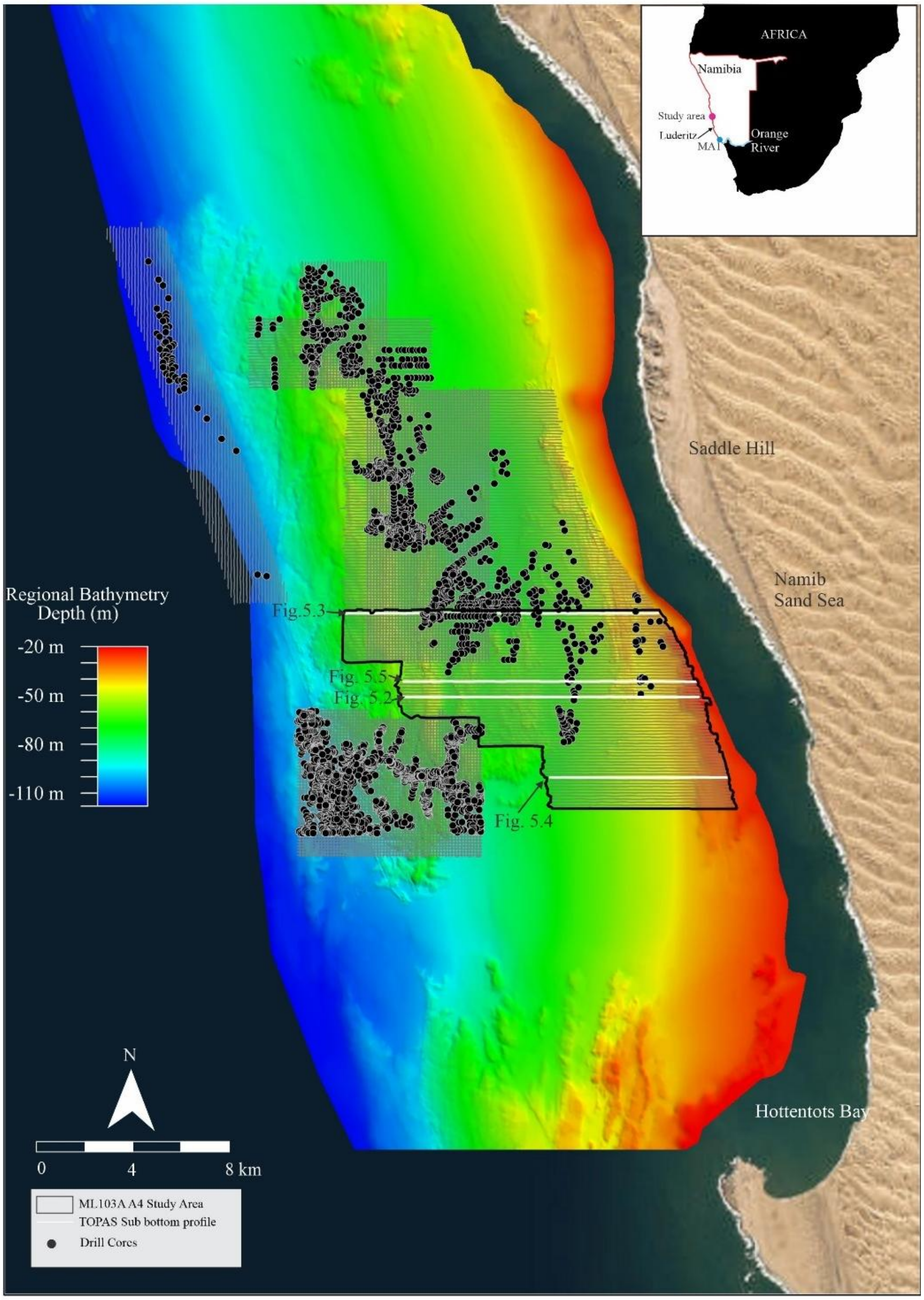

Figure. 1.1. Locality map of the study area highlighting the geophysical data collected, and drill core sample distribution. The area of focus is concerning the Namibian inner shelf offshore Hottentots Bay.

Chapter 2: Literature Review

2. Seismic Stratigraphic analysis of Surfaces

As per Mitchum and Vail, 1977 initial steps of seismic stratigraphic analysis of basin fills entails delineating genetically linked units, termed Depositional Sequences. These sequences hold regional significance and are subsequently subdivided into individual system tracts (Van Wagoner et al., 1987), delineated by the occurrence of local unconformities and their laterally equivalent conformities. According to Armentrout and Perkins (1991) these system tracts are found to contain a grouping of deposits from time-equivalent depositional systems.

The depositional sequences consist of a stack of system tracts, which can be categorized into lowstand and highstand system tracts, indicating shifts in relative sea level. The primary technique used for demarcating Depositional Sequence boundaries is termed reflection termination mapping (Vail et al., 1977).

The convention suggested by Sangree and Widmier (1977, 1979) and Mitchum et al. (1977a), whereby three attributes are combined into a single mappable variable, is commonly followed by most published seismic facies analyses. These include the geometric relations of the reflections with reference to the upper and lower sequence boundaries (toplap and downlap, respectively) and the internal reflection configuration (parallel, oblique, divergent, sigmoid) (Cross, 1988).

2.1 Nature of reflection patterns

A seismic facies unit is characterized as a distinct grouping of reflections, distinguishable by variations in elements such as reflection patterns, amplitude, continuity, frequency, and interval velocity, differing from those of neighbouring units (Veeken and Moerkerken, 2013).

Reflection patterns involve the configuration of reflections and the nature of cycle terminations at the boundaries of seismic facies units. Interpreting these patterns aids in deducing substantial information about the transportation processes and depositional environment of the facies.

There are four major groups of systematic reflections observed on seismic sections: (1) sedimentary reflections representing bedding planes. (2) Unconformities/discontinuities in geological time. (3) Artefacts; for example, multiples and diffractions. (4) Non-sedimentary reflections; example fault planes, fluid contacts etc. (Sangree and Widmier, 1979).

2.2 Reflection Configuration patterns

Reflection configuration patterns are cross bedding patterns. These patterns hold vital information on the transporting processes and the environment of deposition of sediment.

There are three principal types of reflection configuration: (1) reflection-free zones areas where limited reflecting surfaces exist (2) stratified patterns which consist of parallel or divergent reflections that possess a sensible degree of continuity; and (3) chaotic patterns in which reflections are discontinuous or internally contorted (Veeken and Moerkerken, 2013). The reflection configuration geometries can be defined as stratified (parallel, oblique, divergent, sigmoid), reflection-free or chaotic (Sangree and Widmier, 1979) (Fig. 2.1a).

2.3 Reflection termination patterns/ Stratal termination patterns

According to Catuneanu (2006), stratal terminations are defined by the geometric relationship between strata and the stratigraphic surface against which they terminate. Stratified configurations consist of both simple and complex stratified configurations. Both formations emerge through the progressive development of depositional surfaces that slope from a gently inclined, relatively shallow water area into deeper water. The resulting reflection configuration can be categorized into upper (topset), middle (foreset), and lower (bottomset) zones (Sangree and Widmier, 1979). The primary types of stratal terminations are defined by truncation, toplap, onlap, downlap and offlap which have been introduced with the development of seismic stratigraphy in the 1970s to describe the architecture of seismic reflections (Mitchum and Vail, 1977) (Fig. 2.1b).

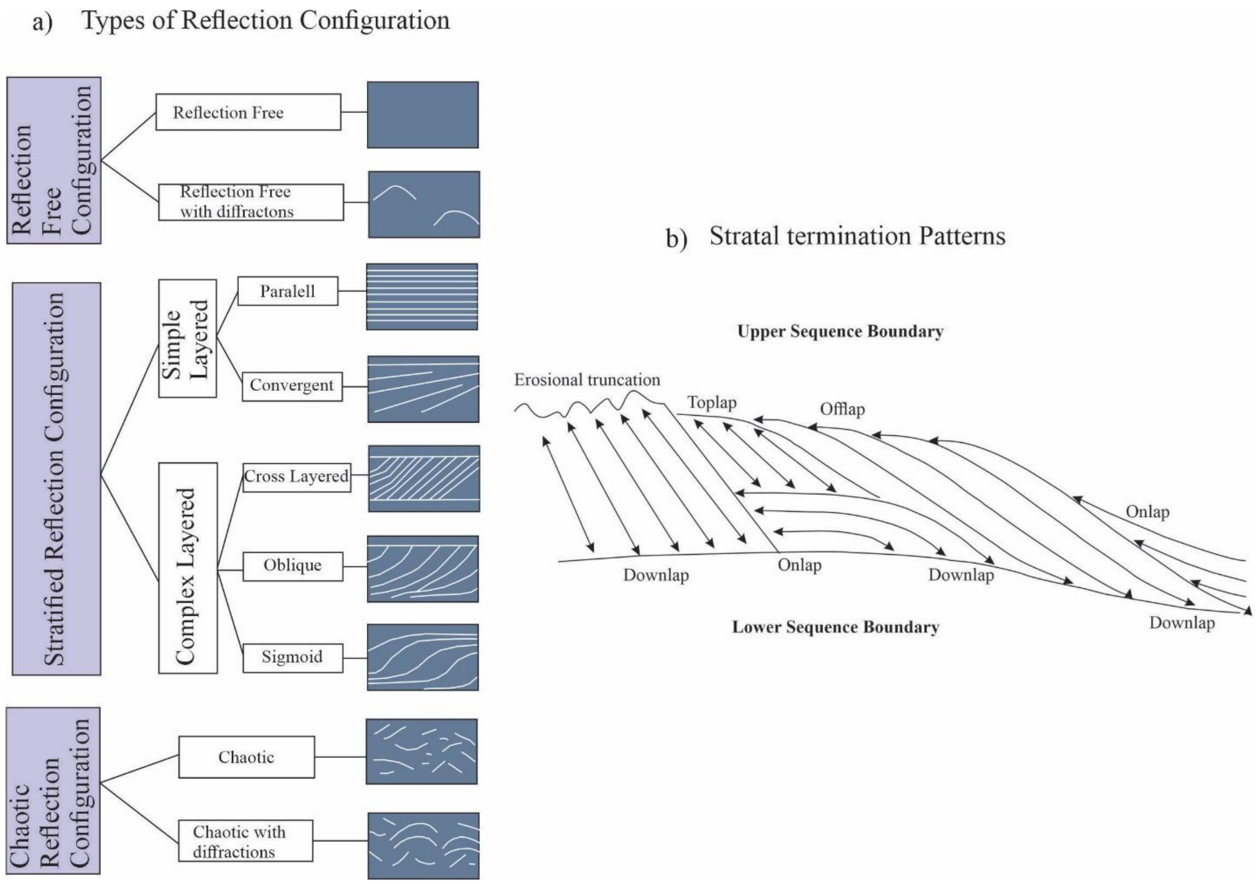

Figure. 2.1. a. Diagram depicts the basic types of reflection configuration (Modified after Roksandik, 1978). b. Types of stratal terminations (modified from Catuneanu, 2006).

2.4 Incised Valleys

Incised-valley systems are preserved features typical of Quaternary stratigraphy found on most continental shelves (Duncan et al., 2000; Foyle and Oertel, 1997; Warren and Bartek, 2002). They are typically elongated depressions, which are larger than a single channel, (Dalrymple et al., 1994), formed through the process of fluvial incision during shelf exposure. Incised-valley systems provide evidence of paleo-flow conditions during times of lowered sea level (Nordfjord et al. 2006).

According to Van Wagoner et al. (1990), incised valleys are the keystone for sedimentary record of sea-level fluctuations on continental margins. As coastal lowlands these valleys are vital in maintaining shelf environments as they provide accommodation for lowstand and early transgressive sedimentation (Vail 1987; Posamentier and Allen 1993).

These features also aid in entraining and protecting sediment from transgressive erosion (Swift and Thorne, 1991) and have potential to offer the most comprehensive sedimentary record of lowstand intervals (Thomas and Anderson, 1994; Payenberg et al., 2006). This makes them essential in deducing processes that create, change, and preserve continental-margin sequence stratigraphy.

Incised valleys are characterized by two types of sediment fills (Zaitlin et al., 1994) namely:

Simple fills have one sequence boundary found at the base of the valley (Lericolais et al., 2001) and compound fills has a series of sequence boundaries formed from multiple cycles of superimposed incision and deposition. (Thomas and Anderson, 1994).

A series of conceptual models have been proposed by Zaitlin et al (1994) which explains how incised valleys' morphology and general sediment facies respond to environmental forcing. These environmental forcing encompasses variations in sediment supply and associated physio-graphic alterations, occurring as a consequence of rising sea levels leading to drowning.

Drowned valley fills are categorised into: (1) a landward zone, predominantly influenced by riverine sedimentation, which may include features like bay head deltas or straight tidal and fluvial channels, (2) a seaward zone characterized by dominance of wave and/or tidal processes, exemplified by features as an estuary mouth complex, (3) an intermediate area with mixed energy, essentially acting as a sediment sink subject to both marine and non-marine influences. Muddy central basin sediments are indicative deposits of such an area (Hughes and Masselink, 2003) (Fig. 2.2).

Models of this nature serve as a foundation for globally comparing drowned valley systems and exploring the evolution process whereby incised valleys transform into estuaries during transgression (Nordfjord et al., 2006). These models range from the proximal to the distal environment of incised-valleys. The characteristics and arrangement of facies within incised-valley estuaries are governed by the interaction between marine processes (wave and tides), which typically diminish in intensity upstream, and fluvial processes, which weaken downstream. According to Dalrymple et al. (1992), all estuaries ideally exhibit a three-fold structure. Estuaries typically possess an outer marine-dominated portion characterized by net bedload transport moving seaward; a relatively low-energy central zone where bedload convergence occurs; and an inner river-dominated segment which is influenced by marine forces where transport is directed seaward. The degree of development of these three zones varies across estuaries due to factors like sediment availability, coastal zone gradient and the estuary's evolutionary stage.

Estuaries are classified into two distinct yet intergrading types, namely wave-dominated and tide dominated, based on the prevailing marine process.

2.4.1 Wave-dominated Estuary

In wave-dominated estuaries the transportation of sand alongshore and onto the shore in this type of estuary results in the deposition of a sandy plug at the head of the estuary. The sand plug typically consists of two components, (1) a barrier accompanied by washover deposits, and (2) a tidal inlet that breaches the barrier, allowing the exchange of tides with the estuary and subsequently forming a flood tidal delta (Catuneanu, 2006). The central portion of the estuary found in the landward part of the sand plug is found to be low-energy zone typical of muddy facies. Wave-dominated estuaries usually exhibits a clearly distinct three-part zonation: a marine sand body containing barrier islands, washovers, tidal inlets, and tidal delta deposits; a central basin characterized by fine-grained, predominantly muddy sediments; and a bay-head delta influenced by tidal and/or saltwater influences (Dalrymple et al., 1992).

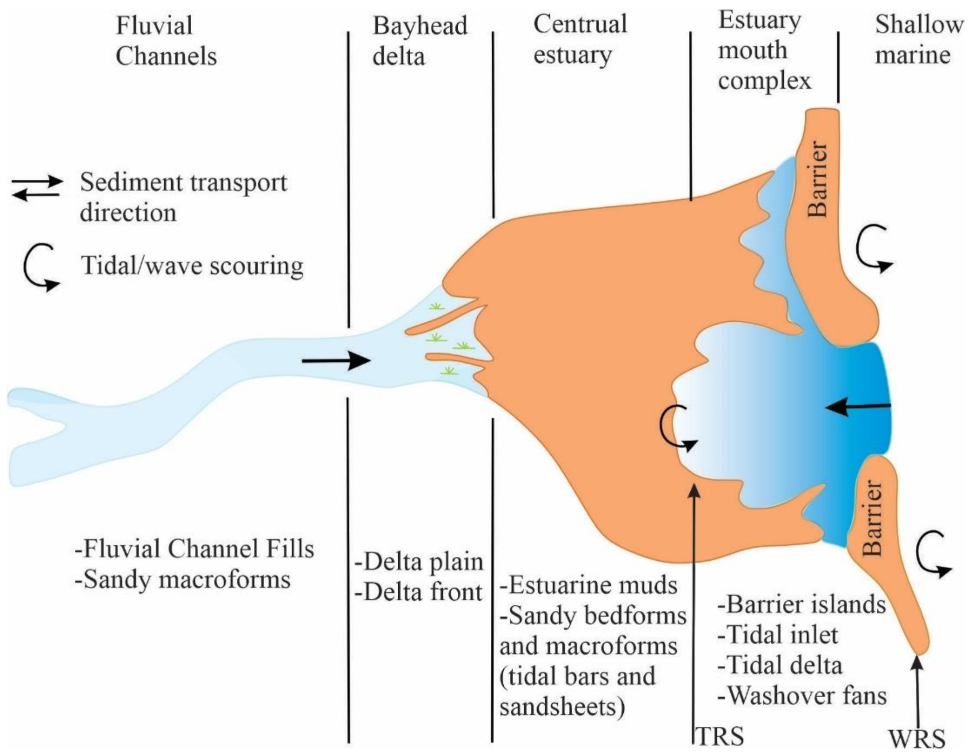

Figure. 2.2. Tidal and wave-ravinement surfaces in a wave-dominated estuarine setting (modified after Dalrymple et al., 1992, Zaitlin et al., 1994 and Catuneanu, 2006). Both tidal and wave ravinement surfaces (TRS and WRS respectively) expand in a landward direction as facies retrograde during transgression.

2.4.2 Tide-dominated Estuary

According to Cooper et al. (2001), tide-dominated estuaries are described to have adequate tidal prism to maintain their inlets by tidal currents against littoral sediment transport driven by longshore and cross-shore waves. Tide-dominated estuaries have been studied in various localities across the globe and are regarded as a microtidal estuary (Cooper, 1993). There is significant bedload of sediment transported upstream due to tide deformation during propagation. Sediment is found to be received from both the shelf and the river with most of the sediment received by the river being transported and deposited by tidal currents. Such estuaries are generally characterized by a funnel-shaped that have a high width to depth ratio. Distributary channels typically have low sinuosity (Wells, 1995). Elongated sand bars are characteristic of tide-dominated estuaries

(Dalrymple et al., 1990). These sand bars are formed at the mouth of the estuary due to the prevalence of tidal-current energy over wave energy, subsequently these sand bars also dissipate existing wave energy as it travels up the estuary. Due to the funnel shaped geometry of these estuaries (Langbein in Myrick and Leopold, 1963), incoming flood tide experiences a gradual compression into the narrow cross-sectional area. This results in the intensification of flood-tidal currents' velocities within the estuary. The phenomenon of this tidal intensification is called hypersynchronous (Nichols and Biggs, 1985).

Cooper (2001) describes tide-dominated estuaries to display a distinct tripartite arrangement of facies. This arrangement consists of marine inputs at the inlet, fluvial inputs at the tidal head and a central zone dominated by suspended sedimentation. It is observed that the upper tidal limit of the estuary, the fine-grained sedimentation transitions to the deposition of fluvial sediment, forming a delta characterized with varying textures according to the geological composition of the river catchment (Cooper, 2002).

Within the seaward section, known as an estuarine bay, a conceptualized incised valley succession exhibits at least three superimposed transgressive surfaces in response to steady sea level rise and continuous sediment supply (Hughes and Masselink, 2003): (1) The bay flooding surface arises as a result of inundation of the fluvial system (Nummedal and Swift, 1987), distinguishing the underlying fluvial deposits from the overlying estuarine deposits. (2) Zaitlin et al. (1994) had described that tidal ravinement surface form as tidal currents erode coastal inlets or channels within the established estuary, which then erodes the underlying deposits confined within this particular part of the system (Allen and Posamentier, 1993). As the tidal ravinement develops in or near the mouth of the submerging incised valley, a locally occurring bay head channel system diastem forms within the landward portion of the estuary-mouth complex. This diastem arises from the seaward propagation of a bay head delta. (3) Lastly, a broad wave ravinement surface forms as the shore recedes inland during transgression. Underlying estuarine deposits are truncated by an erosional event. To form this surface, wave and current erosion must remove both flood tidal-deposits and potentially some central-basin facies.

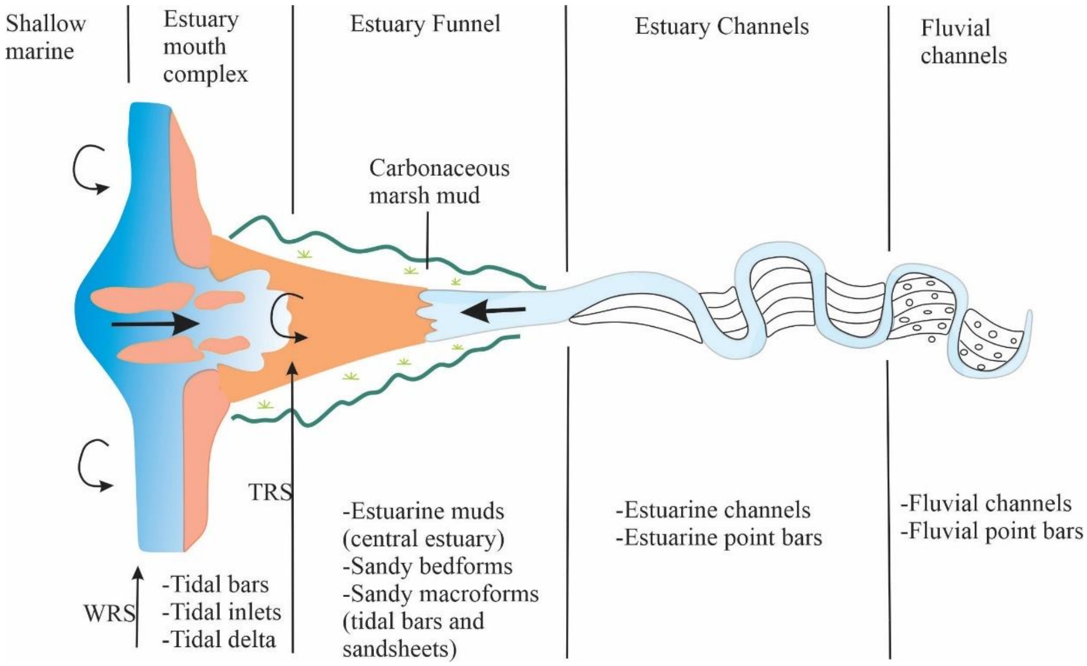

Figure. 2.3. Tidal and wave ravinement surfaces in a tide-dominated estuarine setting (modified after Dalrymple et al., 1992, Reinson et al., 2000, Zaitlin et al., 1994 and Catuneanu, 2006).

2.5 Depositional Sub-environments of gravel beaches

The morphology, dynamics, and growth of gravel beaches have been extensively studied (Spaggiari et al., 2006), but only in the past few decades has their internal structure been recognized, beginning with an initial and preliminary study by Bluck. (1967). According to Bluck et al. (2001) gravel will accumulate in three major areas and thus their deposits are classified into three main zones. These deposits are the subtidal, intertidal and back barrier deposits.

2.5.1 Intertidal zone

The intertidal unit is structurally complex, featuring a variety of bed assemblages and depositional sub-environments. There is a wide variety of foreshore deposits and the morphology and structure of the gravel bars, which include the foreshore, are notably diverse (Spaggiari et al., 2006). Bluck et al. (2001) has recognized four beach types which are: spits, barrier beaches, linear beaches and pocket beaches, they are in order of sediment accretion rate. These beach types are all classified according to the range and combination of bed assemblages. One distinguishing feature that connects these beaches is the sorting of their gravel clasts, serving as a clear identifying factor.

In most gravel beaches there is a noticeable segregation of clast shapes. Large oblate to discoidal clasts of varied shapes accumulates at beach crests, while large equant or spherical clasts and small discoidal clasts accumulate at the base of the intertidal zone. Therefore, the beach surface is regarded as a zone of varying steepness where particle acceptance and rejection take place according to their shape and size due to strong swash and backwash energy. Gravel beaches can vary greatly in morphology and subsequently in the sedimentary environments that influence the distribution of sediment (coarse and fine) (Bluck, 1998).

There are four zones to gravel beaches: (1) Infill zone; (2) Zone of selection pavements; (3) Zone of beach and cusps; (4) Berm.

In the Infill zone are typically observed to have alternating beds of smaller spheres and sand. Towards the seaward edge of the beach, there is a zone where displaced clasts fill the gaps between the spherical clasts forming the outer boundary (Spaggiari et al., 2006).

The infill zone merges into the zone of selection pavements which is an inclined surface that typically consists of a mix of gravel and sand. Stratified marine gravels are formed here as clasts are hydraulically sorted to accumulate on the beach as seaward inclined strata usually characterised by good shape and size segregation. This zone may also constitute of cusps (Spaggiari et al., 2006).

The zone of berm and cusps lies in the landward section of the zone of the selection pavements. Due to a high degree of sorting this zone exhibits steep surfaces and beds steeper than that found in the selection pavements. These steeply dipping beds extends seaward in the direction of beach progradation and show pronounced shape and size sorting. A berm may replace the area where the beach and cusps form which is strike-aligned along the coast without significant evidence of cuspate development (Spaggiari et al., 2006).

2.5.2 Subtidal deposits

Subtidal deposits commonly consist of sand with cross strata that may exhibit bimodal dip directions. These beds, often containing abundant shell debris are believed to be equivalent to shallow marine mega-rippled sand fields. In addition, sand sheets up to several metres thick with heavy bioturbation are present in this zone (Spaggiari et al., 2006).

The subtidal zone may be divided into three zones (Boggs Jr, 2006), which are: 1) The upper shoreface; 2) Middle shoreface; 3) Lower shoreface.

Boggs Jr (2006) described the upper shoreface as the energetic surf zone. Sediment sizes in this zone ranges from fine to medium with gravel. Waves generate shore-normal currents that interact with shore-parallel currents, resulting in intricate sedimentary sequences characterised by multi-directional structures. The upper shoreface is primarily characterised by trough cross-stratification, which forms as ripples and dunes migrates (Reinson, 1984; Spaggiari, 2011).

The middle shoreface is also observed to be an area subjected to high energy and wave action. This zone constitutes of the breaker zone where shell material, fine to medium grained sand, silt and gravel accumulate. Longshore bar development is associated with this zone. Sedimentary structures present in this area are similar to that of the structures found in the upper shoreface. Sedimentary structures present are intricate which consists of landward-dipping ripple cross lamination through seaward-dipping, low angle planar stratification to trough cross stratification (Boggs Jr, 2006).

The seaward section of the surf and breaker zone is exposed to oscillating wave currents through fair-weather hence giving rise to the lower shoreface. Sediments found in this area is typically fine sand interbedded with silt and mud. Dominant sedimentary structures include near horizontal lamination, landward migrating ripples and hummocky cross-stratification (Boggs Jr, 2006; Spaggiari, 2011).

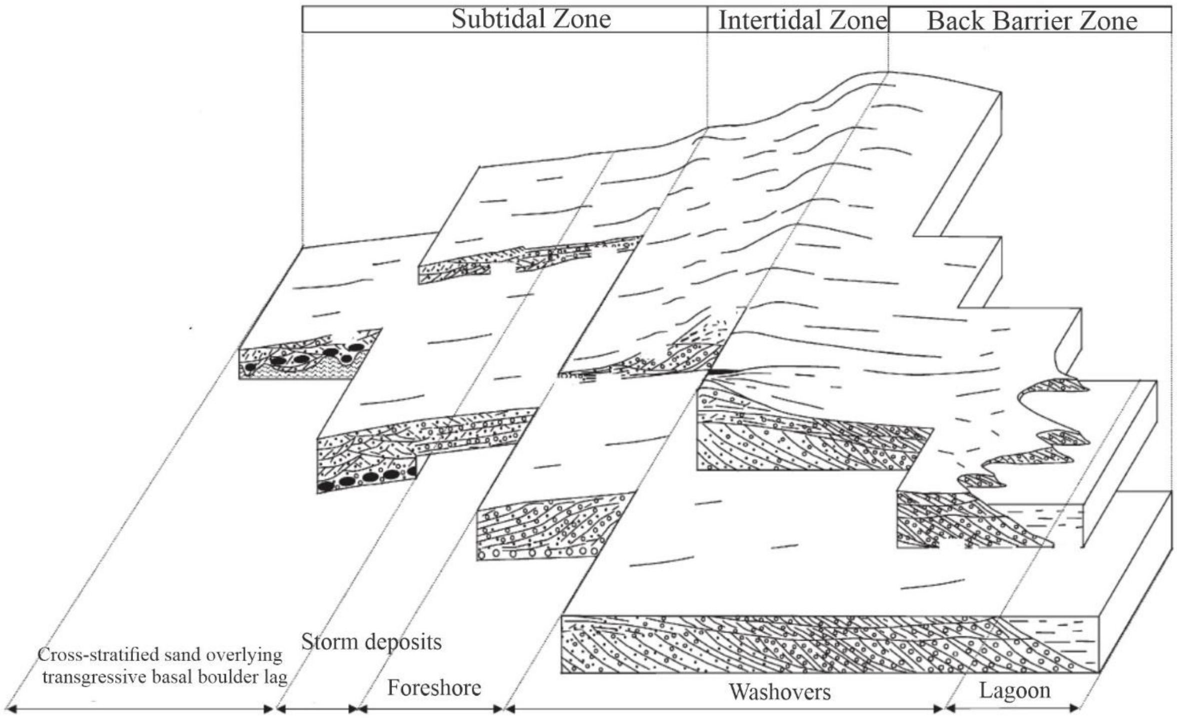

Figure. 2.4. Diagram showing internal structures of beach depositional environments (Adapted from Spaggiari et al., 2006).

Chapter 3: Regional setting

3.1 Offshore regional stratigraphy

The Namibian continental margin is one of the worlds widest and deepest shelves which far exceeds the global average width of 86 km and depth of 130 m. The margin is of volcanic origin (Clemson, 1997). It encompasses an extensive and stable shelf that spans up to 230 km offshore and lies up to 500 m below sea level (Dingle et al., 1983).

The shelf comprises a thick wedge (3-5 km) of predominantly clastic post-rift sediments, overlying a rifted Proterozoic continental basement (Light et al., 1993), this is subsequently overlain by syn-rift siliciclastics and volcanics deposits dating from the late Jurassic to the early Cretaceous period (Clemson et al., 1999). Karoo Supergroup rocks from the Late Carboniferous to Early Jurassic era are potentially preserved withing small half-grabens, truncated by an angular unconformity which subsequently reflects significant erosion of the Karoo Supergroup material over an extended period (Clemson et al., 1999; Aizawa et al., 2000).

3.2 Sediment supply and coastal regime

The Orange River, formed during the Early Cretaceous, currently serves as the primary channel for coarse sediments and diamonds to the west coast of southern Africa (Dingle and Scrutton, 1974). The discharge point of the Late Cretaceous predecessor to the Orange River was a finer-grained transporting system that supplied sediment to a significant, enduring palaeo-delta located offshore from the present-day mouth of the Orange River (Ward and Bluck, 1997; Aizawa et al., 2000). During the late to end of Cretaceous period, regional subcontinent uplift commenced fluvial incision, which persisted intermittently throughout much of the Cainozoic era (Spaggiari et al., 2006), altering the deposition at the river mouth from fine (silt and clay) to coarse-grained (gravel and sand) sediment (Spaggiari et al., 2006). Since then, the Orange River has transported sediment of up to boulder sizes to the coast (Bluck et al., 2007).

The present-day Orange River has a wave-dominated delta, which experiences significant northward longshore drift due to the prevailing southerly swell, wind and wave patterns (Rogers, 1977). From the south-southwest direction, the coastline receives prolonged-period swells, with an average swell height surpassing 3 m, originating in the Southern Atlantic Ocean. During summer wave heights can average 1.5 m, increasing to approximately 1.9 m in winter but throughout the year wave heights can be found to exceed 4.75 m (Kirkpatrick et al., 2019). The average wave periods range between 10.5 s in summer and 12.5 s in winter. Shorter-period waves, induced by persistent southwest winds, which are in turn generated by the South Atlantic Anticyclone system superimpose the long-period swells. Approximately 90% of the shorter period waves attain a height ranging from 0.75-3.25 m (De Decker, 1988).

The estimated water depth of the wave base is ~ 40 m, but submersible dives suggest that it can extend significantly deeper to ~110 m (Bluck et al., 2007). The swell and wind regime gives rise to the northward-directed littoral drift and the average wave conditions along this coast have enough energy to transport coarse sand to depths of 30 m. It is also found that storm waves have the ability to transport medium sized pebble at the same depth (De Decker, 1988). At ~ 15 m water depth, cobbles are frequently transported while storm events induce significant sediment transport on the inner shelf at a ~ 30 m water depth (De Decker, 1988; Bluck et al., 2007). The Orange Rivers' coarse-grained discharge has been exposed to yearly high-wave energy since mid to late Tertiary times (Spaggiari et al., 2006). Over a narrow zone of the coastline these high wave energy conditions are concentrated by a micro-tidal range of 1.8m. Discharge of the Orange River is dispersed northwards and westwards by the dynamic longshore drift system (Bluck et al., 2007). Gravels are found to be deposited along the coastline spanning more than 300 km north of the Orange River mouth, sand fractions are transported > 700 km along the coast and mud is found to be more dispersed westwards, northwards and southwards into basins on the shelf and onto the continental shelf edge (Bluck et al., 2007). A significant portion of the sandy or finer sediment fraction is entrained into the Namib Sand Sea (Corbett, 1993). This is exacerbated by the presence of the nearshore geological framework that limits accommodation during lowstands (Green et al., 2024).

3.3 Gravel Pulses of the Orange River

The orange River is the principal conduit for the transportation of diamondiferous gravels from the southern African interior to the Atlantic coast (Jacob et al., 1999).

In the late Cretaceous, the Orange River flowing into the Atlantic Ocean transported fine sediment thus creating a large, fine-grained delta offshore from its current position (Bluck, 1997; Spaggiari and Bordy, 2023). By the Middle Eocene the river had evolved into a highly energetic, gravel dominated system that incised into bedrock, transporting small cobble-sized gravels from the interior of southern Africa to the Atlantic coast (Ward and Buck, 1997; Bluck et al., 2005). This shift from a suspended to a bed load-dominated Orange River resulted from continental uplift. Due to the lack of precise dating this change is attributed to the Late Cretaceous to Early Paleogene (Aizawa et al., 2000).

According to Bluck (2005), during the Miocene and later, the bedload of the Orange River coarsened notably, particularly during the Plio-Pleistocene when the dissection of coastal Neoproterozoic bedrocks supplied the majority of gravel. During the Plio-Pleistocene, multiple incisions occurred which was influenced by uplift or sea level changes This resulted in the transport of boulder-sized gravel, with clasts exceeding 1 m, into the Atlantic coast which constituted the main sediment input to the paleo-beaches of southern Namibia (Bluck et al., 2005; Jacob, 2005).

Three distinct terrace (gravel) deposits along the lower Orange River are recognized by their elevation, bedrock strath levels and unique clast compositions (Nakashole, 2018). These three gravel terraces were formed from gravel pulses, of different characteristic sediment composition, supplied by the palaeo-Orange River which Bluck, (2005) termed them, Pre-Proto Orange River, Proto Orange River, and Meso Orange River.

The overall composition of each of this gravel is a combination of both exotic and locally derived clasts. A Pliocene uplift occurring after the deposition of the Proto Orange River gravel, may have caused drainage re-organization and influenced the differences in clast assemblage between Proto and Meso Orange River gravels.

The gravel is composed of a mix of exotic and locally sourced clasts with the large cobble-sized fractions (>25 mm) being primarily made up of quartzite clasts. Agate, Karoo Supergroup shales and sandstones, Karoo Supergroup basalt and banded iron formation (BIF), are known as exotic clasts.

There is no diagnostic clast lithology in either Proto or Meso gravels. Therefore, the dominant exotics in each gravel aids in dating the gravel pulses. The dominance of an exotic is influenced by the timing, rivers sinuosity and river energy (geomorphic evolution of Orange River basin) (Nakashole, 2018).

Table. 3.1. Timing of the main gravel pulses, clast assemblages, clast roundness and deposit thickness

Gravel Pulses						
Pulse type	Age	Clast Assemblage	Exotic mineral Distribution	Clast roundness	River sinuosity at deposition period	Thickness
Pre-Proto	Not sufficiently dated. Late Oligocene age (Bluck et al., 2005; Spaggiari, 2011; Jacob 2005)	High Namaqua Metamorphic Complex clasts.	Dominance of Epidote - rich minerals.	Low degree	Low sinuosity	Unknown due to lack of preservation.
Proto	Early to mid-Miocene, associated with *Lopholistriodon moruoroti* (Jacob et al., 1999; Jacob, 2005)	Minor Namaqua Metamorphic Complex clasts.	Dominance of Karoo Supergroup, shale and sandstone clasts and minor BIF. Minor amphibole-epidote content (Increase in river energy). 22% Sandstone, 6% BIF.	High degree	High sinuosity, reinforced by preservation of cut-off meander loop terraces. Associated with High incision depth and increase sediment transport.	Up to 50m
Meso	Plio-Pleistocene (Jacob et al., 1999; Jacob, 2005)	High Namaqua Metamorphic Complex clasts.	Dominance of BIF clasts with minor Karoo Supergroup, shale and sandstone clasts. Abundance amphibole-epidote content (due to decrease in river energy). 7% Sandstone 10% BIF.	Low degree	Low sinuosity, similar to sinuosity of modern Orange River. Associated with shallower incision depth and decreased sediment transport.	6-23 m

3.4 West Coast sea-level fluctuations and palaeo-shorelines

Similar methods employed in marine heavy mineral exploration, which relies on identifying appropriate environments such as strandlines/beach ridges and embayments (Hou et al., 2017) have been applied to the inner shelf marine placer deposits along the west coast of Namibia. These revealed major concentrations of diamonds along palaeo-shorelines at different elevations. These enrichment concentrations of placer deposits occurred in response to cycles of sea-level transgression and regression (Hallam, 1964; De Decker, 1988).

It is found that the breaker zone has the highest concentration of energy (Jacob, 2001); reworking in this zone upgrades the concentration processes that subsequently occur. As a result, higher-grade diamonds and associated gravel deposits are correlated with the approximate sea level during the deposition period (Oelofsen, 2008).

High diamond concentrations (grades) are often observed within bedrock gullies carved into marine-cut platforms of Mining Area 1 (MA1) at Oranjemund. These formations are thought to have formed during prolonged periods of sea level stability (Hallam, 1964; Oosterveld et al., 1989). A similar situation is predicted in the offshore environment, with platforms associated with still stands considered effective diamond and gravel repositories (Kirkpatrick et al., 2019; Kirkpatrick and Green, 2021).

Throughout the last 40 million years, there have been significant fluctuations in sea level observed along this coastal region, ranging from a high of ~180 m above current sea level during the Eocene and to a Pleistocene low of ~120 m below current sea level (Green and Uken, 2005). This significant drop in sea-level coincided with the Last Glacial Maximum (LGM) ~22 000 BP. Following the LGM, the subsequent rise of sea-level has occurred intermittently, with intervals of slow rising sea level interspersed with rapid rates of sea-level rise (Green et al., 2024).

In the past where climatic and oceanic conditions were characterized by higher energy levels (Bluck et., 2001), it is reasonable to expect lower than present sea-level stillstands would have generated similar erosional morphologies in the bedrock. Consequently, palaeo-shorelines should exhibit equal or greater distinctiveness compared to those observed in the onshore environment (Kirkpatrick and Green, 2021).

A regionally developed palaeo-shoreline at -100 m has been identified along the southern African coast, associated with a still-stand during the Bølling-Allerød transition period ~14 500

BP (Green et al., 2014; Green et al., 2020, Green et al., 2024). Global records have proven that this still-stand was succeeded by a rapid warming in the Northern Hemisphere ~ 14 650 yr BP. Shortly thereafter, rapid melting of ice sheets resulted in a surge in the rate of sea level rise, termed Meltwater Pulse (MWP)1 A (Blanchon and Shaw, 1995).

MWP 1A induced a 12-14 m sea-level rise over ~340 yr which was then followed by slower sea-level rise. It was during this period of gradual sea level the formation of barrier shorelines along the southern Nambian coastline occurred between 14 000 and 13 300 cal BP (Runds et al., 2019; Green et al., 2024), these shorelines were preserved by another surge in sea level which was linked to the MWP -1 B (sea levels rose by approximately 18 m between ~ 11 500 and 11 200 yr BP). In the late Holocene, sea levels rose to a maximum highstand of ~ 3m at 6280 cal BP preceding to present-day sea level of ca. 3000 cal BP (Cooper et al., 2018).

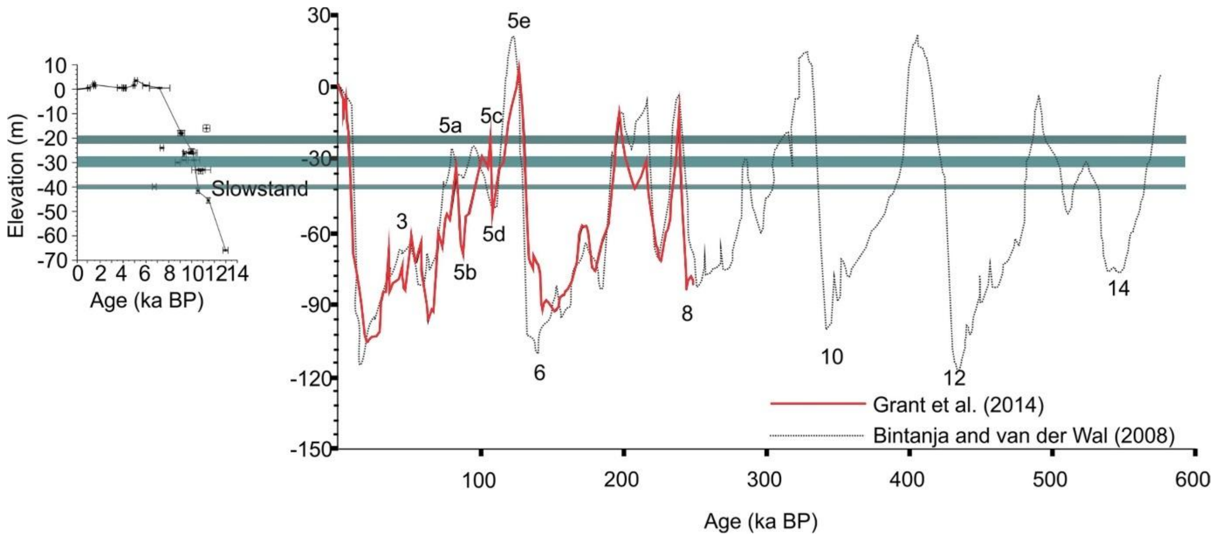

Figure. 3.1. Graph depicting Mid to Late Pleistocene sea level curve (Modified after Cooper et al., 2018)

Chapter 4: Methodology

4.1 Geophysical Data

The study area was mapped in September 2019 using a high-resolution Kongsberg EM 710 multibeam echosounder mounted on the MV DP Star. Data positioning was via a C-Nav 3050 DGPS and a Kongsberg Seapath 200 IMU, while sound velocity adjustments were conducted using a Sound Velocity Probe (Midas Mini). Backscatter was collected simultaneously with the multibeam data.

QPS Qimera was used to process and grid the bathymetry data to a 0.5 m cell size. Any anomalies found in the data were corrected and soundings reduced to MSL datum using predicted naval tide charts for the area. The backscatter data were processed using the Geocoder utility in Qimera and gridded to a mosaic pixel size of 0.5 × 0.5 m. Additional legacy side scan sonar data were employed with the backscatter data, as described in Green et al. (2024).

Approximately 12 000-line km of sub-bottom data were collected along coast perpendicular lines with a line spacing of 100 m using a Topas PS40 parametric-sub bottom profiler. A chirp LFM pulse was employed, and the data were subsequently match-filtered using the Kongsberg SBP utility. Transducer motion was modelled based on the inputs from the Seapath 200. The final RAW TOPAS files were then exported as full waveform data to SEG Y format with a resolution of <20 cm.

The processing and interpretation of the seismic SEGY data were done using Geosuite Allworks. A nominal gain of 10dB was initially applied before the seabed was manually digitised. Once the seabed was established, AGC, water column muting, and swell filtering were applied, and the key stratigraphic horizons digitised. Each horizon was converted from two-way travel time (TWT) to depth by using the standard published values for shallow Namibian shelf stratigraphy which are 1500 m/s for seawater and 1600 m/s for sediments (Kirkpatrick et al., 2019)

4.2 Lithological Data

A total of 6420 borehole samples were collected in the study area from the MV Explorer. Samples were acquired using a 5m^2 reverse circulation drilling apparatus capable of drilling up to 8 m. These sampling sites were chosen to validate the seismic stratigraphy to the greatest extent possible and to establish chronological or lithological constraints on the deposition of certain units. Due to the drilling method used to acquire samples, the cores are retrieved in the form of fragments. Sampling was restricted in areas where water depth was below 30 m to reduce the risk of vessel grounding and damage to the ship hull.

Chapter 5: Results

5.1. Seafloor geological framework and morphology

The seafloor geology of the area is dominated by high backscatter acoustic facies, the majority of which comprise uneven and irregular, moderate to high relief facies (Fig. 5.1). Slightly less intense, moderate backscatter facies with occasional mottling fringe the higher relief seafloor areas. Low, even-toned backscatter seafloor forms a prominent nearshore coast parallel swath. A narrower (1 km-wide) seaward swath of lower backscatter is separated from the inshore corridor by a significant area of high relief, high backscatter, where it forms a characteristic dendritic pattern along the inner shelf edge.

Ground truthing of the seafloor facies reveals these to comprise:

1) Competent rocky outcrop (high backscatter, high relief)
2) Gravel or thin sediment veneer mantling rock (moderate backscatter, mottled tone)
3) Sandy to muddy unconsolidated sediment (low backscatter, even tone)

The inshore rocky material is composed of Precambrian schists of the Spencer Bay Formation, with schists and quartzites of the Gariep Belt more prominent to seaward (Fig. 5.1). These form two main ridges, a western and eastern ridge that frame a low-lying depression (Fig. 5.1c). The rocky framework of these ridges compartmentalises an inshore and offshore fine sediment field, with fringing gravels along the eastern edges that interfinger with the fine sediment. To landward, rocky outcrop appears to form a peninsula in which fine sediment has accumulated.

5.2 Seismic stratigraphy, lithostratigraphy and unit distribution

Six seismic units were identified in the underlying stratigraphy (Units A-F) (Figs. 5.2-5.5). These were defined accordingly by their termination patterns, internal reflection configurations and reflection amplitudes. Their distributions are depicted in figures 5.6 and 5.7. Accompanying the sub-bottom profiles were 6652 drill samples (Fig.1.1) which helped constrain the sub-bottom lithological interpretations (Fig. 5.8).

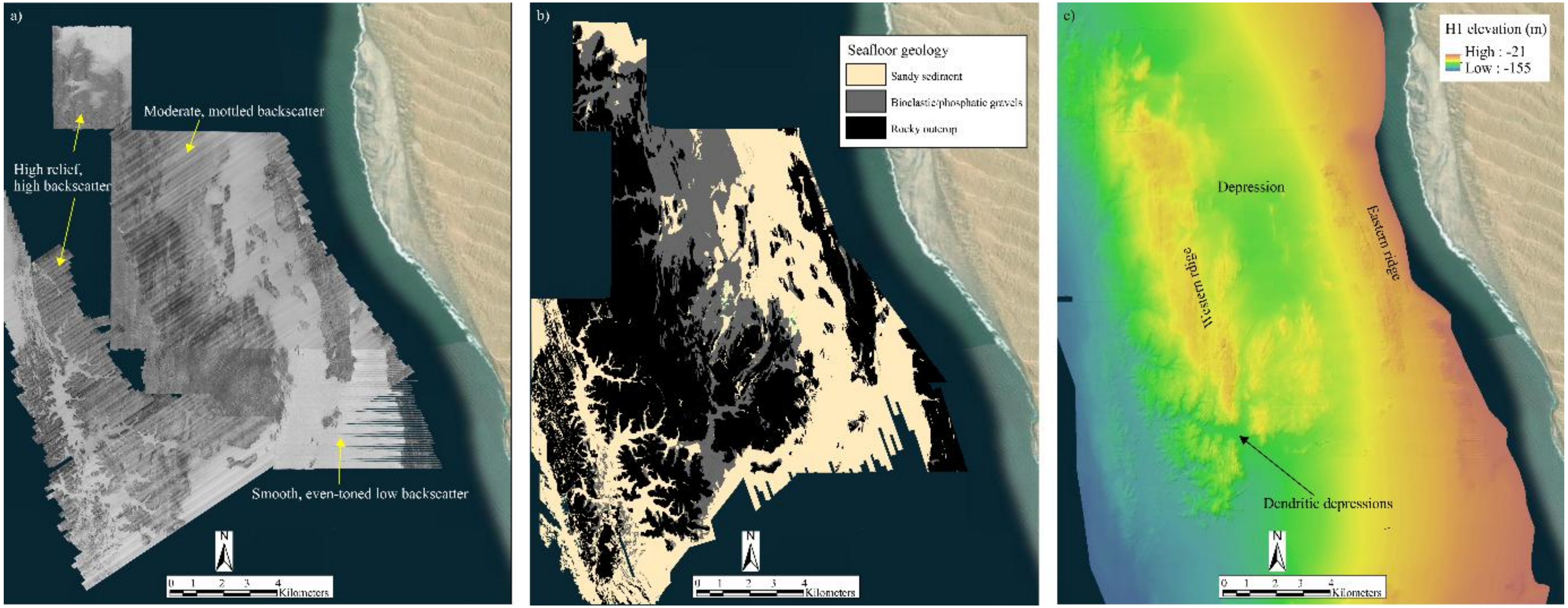

Figure. 5.1. Merged side scan sonar and backscatter mosaic. b. Seafloor interpretation of the acoustic facies of the inner shelf.

Unit A: schists, quartzites (acoustic basement) and weathering residues (saprolites and clays)

The seismic facies of the acoustic basement and associated weathering residues is characterised by high amplitude, low to medium frequency, chaotic internal reflections. The residues that occur above the acoustic basement present as parallel-layered weakly reflective material near the resolution of the data. The acoustic basement crops out to form the rocky seabed (Figs. 5.2-5.5). Overlying the acoustic basement are isolated patches of very thin saprolites and clays, derived as weathering residues from the schists. Their location was mapped predominantly by their occurrence in drill samples where they appear as < 20 cm-thick horizons. Saprolite distribution throughout the study area is confined to depressions the dendritic channel feature in the southwest, and along the landward lee of the western rock ridge (Fig. 5.6a). Drill cores reveal the presence of mudballs which indicate the reworking of saprolite and clay (Fig. 5.8a-b).

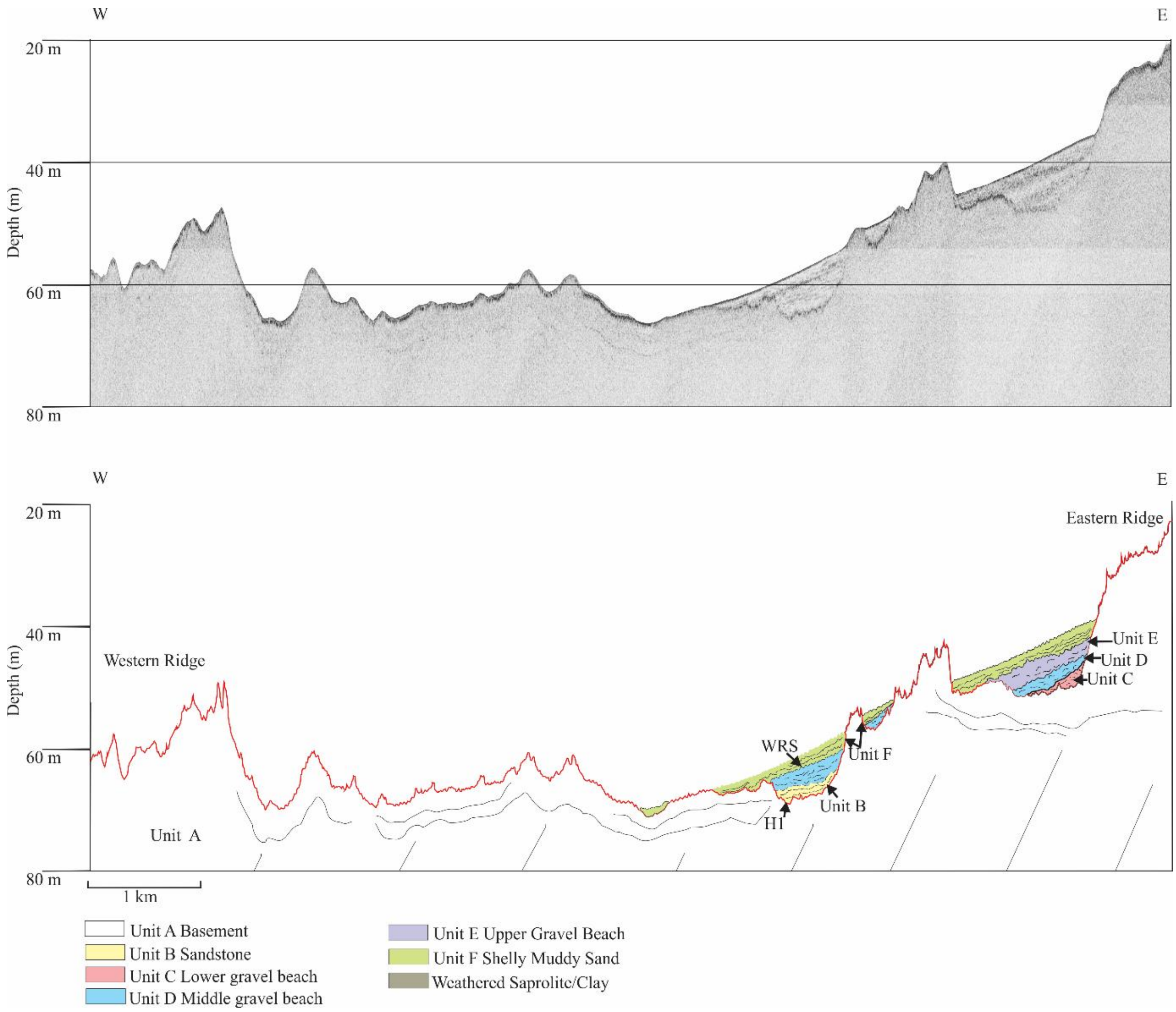

Figure. 5.2. (Top) Uninterpreted sub-bottom profile. (Bottom) Interpreted shore-perpendicular sub-bottom profile, ML103A_A4_13800, with Units A-F including WRS (wave ravinement surface) and H1 Reflectors.

5.2.1 Unit B: sandstone

In the offshore parts of the study area, isolated bodies of Unit B are found between highpoints of the acoustic basement and in channels cut into the bedrock. Unit B typically has a high amplitude surface reflection with chaotic to wavy internal reflections, and forms pinnacled acoustic bodies (Fig. 5.2-5.5). General thickness reaches 1.5 m in the depression between the eastern and western ridges, where the unit forms a discontinuous coast-parallel linear body (Fig. 5.6b).

Drill core from the area reveals Unit B to be an indurated, fossiliferous sandstone (Fig. 5.8c-e). The presence of several key fossils, most importantly *Diplochaetetes longitubus*, constrains the depositing environment and age to that of a shallow shelf during the early Eocene (Green et al., 2024).

5.2.2 Surface H1

A moderate amplitude regional reflector (H1) truncates the sandstones, weathering remnants and basement schists to form an irregular, high relief surface that mimics the contemporary bathymetry (Fig. 5.7a). Like the bathymetry, a NNW-SSE trending depression occurs between the two bedrock ridges, where gradients are less than 0.3° (Fig. 5.7b). The rocky ridges mark a significant steepening of the surface, mostly from the influence of the schists and quartzites as they crop out to form terraces 16 m high and with slopes of 4° or more (Fig. 5.7b). The remaining post-H1 cover comprises unconsolidated materials up to 16 m-thick (Fig. 5.7c).

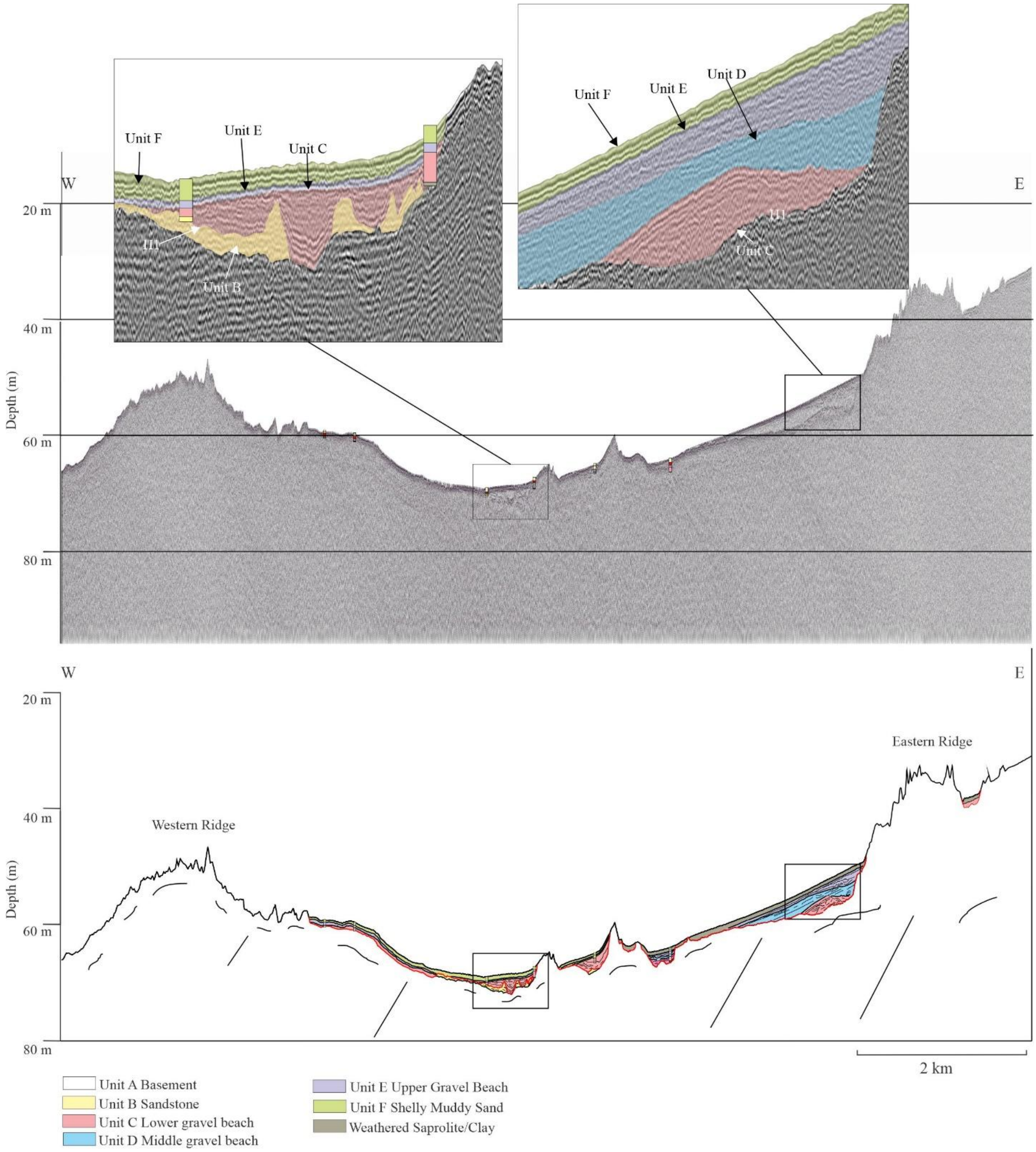

Figure. 5.3. (Top) Uninterpreted sub-bottom profile. (Bottom) Interpreted shore-perpendicular sub-bottom profile, ML103A_A4_16500, with Units A-F including WRS (wave ravinement surface) and H1 Reflectors.

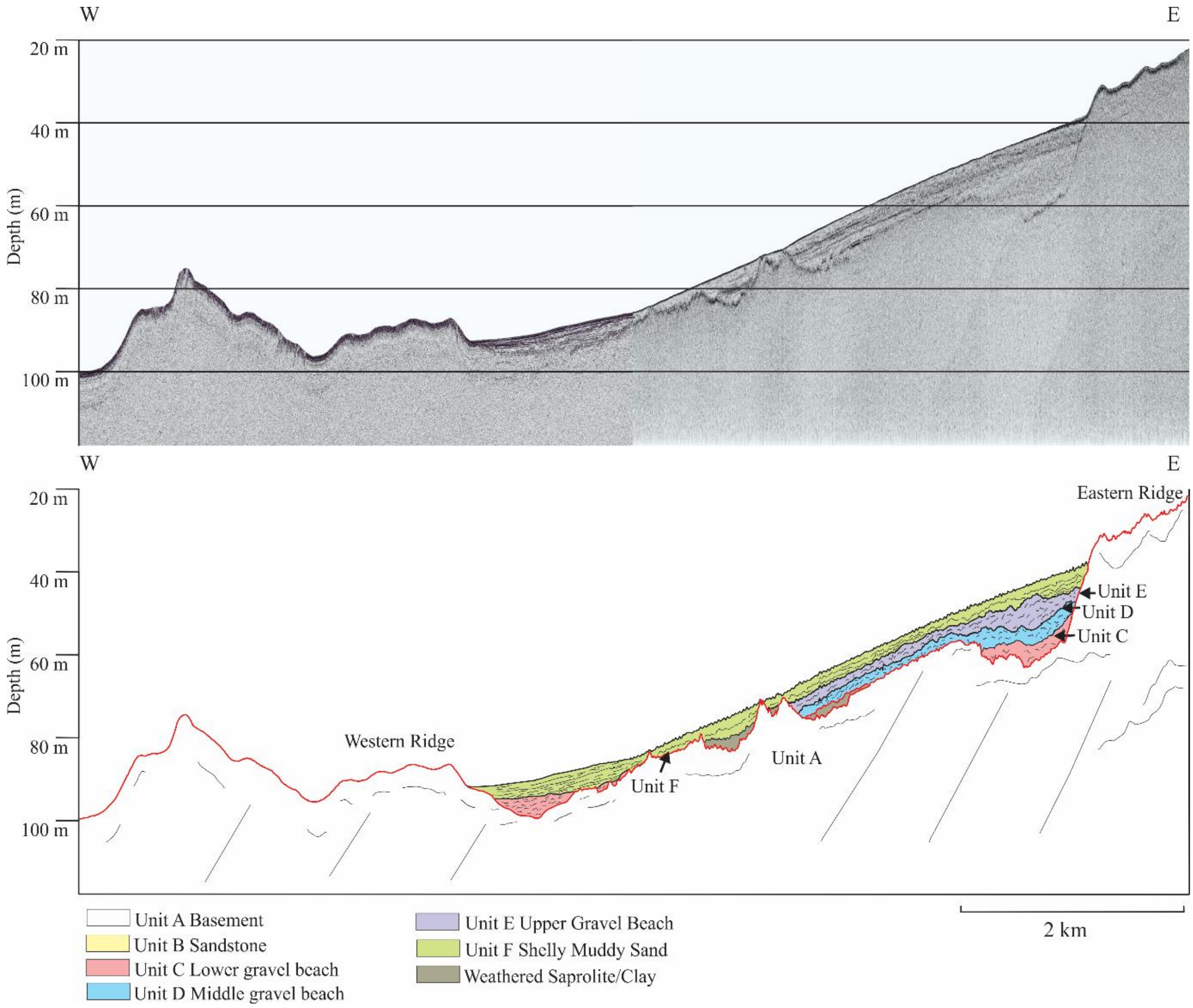

Figure. 5.4. High resolution, coast perpendicular TOPAS sub-bottom profile of line ML103A_A4_11200 (top-uninterpreted, bottom interpreted) detailing the fill succession of H1.

5.2.3 Unit C: lower gravel unit

Unit C occurs as a thin deposit immediately overlying H1, with isolated thickenings in the dendritic portions of the H1 surface to the southwest (Fig. 5.6). The deposits thicken substantially to the east where a 7 m-thick package is observed, confined within the embayment formed by the eastern bedrock ridge. This unit exhibits chaotic internal reflections, often with weak amplitudes from masking of the signal, and with limited reflection continuity (Fig. 5.2-5.5). Occasionally, the internal architecture of the deposit is clear (e.g. Fig. 5.3). In these examples, flat-lying, irregular and wavy reflections interpose with steeper, seaward dipping reflections. Drill cores reveal that this unit is composed of a variety of clast sizes and compositions including an abundance of sub-angular schist and gneiss with common sub-rounded quartzite, quartz pebbles, cobbles, boulders and Karoo Supergroup sandstone pebbles (Fig. 5.8f).

5.2.4 Unit D: middle gravel unit

Unit D is very like Unit C, with a similar reflection arrangement and character but with a more aggradational component. It has an erosional lower contact, with some reflections downlapping and prograding over the upper surface of Unit C (Fig. 5.5). Chaotic irregular reflections often onlap the H1 surface and are overlain by seaward dipping reflections that onlap H1 progressively landward and up-profile (Fig. 5.4).

Unit D is best developed in the bedrock embayment, where it reaches a maximum thickness of 4.6 m. A limb of Unit D bifurcates to the north around the peninsula and extends along the bedrock cliff line for ~ 3.5 km. Drill cores reveal this unit to be composed of an abundance of sub-rounded to well-rounded vein quartz, and angular to subrounded small cobbles of quartzite. Minor traces of angular phyllite fragments, platy schist and disc-shaped banded ironstone were observed (Fig. 5.8g).

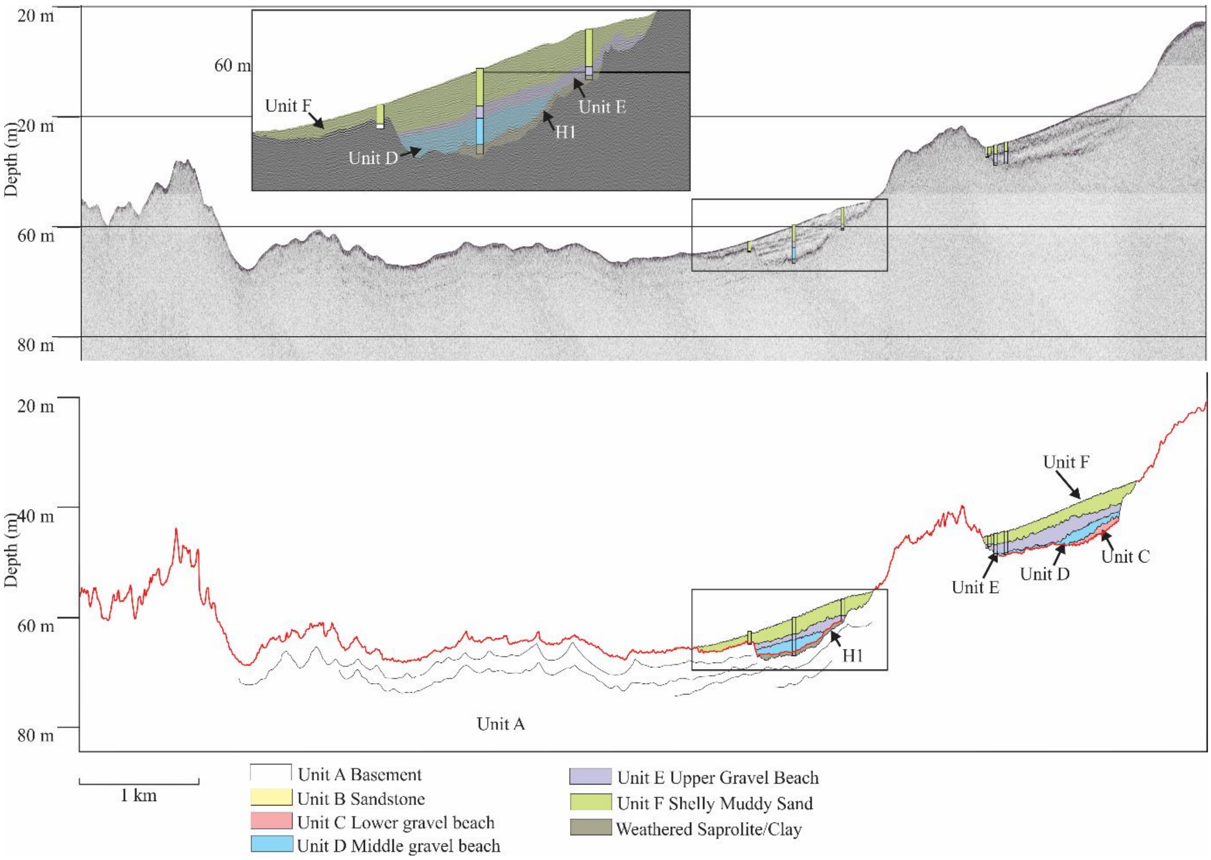

Figure. 5.5. High resolution, coast perpendicular TOPAS sub-bottom profile of line ML103A_A4_143000 (top-uninterpreted, bottom interpreted) detailing the fill succession of H1.

5.2.5 Unit E: upper gravel unit

Unit E mirrors the distribution of Unit D but extends farther into the shelf out of the embayment. It mantles Unit D and exhibits chaotic internal reflections, moderate to high amplitudes and a retrogradational stacking pattern (Fig. 5.3). It is up to 8.9 m-thick in the embayment and consists of an abundance of shelly materials (*Lucinoma* sp and *Dosinia* sp). Angular to subrounded quartzite pebbles, minor small pebbles, cobbles, with common mica-schist flats and bioturbated sandstone pebbles are also common (Fig. 5.8h). This unit commonly occurs at a depth of ~ 70 m and represents the most landward and highest elevation gravel deposit in the area.

5.2.6 WRS

Surface WRS erosionally truncates the gravel units (C-E) throughout the study area from the nearshore to the inner shelf edge (Figs. 5.3-5.5). The surface forms a generally planar, seaward dipping horizon that manifests as a high amplitude continuous reflector that merges with the bedrock surfaces, or H1, if exposed at the seabed. There is a slight deepening of the surface to the NNW.

5.2.7 Unit F: Shelly muddy sand: Younger unconsolidated and semi-consolidated sediments

WRS marks the change from gravel to the finer sediments of Unit F. This unit caps the stratigraphy throughout depressions between high lying regions of the study area and comprises horizontal-parallel reflections with low-high amplitudes thick. Cores reveal the material to consist of muddy sand with an abundance of *Lucinoma* sp and *Dosina* sp shell fragments. The post WRS sediment thickness may reach up to 4 m, associated with the dendritic channel-like features in the south, and the central parts of the H1 depression between the western and eastern bedrock ridges.

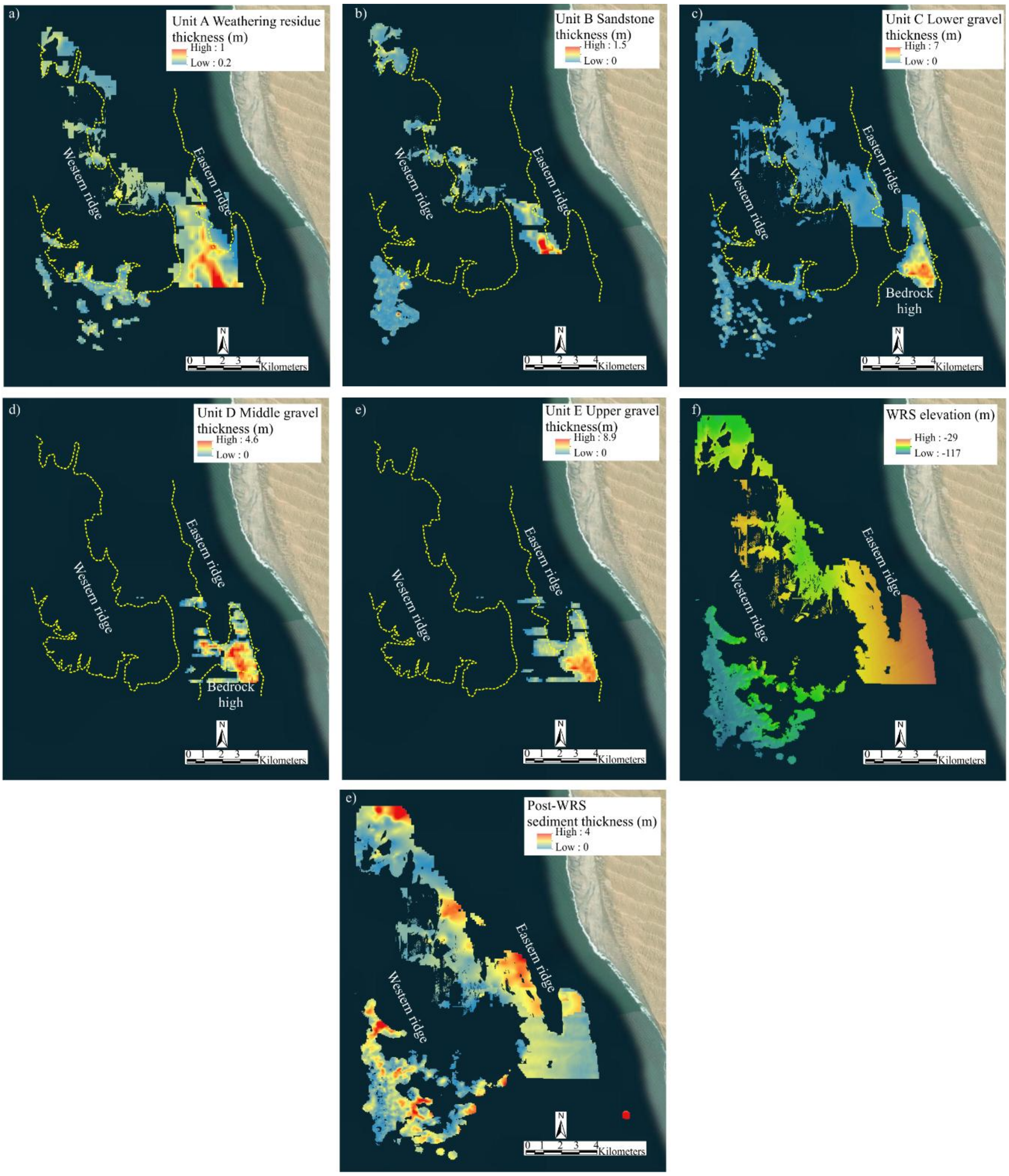

Figure. 5.6. Key horizon structure maps and isopachs of the various stratigraphic surfaces and units in the study area.

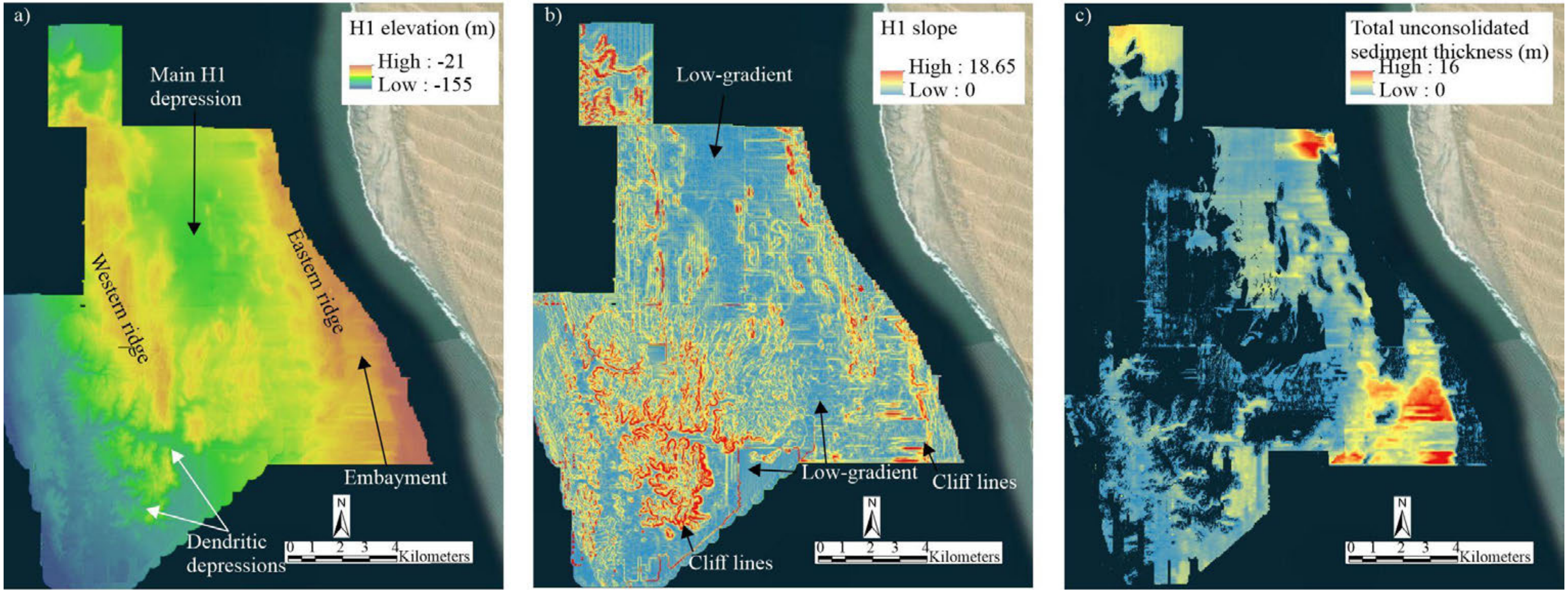

Figure. 5.7.a. H1 elevation throughout the study area. b. Gradient of H1, with several steep cliffed areas evident in the surface. c. Total unconsolidated sediment thickness.

Table.5.1. Seismic stratigraphic units including the description of seismic facies and interpreted depositional environments and age.

Unit/Surface	Underlying Surface/Units	Description	Internal Reflection	Interpreted Depositional environment	Primary Lithology	Age
Unit A	n/a	Rugged topography	High amplitudes and low-medium frequency	Basement	Quartzite and Schists	Precambrian/Proterozoic
	n/a	Smooth and gradational topography	Low amplitude and frequency. Exhibits parallel or sub-parallel patterns. Weak and discontinuous internal reflectors.	Chemical erosion and weathering of schist	Saprolite	Precambrian
	n/a	Smooth and continuous topography	Low amplitude. Low-medium frequency. Parallel and horizontal patterns.	Wave transport and mechanical weathering of eroded weathered material	Clay	Palaeocene
Unit B	H1	Localized body	Medium-high amplitude and frequency. Layered and parallel patterns.	Shallow marine environment, continental shelves	Sandstone	Eocene

H1	Unit A	Continuous surface	High amplitude	Subaerial unconformity	n/a	Early Eocene
Unit C	Units A, B, and H1	Irregular and continuous topography	Variable amplitude with high frequency. Layered and chaotic	Lowstand gravel lag deposit	Lower gravel	Late Oligocene
Unit D	Units A, B, C, and H1	Irregular and continuous topography	Variable amplitude with high frequency. Layered and chaotic	Embayed gravel beach and linear beach	Middle gravel	Early to mid-Miocene
Unit E	Units A, B, C, D, E, and H1	Irregular and continuous topography	Variable amplitude with high frequency. Layered and chaotic	Embayed gravel beach and linear beach	Upper gravel	Pilo-Pleistocene
Unit F	Units A, B, C, D, E, and H1	Capping Stratigraphy		Shoreface	Mixed	Holocene

Figure. 5.8. Drill core screens showing a) Saprolite b) Mudballs c-d) Sandstone tubes formed by reef-building tubeworms, *Diplochaetetes longitubus*. e) Traces of of *Diplochaetetes longitubus* bioturbation in sandstone. f) Lower gravel beach material. g) Middle gravel beach material with abundant banded ironstone clasts. h) Upper gravel beach material containing shell hash and finer gravels.

Chapter 6: Discussion

The stratigraphy offshore Saddle Hill displays a diverse assemblage of Quaternary sand, gravel and mud deposited in shallow bathymetric lows carved into weathered bedrock (H1-Green et al., 2024). To the southeast, the stratigraphy is more complex, comprising a sequence of unusually stacked barrier beach units that rest atop a topographically variable bedrock and weathered bedrock surface, interposed with pinnacles of sandstone. To the southwest, the sequences preserved are significantly thinner, and almost exclusively housed within a dendritically-arranged series of topographic low points.

6.1 Interpretation of units

6.1.1 H1: Regional scale subaerial unconformity

H1 is interpreted as a regional scale subaerial unconformity that carved into the uplifted mid Neoproterozoic basement rocks that frame the inner shelf (Rund et al 2019, Kirkpatrick et al., 2019; Green et al., 2024). H1 truncates the schists, quartzites and sandstones (Fig. 5.3-5.5), and is lined by a thin layer of weathered and reworked regolith comprising clay and rolled mudballs, often juxtaposed with saprolite (Fig. 5.8). Atop this surface, the unconsolidated succession rests. The occurrence of *Diplochaetetes longitubus* (Pickford and Senut, 2002) in the Unit B sandstone, truncated by the subaerial unconformity, restricts the age of H1 to early Eocene or younger.

During the lowstands of the early Paleogene, the acoustic basement of Unit A was first exhumed and exposed to subaerial processes (Baby et al., 2018; Green et al., 2024). This surface is interpreted to represent a subaerial unconformity which was further excavated during later sea level regressions during the late Oligocene (Green et al., 2024). Figure 6.1 provides an outline of the palaeo-fluvial courses (incised valleys) of the area, with several sheltered pockets of accommodation to landward. It appears that when submerged, the main H1 depression and older fluvial conduits likely acted as a strait, framed by rocky coastline to both seaward and landward. Further seaward, the dendritic depressions are valleys incised into H1 (Meltzer, 2023; Green et al., in review-Appendix 2).

6.1.2 Unit B: Sandstone

The Eocene sandstones of Unit B (Pickford and Senut, 2002) were deposited during an early Eocene sea level high which subsequently caused shallow marine flooding of the proto-H1 depression. The sandstone distribution is almost entirely restricted to the shallow basin formed between the eastern and western ridge (Fig. 5.6b).

6.1.3 Unit C: Lowermost Gravel Unit

The lower gravel unit consists mainly of angular schist cobbles and pebbles, with some sub rounded quartzite cobbles, vein quartz clasts and pebbles of Karoo sandstones. These clast assemblages match those of the Pre-Proto and Proto Orange River gravels and are associated with an end of Eocene to Mid-Oligocene age incision of the Orange River (Jacob et al., 1999; Nakashole et al., 2018). This explains to some degree the remnants of these gravels in the dendritic, channel like features of H1, where the gravels likely comprise the basal lowstand component to the valley fills (Zaitlin et al., 1994; Nordfjord et al., 2006).

The thickest accumulation of this unit on the inner shelf is in the rock-bound and submerged embayment to landward. This is located on a flat bedrock platform within the embayed zone of accommodation sheltered from fluvial processes (Fig. 6.1). Here the lower gravels form a northward thinning elongate finger of material attached to an ~ 10 m-high raised bedrock platform (Fig. 5.6c). The morphology of the deposit resembles several examples of modern, swell-dominated embayed gravel beaches (Buscombe and Masselink, 2006; Loureiro et al., 2009) and its internal structure is comparable to prograding beach sequences in microtidal, high wave energy environments (Massari and Parea, 1988; Neal et al., 2002). When compared to strait-margin gravel beaches and shorefaces, the general internal geometry and lithology of Unit C compares well with Zones 1 and 2 (Backshore and Intertidal) (Frey and Dashtgard, 2011). The flat-lying reflections are interpreted as a back beach facies, with the steeper, seaward dipping packages representing the foreshore/swash zone. Similar internal structures are reported for the foreshore and spit platforms of raised Plio-Pleistocene barrier spits from the Oranjemund coastline (Spaggiari and Bordy, 2023), however these spits are significantly narrower (< 500 m-wide) when compared to the ~ 2 km width of Unit C.

6.1.4 Unit D: Middle Gravel Unit

Unit D comprises rounded pebbles and cobbles of vein quartz together with clasts of banded ironstone, indicative of the Plio-Pleistocene age Meso Orange River gravels. The shallowly seaward dipping reflections of the unit are again similar to those of the backshore for strait-margin gravel beaches, interposed with the more steeply seaward dipping foreshore sets (Massari and Parea, 1988; Frey and Dashtgard, 2011). The aggradational component of the unit may be related to the limited accommodation provided in the embayment, coupled to stable sea levels causing normal regression (the prograding foreshore reflections) and the eventual progradation out of the embayment into the strait (Fig. 5.6). This has resulted in a linear, coast-parallel extension of the gravels for 3.5 km.

The general morphology and thickness of this linear extension is similar to the linear beaches recognised by Spaggiari et al., 2006). Mature linear beaches are characterised by seaward-dipping foresets attributed to seaward-prograding gravel sheets comprising disc assemblages that get progressively coarser up-section

(Bluck and Spaggiari, 2001) (Fig. 6.2). The absence of fines to landward supports the idea of a beach as opposed to barrier spit where clays and silts are found juxtaposed to landward and then stacked in a transgressive manner (e.g. Runds et al., 2019; Spaggiari and Bordy, 2023). This is further reenforced by the absence of landward dipping reflections that would represent washover events (e.g. the spit recurve facies of Spaggiari and Bordy, or the interbedded washover gravel-sand associations of modern barrier lagoons-Green et al., 2019).

According to Spaggiari and Bordy. (2023), during the Plio-Pleistocene uplift or forced regression caused a flushing out of large clasts up to boulder size into the Atlantic Ocean. It was this sediment, brought by the Orange River that supplied the palaeo-beaches of the late Pliocene to the Holocene along southern Namibia, including Unit Cs embayed and linear beaches.

6.1.5 Unit E: Upper Gravel Unit

Unit E comprises variable mixtures of locally derived angular clasts, reworked local marine sandstones (*Diplochaetetes longitubus* hosting) and well-rounded, fluvially-introduced exotic quartzites. A significant amount of shell content is also apparent. The unit distribution (Fig. 5.6d and e) mirrors that of the middle gravel but with a slight extension seaward. The general backstepping nature of the unit suggests that it initiated at a depth of ~ 70 m and has undergone partial overstepping and rollover (Pretorius et al., 2016). The general seaward dips of the reflections point to deposition along a gravel beach foreshore (Fig. 6.2) that has migrated landward and survived shoreface and beachface ravinement.

When compared to the middle gravel unit, the clasts of the upper gravel are better rounded, indicating a prolonged history of reworking and redistribution, likely in the lower foreshore (Spaggiari et al., 1999). Though ~ 250 km away, cores from the uppermost gravels in a submerged gravel barrier revealed similar clast assemblages, and dates from insitu *Choromytilus meridionalis* and *Tellina trilatera* returned a time of deposition of between 10.5 and 10.2 cal. Ka BP (Kirkpatrick et al., 2019). The upper portions of this unit are thus considered Holocene and related to the Holocene transgression.

6.1.6 WRS

Sub-bottom profiles reveal a distinctive high amplitude surface that caps the gravels of the Holocene. This is interpreted as a scour surface incised by high to moderate energy waves in the upper shoreface during rapid sea level and subsequent transgression (Catuneanu et al., 2011; Runds et al., 2019). A series of cores retrieved from the main H1 depression (Compton et al., 2001) intersected the upper gravel succession and dated it to 10.23 cal Ka BP, confirming this surface as the most recent wave ravinement.

6.1.7 Unit F: Younger unconsolidated sediment

Unit F caps the WRS, except where the acoustic basement crops out. According to Swift, (1968) during the erosional processes of wave ravinement, material is stripped from the upper shoreface and deposited down-profile where they accumulate to form the modern shelf sediment cover. The variation in hydrodynamic regime, as driven by the geological controls of the two main bedrock ridges transgression has given rise to the fractionation of the seabed sediments into bedrock-proximal gravels (with greater turbulent winnowing), and a proximal sand sheet where geological controls are less pronounced (Fig. 5.1) (Green et al., 2024).

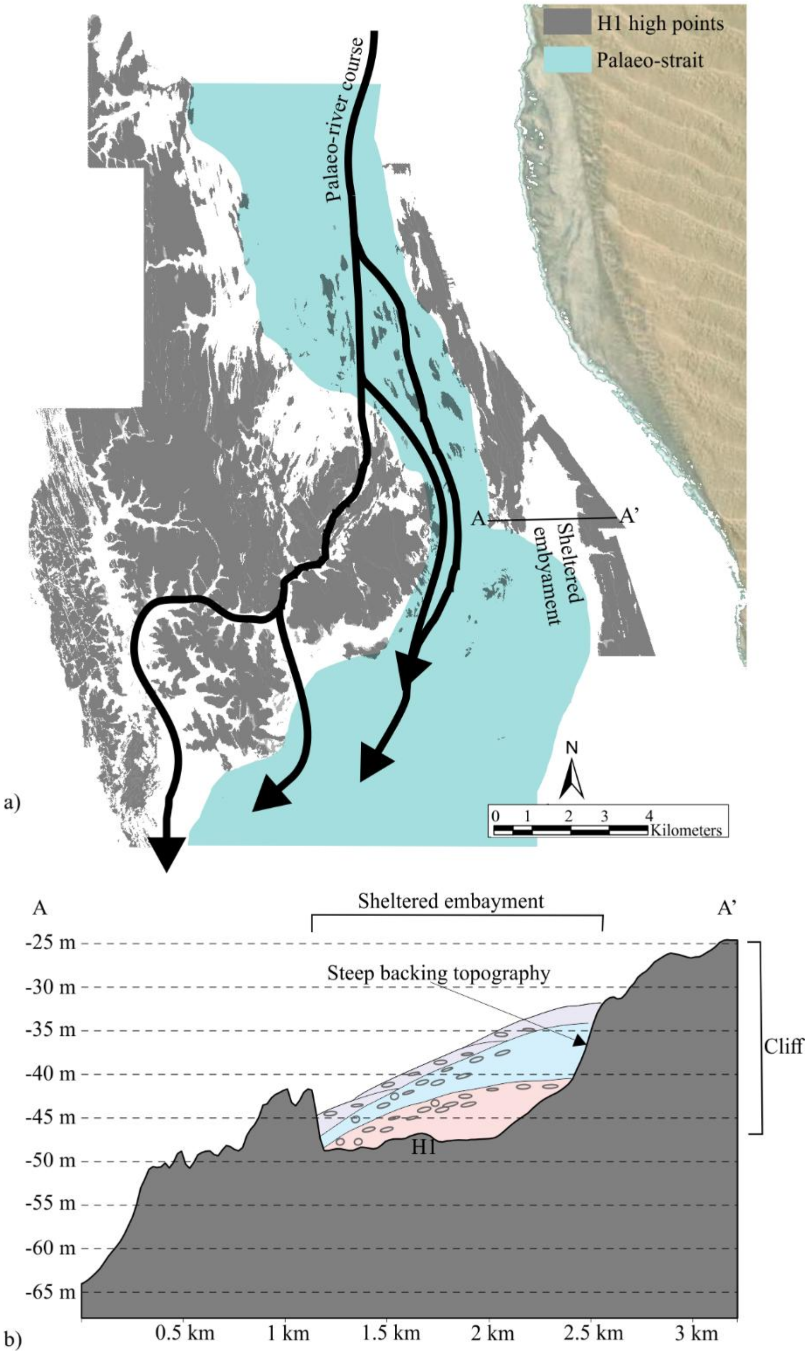

Figure. 6.1. Palaeodrainage. a. Low points in the H1 surface where fluvial courses were likely to have followed. When water levels were ~ -70 to -65 m, a bedrock-framed strait is apparent. b. cross section through the sheltered embayment demonstrating the steep backing topography and preferential accommodation. Schematic stacking pattern of Units C-E shown.

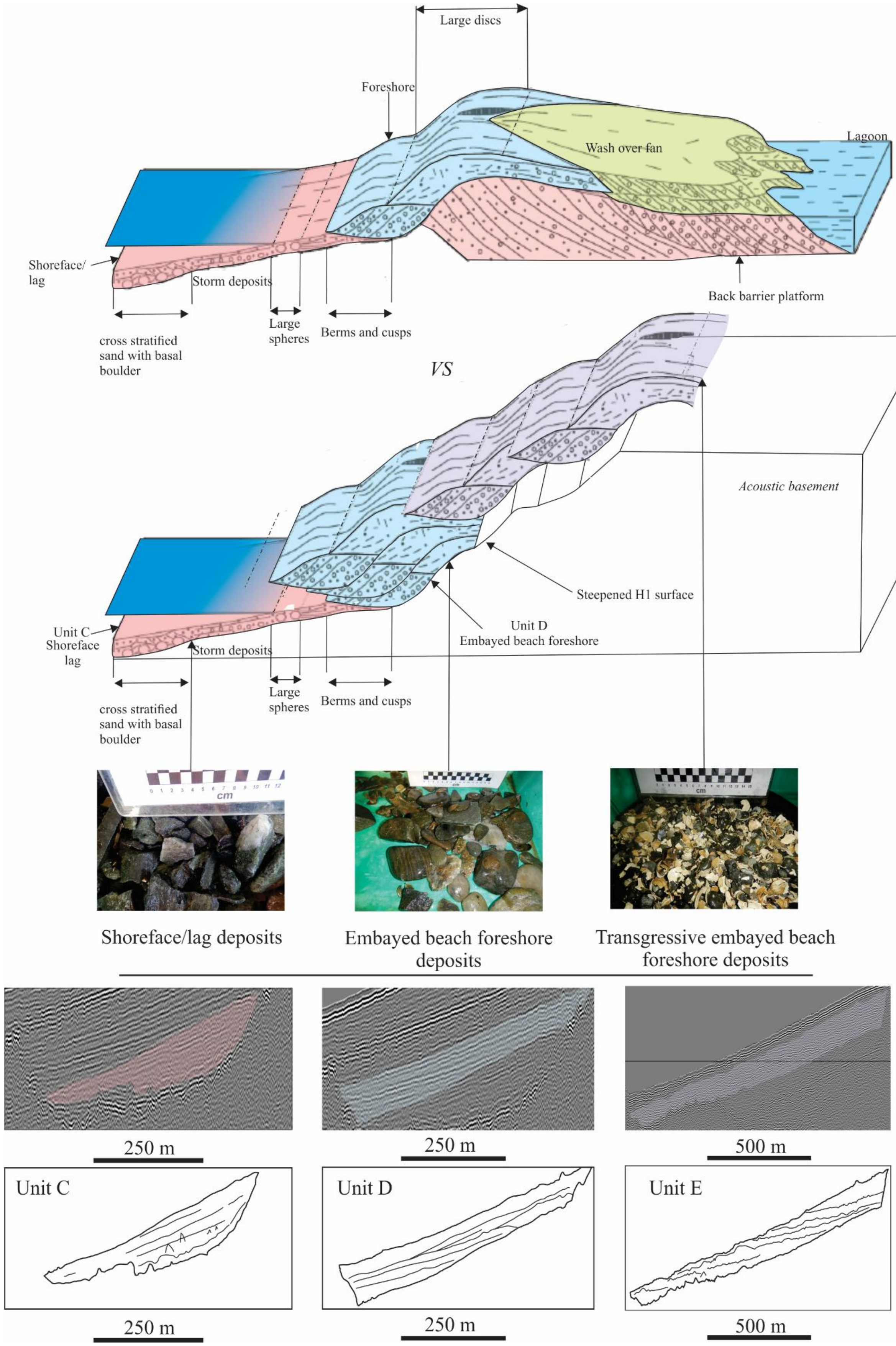

Figure. 6.2. Schematic representing the various depositional environment of a barrier beach (after Spaggiari et al., 2006), compared to the stratigraphic/seismic architecture and lithology of the stacked gravel beaches of Hottentot’s Bay.

6.2 Submerged gravel beach evolution on the inner shelf

The formation and preservation of coastal sequences are influenced by several factors such as tidal and wave processes, sea-level fluctuations, antecedent geology, and sediment supply (Catuneanu, 2006; Spaggiari, 2011; Runds et al., 2019; Green et al., 2024). The southern Namibian shelf is known to be one of the most energetic shelf environments in the world, with a significant degree of sediment bypass associated with uplift of the hinterland during the Late Cretaceous to early Cenozoic (Bluck et el., 2007). For this reason, there has been little subsidence-induced accommodation space available in the inner shelf. Much of the sediment accumulation has been influenced by antecedent controls of the shallow bedrock framework, the long-lasting wave energy, and the allocyclic controls of sea level and hinterland denudation.

Lowstands of the Miocene to Pleistocene promoted the transport and deposition of gravels by the Orange River, onto an inner shelf dominated by waves and sand bypassing (Green et al., 2024). The gravels have thus subsequently become concentrated, with repeated regressive/ transgressive cycles over the Pleistocene creating merged gravel bodies that on the southern Namibian shelf, are difficult to distinguish from each other (Kirkpatrick, Green, et al., 2019). The distribution of gravel in the study area reflects an initial thin blanketing of Pre-Proto and Proto-Orange gravels of end Eocene to late Oligocene age. These correspond well with the assumed late Oligocene age of the underlying H1 surface (Green et al., 2024). Their occurrence in the dendritic channels to seaward possibly relates to the development of lowstand channel lags (cf. Nordfjord et al., 2006) and the preferential accommodation offered by the channel forms. Elsewhere, the thin cover of Proto-Orange gravel is likely related to gravel dispersion by the long-prevailing energetic littoral processes (Bluck et al., 2007) coupled to the shallow bedrock-controlled accommodation of H1.

One of the few areas where abundant accommodation existed was in the rocky embayment formed in the western bedrock ridge. No fluvial paths can be traced through the embayment; therefore, subaerial erosion of the deposits was likely limited (Fig. fluvial courses). Further, the steep backing topography in the bedrock created a backstop for barrier-beach rollover following the rising sea levels of the Miocene (Fig. 6.3). The initial pulses of gravel to the area could thus be reworked and stored in this repository forming an embayed gravel beach, fronted by a strait to seaward.

The second pulse of gravel deposition, Unit D, likewise blanketed the shelf and exploited low points that were not completely filled by the previous gravel pulse. Figure 5.6d shows that much of the remaining accommodation in the bedrock embayment was filled, and that the gravels prograded and were entrained into the strait. There they were subjected to wave action and littoral drift processes, causing a northward extension of the gravel body which remained pinned against the linear portion of the western ridge to form a linear beach (e.g. Spaggiari et al., 2006). The final gravel pulse caused a similar pattern to emerge, but with a significantly thicker accumulation of material in the embayment (Fig. 5.6e). The composite linear beach that formed is of a similar internal structure and morphology to zones A and B of Spaggiari et al.'s (2006) model (Fig. 6.2).

The linear beaches along the exposed mid-inner shelf of the area were ultimately preserved due to two main reasons. 1) the thick gravel accumulation of up to 10 m of cobbles and pebbles has a substantial inertia to overcome by wave base reworking during transgression (e.g. Cooper et al., 2018). 2) the Holocene material was overstepped by the punctuated rises in sea level of the Holocene (e.g. Green et al., 2014) (Fig. 6.3). The seaward depth of the youngest gravel beach (~70 m) matches a period of very slowly rising sea level preceding MWP-1B (Fig. 6.3), allowing the beach to prograde (as seen in the sub bottom data-Fig. 5.3). This phase of progradation was followed by MWP-1B where a subsequent rapid rise in sea level from -58 to -40 m occurred between 11.5 and 11.2 cal Ka BP (Runds et al., 2019).

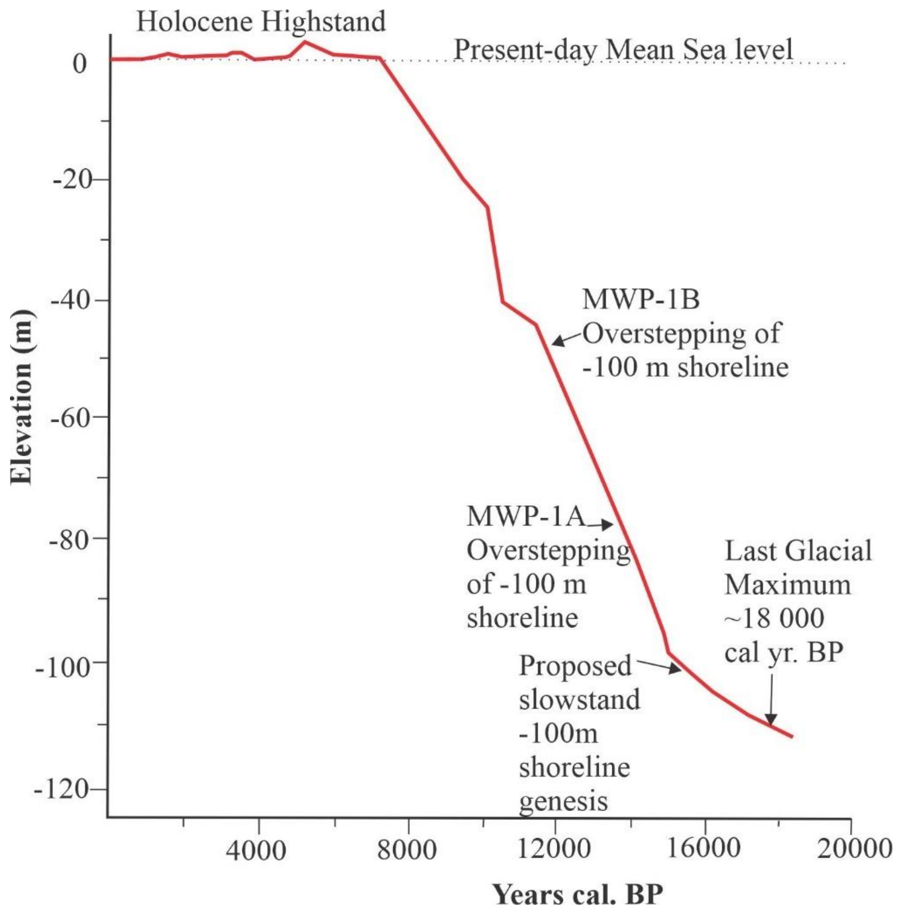

Figure. 6. 3. Regional sea-level curve for southern Africa (Adapted from Cooper et al., 2018).

Runds et al. (2019) and Kirkpatrick et al. (2019) describe the development of gravel beaches offshore the Oranjemund area of southern Namibia. The southernmost examples were considered to be wave-sheltered, with steeply dipping foresets to both landward and seaward, and with beach accretion at its maximum and sediment supply coarsest due to the proximity to the Orange River mouth (Kirkpatrick et al., 2019). When compared to the more northern examples, the beaches had no lagoonal components to landward and thus differed fundamentally from the barrier spit examples recognised onshore by Spaggiari et al. (2006) and offshore by Runds et al. (2019).

The submerged gravel beaches offshore Hottentot's Bay displays a combination of the southern submerged beaches of Kirkpatrick et al. (2019), with the inner-shelf being wave-sheltered by the eastern ridge and protected by the embayment. Likewise, the steep backing topography limited accommodation for any back barrier environments to form, and instead gravel aggradation of multi-stacked beaches has occurred. Cooper et al. (2016), attributed the preservation of overstepped sandy barriers to wave-sheltered locations, rapid sea-level rise and rapid burial of shoreface sediments, giving rise to aggradation.

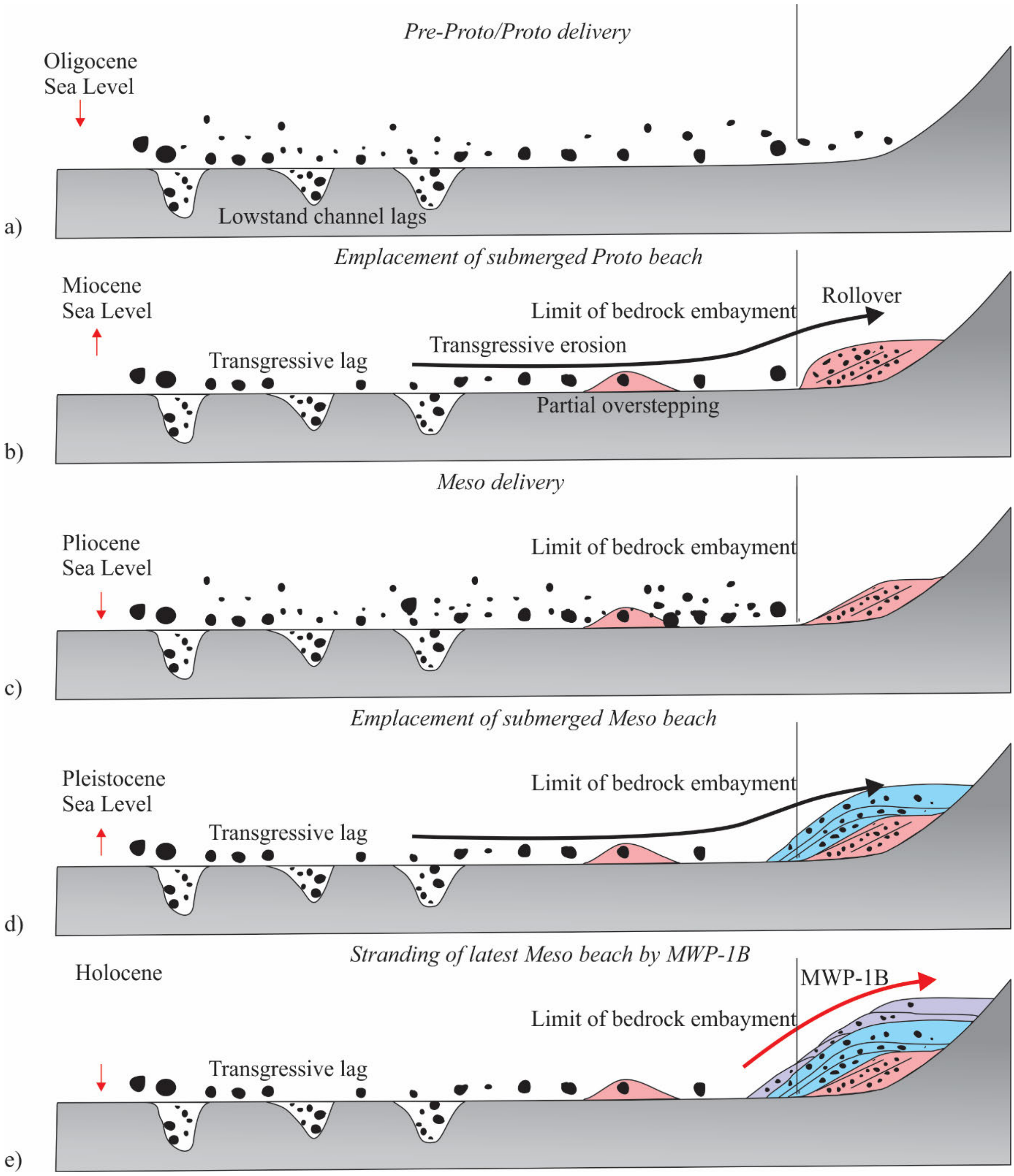

Figure. 6.4. Conceptual model of gravel stacking and development of the Units C-E.

Geological summary:

a) Gravel fills valleys of the dendritic depressions in H1 during the Oligocene phase of gravel delivery.

b) Relative sea-level rise of the Miocene produces a shelf-wide lag of gravel (Unit C), and stacks Unit D gravels into an aggradational/progradational deposit in the available accommodation of the bedrock embayment via rollover. Sporadic deposits are left behind as partially overstepped gravel shorelines.

c) Pliocene relative sea-level fall delivers Meso-Orange gravels.

d) Pleistocene rise and fall in relative sea level produces a lag on the shelf of mixed Proto and Meso components. Another phase of aggradation and progradation occurs of a second stacked gravel beach in the embayment (Unit D). This progrades out of the embayment to form a linear beach along the eastern part of the rocky strait.

e) Holocene transgression causes a retrogradational stacking on top of the older gravel units which is preserved by overstepping due to MWP-1B, in addition to the deposit inertia and anchoring point in the antecedent topography.

Chapter 7: Conclusion

The southern Namibian shelf, one of the most energetic shelf environments globally, experienced significant sediment bypass due to hinterland uplift during the Late Cretaceous to early Cenozoic. Subsidence-induced accommodation was thus limited leading to sediment accumulation predominantly controlled by the shallow bedrock framework, persistent wave energy, and cyclical sea-level changes.

Using a pseudo 3D grid of ultra-high resolution sub bottom profiles, and several thousand boreholes, the morphology of palaeo-land surface (H1) over which the unconsolidated materials of the shelf now lie was reconstructed. H1 comprises a weathered bedrock surface, lined with a thin veneer of saprolite or clay, which in turn is mantled by Eocene-age sandstones. The overlying unconsolidated sediment comprised four seismic and lithostratigraphic units (C-F). The lowermost gravel Units C and D were delivered to H1 in several pulses corresponding to the late Oligocene, early to mid-Miocene and late Pliocene/Pleistocene. These formed widespread deposits that, over multiple phases of regression and transgression formed lowstand lags in small channels of the inner shelf edge, and a thickly developed embayed beach on the innermost shelf. The bedrock-hosted embayment in which the beaches developed fronted a rock-bound strait and provided preferential accommodation for multi-stacked gravel beaches. These contrast with the barrier spit and back barrier sequence preserved to the south, closer to the Orange River and indicate a limited accommodation and depositing surface that was too steep to form lagoonal back barrier conditions.

Once the embayed accommodation was filled, material spilled out into the strait and formed linear beaches subject to littoral drift, anchored to landward by a bedrock high. These linear gravel beaches, with their significant resistance against wave reworking have remained preserved due to overstepping. This was promoted by the coarse grain sizes, and stepped rises in sea level, notably MWP-1B of the Holocene.

It is strongly recommended that further sampling for dateable material be undertaken, so as to better constrain the age of formation of each gravel beach. This should encompass Optical Stimultaed Luminescence dating on the sandier unconsolidated sediments, together with dating of the whole shell gravels by radiocarbon means. Further suvryeing to the south of the study area would allow the beach morphology to be inspected at the regional scale, and linked to modern day littoral processes.

References

Aizawa, M., Bluck, B., Cartwright, J., Milner, S., Swart, R., Ward, J., 2000. Constraints on the geomorphological evolution of Namibia from the offshore stratigraphic record. Communications of the Geological Survey of Namibia 12, 337-346.

Allen, G.P., Posamentier, H.W., 1993. Sequence stratigraphy and facies model of an incised valley fill; the Gironde Estuary, France. Journal of Sedimentary Research 63, 378-391.

Apollus, L., 1995. The distribution of diamonds on a late Cainozoic gravel beach, southwestern Namibia. University of Glasgow (United Kingdom).

Armentrout, J.M., Perkins, B.F., 1991. Sequence stratigraphy as an Exploration tool: Concepts and practices in the Gulf Coast. SEPM Society for Sedimentary Geology.

Baby, G., Guillocheau, F., Morin, J., Ressouche, J., Robin, C., Broucke, O., Dall'Asta, M., 2018. Post-rift stratigraphic evolution of the Atlantic margin of Namibia and South Africa: Implications for the vertical movements of the margin and the uplift history of the South African Plateau. Marine and Petroleum Geology 97, 169-191.

Bellefleur, G., Malinowski, M., Urosevic, M., 2019. Editorial for special issue “seismic methods in mineral exploration”. MDPI, p. 630.

Blanchon, P., Shaw, J., 1995. Reef drowning during the last deglaciation: evidence for catastrophic sea-level rise and ice-sheet collapse. Geology 23, 4-8.

Bluck, B.J., 1998. Clast assembling, bed-forms and structure in gravel beaches. Earth and Environmental Science Transactions of the Royal Society of Edinburgh 89, 291-323.

Bluck, B.J., Ward, J., Cartwright, J., Swart, R., 2007. The Orange River, southern Africa: an extreme example of a wave-dominated sediment dispersal system in the South Atlantic Ocean. Journal of the Geological Society 164, 341-351.
Bluck, B.J., Ward, J., De Wit, M., 2005. Diamond mega-placers: southern Africa and the Kaapvaal craton in a global context. Geological Society, London, Special Publications 248, 213-245.

Bluck, B.J., 1967. Sedimentation of beach gravels; examples from South Wales. Journal of Sedimentary Research 37, 128-156.

Bluck, B.J., Ward, J.D., Spaggiari, R., 2001. Gravel beaches of southern Namibia. Westbury Academic and Scientific Publishing, Otley, West Yorkshire, U.K.

Boggs, S., 2006. Principles of sedimentology and stratigraphy. Pearson Prentice Hall Upper Saddle River, NJ.

Buscombe, D., Masselink, G., 2006. Concepts in gravel beach dynamics. Earth-science reviews 79, 33-52.

Carter, R.W.G., 1988. Coastal Environments: An Introduction to the Physical, Ecological and Cultural Systems of Coastlines. Elsevier, London.

Carter, R.W.G., 2013. Coastal environments: an introduction to the physical, ecological, and cultural systems of coastlines. Elsevier.

Catuneanu, O., 2006. Principles of Sequence Stratigraphy. Elsevier.

Catuneanu, O., 2022. Principles of sequence stratigraphy. Newnes.

Catuneanu, O., Galloway, W.E., Kendall, C.G.S.C., Miall, A.D., Posamentier, H.W., Strasser, A., Tucker, M.E., 2011. Sequence stratigraphy: methodology and nomenclature. Newsletters on stratigraphy 44, 173-245.

Clemson, J., Cartwright, J., Booth, J., 1997. Structural segmentation and the influence of basement structure on the Namibian passive margin. Journal of the Geological Society 154, 477-482.

Clemson, J., Cartwright, J., Swart, R., 1999. The Namib Rift: a rift system of possible Karoo age, offshore Namibia. Geological Society, London, Special Publications 153, 381-402.
Compton, J., Harris, C., Thompson, S., 2001. Pleistocene dolomite from the Namibian Shelf: High 87Sr/86Sr and δ18O values indicate an evaporative, mixed-water origin. Journal of Sedimentary Research 71, 800-808.

Cooper, J.A.G., 2001. Geomorphological variability among microtidal estuaries from the wave-dominated South African coast. Geomorphology 40, 99-122.

Cooper, J.A.G., 2002. The role of extreme floods in estuary-coastal behaviour: contrasts between river-and tide-dominated microtidal estuaries. Sedimentary Geology 150, 123-137.

Cooper, J.A.G., Green, A., Meireles, R.P., Klein, A.H., Souza, J., Toldo, E.E., 2016. Sandy barrier overstepping and preservation linked to rapid sea level rise and geological setting. Marine geology 382, 80-91.

Cooper, J.A.G., Green, A., Smith, A., 2013. Vertical stacking of multiple highstand shoreline deposits from the Cretaceous to the present: facies development and preservation. Journal of Coastal Research, 1904-1908.

Cooper, J.A.G., Green, A.N., 2023. Southern African sandy coasts in the context of near-future sea-level rise. Transactions of the Royal Society of South Africa 78, 149-166.

Cooper, J.A.G., 1993. Sedimentation in the cliff-bound, microtidal Mtamvuna Estuary, South Africa. Marine geology 112, 237-256.

Cooper, J.A.G., Green, A.N., Loureiro, C., 2018. Geological constraints on mesoscale coastal barrier behaviour. Global and Planetary Change 168, 15-34.

Cooper, J.A.G., Masselink, G., Coco, G., Short, A.D., Castelle, B., Rogers, K., Anthony, E., Green, A.N., Kelley, J.T., Pilkey, O.H., 2020. Sandy beaches can survive sea-level rise. Nature climate change 10, 993-995.

Corbett, I., 1993. The modern and ancient pattern of sandflow through the southern Namib deflation basin. Aeolian Sediments: Ancient and Modern, 45-60.
Cross, T.A., Lessenger, M.A., 1988. Seismic stratigraphy. Annual review of earth and planetary sciences 16, 319-354.

Dalrymple, R.W., Boyd, R., Zaitlin, B.A., 1994. History of research, types and internal organisation of incised-valley systems: introduction to the volume.

Dalrymple, R.W., Knight, R.J., Zaitlin, B.A., Middleton, G.V., 1990. Dynamics and facies model of a macrotidal sand-bar complex, Cobequid Bay—Salmon River Estuary (Bay of Fundy). Sedimentology 37, 577-612.

Dalrymple, R.W., Zaitlin, B.A., Boyd, R., 1992. Estuarine facies models; conceptual basis and stratigraphic implications. Journal of Sedimentary Research 62, 1130-1146.

Davis, R.J., 2012. Coastal sedimentary environments. Springer Science & Business Media.

De Decker, R., 1988. The wave regime on the inner shelf south of the Orange River and its implications for sediment transport. South African Journal of Geology 91, 358-371.

Dingle, R., Scrutton, R., 1974. Continental breakup and the development of post-Paleozoic sedimentary basins around southern Africa. Geological Society of America Bulletin 85, 1467-1474.

Dingle, R.V., Siesser, W.G., Newton, A.R., 1983. Mesozoic and Tertiary geology of southern Africa.

Duncan, C.S., Goff, J.A., Austin Jr, J.A., Fulthorpe, C.S., 2000. Tracking the last sea-level cycle: seafloor morphology and shallow stratigraphy of the latest Quaternary New Jersey middle continental shelf. Marine geology 170, 395-421.

Foyle, A.M., Oertel, G.F., 1997. Transgressive systems tract development and incised-valley fills within a Quaternary estuary-shelf system: Virginia inner shelf, USA. Marine geology 137, 227-249.

Frey, S.E., Dashtgard, S.E., 2011. Sedimentology, ichnology and hydrodynamics of strait-margin, sand and gravel beaches and shorefaces: Juan de Fuca Strait, British Columbia, Canada. Sedimentology 58, 1326-1346.

Green, A.N., Cooper, J.A.G, Loureiro, C., Dixon, S., Hahn, A., Zabel, M., 2022. Stormier mid-Holocene southwest Indian Ocean due to poleward trending tropical cyclones. Nature Geoscience 15, 60-66.

Green, A.N., Cooper, J.A.G., Salzmann, L., 2014. Geomorphic and stratigraphic signals of postglacial meltwater pulses on continental shelves. Geology 42, 151-154.

Green, A.N., Cooper, J.A.G., Salzmann, L., 2018. The role of shelf morphology and antecedent setting in the preservation of palaeo-shoreline (beachrock and aeolianite) sequences: The SE African shelf. Geo-Marine Letters 38, 5-18.

Green, A.N., Pillay, T., Cooper, J.A.G., Guisado-Pintado, E., 2019. Overwash-dominated stratigraphy of barriers with intermittent inlets. Earth Surface Processes and Landforms 44, 2097-2111.

Green, A.N., Senna, W., Cooper, J.A.G., Heeralal, T., Labuschagne, H., 2024. Antecedent bedrock control on the sediment-starved continental shelf of south/central Namibia. Marine geology, 107242.

Green, A.N., Uken, R., 2005. First observations of sea-level indicators related to glacial maxima at Sodwana Bay, northern KwaZulu-Natal: Research in action. South African Journal of Science 101, 236-238.

Gutierrez, B., Uchupi, E., Driscoll, N., Aubrey, D., 2003. Relative sea-level rise and the development of valley-fill and shallow-water sequences in Nantucket Sound, Massachusetts. Marine geology 193, 295-314.

Hallam, C., Haughton, S., 1964. The geology of the coastal diamond deposits of southern Africa. The Geology of Some Ore Deposits in Southern Africa, edited by: Haughton, SH 2, 671-729.

Hou, B., Keeling, J., Van Gosen, B.S., 2017. Geological and exploration models of beach placer deposits, integrated from case-studies of Southern Australia. Ore Geology Reviews 80, 437-459.

Hughes, M., Masselink, G., 2003. Introduction to coastal processes and geomorphology.
Jacob, J., 2001. Late Proterozoic bedrock geology and its influence on neogene littoral marine diamondiferous trapsites, MA1-Sperrgebiet, Namibia, Department of Geological Sciences University of Cape Town.

Jacob, R., Bluck, B.J., Ward, J., 1999. Tertiary-age diamondiferous fluid deposits of the lower Orange River valley, Southwest Africa. Economic Geology 94, 749-758.

Jacob, R.J., 2005. The erosional and Cainozoic depositional history of the Lower Orange River, southwestern Africa. University of Glasgow.

Kirkpatrick, L.H., Green, A.N., 2018. Antecedent geologic control on nearshore morphological development: the wave dominated, high sediment supply shoreface of southern Namibia. Marine geology 403, 34-47.

Kirkpatrick, L.H., Jacob, J., Green, A.N., 2019. Beaches and bedrock: How geological framework controls coastal morphology and the relative grade of a Southern Namibian diamond placer deposit. Ore Geology Reviews 107, 853-862.

Kirkpatrick, L.H., Green, A.N., Pether, J., 2019. The seismic stratigraphy of the inner shelf of southern Namibia: the development of an unusual nearshore shelf stratigraphy. Marine geology 408, 18-35.

Kirkpatrick, L., Green, A.N., 2021. Mapping diamondiferous palaeo-shorelines in complicated terrain: seismic and GIS-based methods from the inner shelf of southern Namibia. Geo-Marine Letters 41, 41.

Lericolais, G., Berné, S., Féniès, H., 2001. Seaward pinching out and internal stratigraphy of the Gironde incised valley on the shelf (Bay of Biscay). Marine geology 175, 183-197.

Li, C., Wang, P., Sun, H., Zhang, J., Fan, D., Deng, B., 2002. Late Quaternary incised-valley fill of the Yangtze delta (China): its stratigraphic framework and evolution. Sedimentary Geology 152, 133-158.

Light, M., Maslanyj, M., Greenwood, R., Banks, N., 1993. Seismic sequence stratigraphy and tectonics offshore Namibia. Geological Society, London, Special Publications 71, 163-191.

Locker, S.D., Hine, A.C., Tedesco, L.P., Shinn, E.A., 1996. Magnitude and timing of episodic sea-level rise during the last deglaciation. Geology 24, 827-830.

Long, A., Waller, M., Plater, A., 2006. Coastal resilience and late Holocene tidal inlet history: The evolution of Dungeness Foreland and the Romney Marsh depositional complex (UK). Geomorphology 82, 309-330.

Loureiro, C., Ferreira, O., Cooper, J., 2009. Contrasting morphologic behaviour at embayed beaches in Southern Portugal. Journal of Coastal Research, 83-87.

Malehmir, A., Durrheim, R., Bellefleur, G., Urosevic, M., Juhlin, C., White, D.J., Milkereit, B., Campbell, G., 2012. Seismic methods in mineral exploration and mine planning: A general overview of past and present case histories and a look into the future. Geophysics 77, WC173-WC190.

Massari, F., Parea, G., 1988. Progradational gravel beach sequences in a moderate-to high-energy, microtidal marine environment. Sedimentology 35, 881-913.

Matias, A., Williams, J.J., Masselink, G., Ferreira, Ó., 2012. Overwash threshold for gravel barriers. Coastal Engineering 63, 48-61.

Mellett, C.L., Hodgson, D.M., Lang, A., Mauz, B., Selby, I., Plater, A.J., 2012. Preservation of a drowned gravel barrier complex: A landscape evolution study from the north-eastern English Channel. Marine geology 315, 115-131.

Mitchum Jr, R., Vail, P., 1977. Seismic stratigraphy and global changes of sea level: Part 7. Seismic stratigraphic interpretation procedure: Section 2. Application of seismic reflection configuration to stratigraphic interpretation.

Myrick, R.M., Leopold, L.B., 1963. Hydraulic geometry of a small tidal estuary. US Government Printing Office.

Nakashole, A.N., Hodgson, D.M., Chapman, R.J., Morgan, D.J., Jacob, R.J., 2018. Long-term controls on continental-scale bedrock river terrace deposition from integrated clast and heavy mineral assemblage analysis: An example from the lower Orange River, Namibia. Sedimentary Geology 364, 103-120.

Neal, A., Pontee, N.I., Pye, K., Richards, J., 2002. Internal structure of mixed-sand-and-gravel beach deposits revealed using ground-penetrating radar. Sedimentology 49, 789-804.

Nichols, M.M., Biggs, RB, 1985. Coastal sedimentary environments. Springer-Verlag, New York.

Nordfjord, S., Goff, J., Austin Jr, J., Gulick, S., 2006. Seismic facies of incised-valley fills, New Jersey continental shelf: implications for erosion and preservation processes acting during latest Pleistocene–Holocene transgression. Journal of Sedimentary Research 76, 1284-1303.

Nummedal, D., Swift, D.J., 1987. Transgressive stratigraphy at sequence-bounding unconformities: some principles derived from Holocene and Cretaceous examples.

Oelofsen, A., 2008. Late cenozoic shallow marine diamond placers off the northern Sperrgebiet, Namibia.

Oosterveld, M., Campbell, D., Hazell, K., 1989. Geology related to statistical evaluation parameters for a diamondiferous beach deposit, International Journal of Rock Mechanics and Mining Sciences and Geomechanics Abstracts. Elsevier Science, pp. 74-74.

Payenberg, T.H., Boyd, R., Beaudoin, J., Ruming, K., Davies, S., Roberts, J., Lang, S.C., 2006. The filling of an incised valley by shelf dunes—an example from Hervey Bay, east coast of Australia.
Pickford, M., Senut, B., 2002. The fossil record of Namibia.

Pretorius, L., Green, A.N., Cooper, J.A.G., 2016. Submerged shoreline preservation and ravinement during rapid postglacial sea-level rise and subsequent "slowstand". Bulletin 128, 1059-1069.

Pretorius, L., Green, A.N., Cooper, J.AG., 2017. Submerged beachrock preservation in the context of wave ravinement. Geo-Marine Letters 38, 19-32.

Pretorius, L., Green, A.N., Cooper, J.A.G., Hahn, A., Zabel, M., 2019. Outer-to inner-shelf response to stepped sea-level rise: Insights from incised valleys and submerged shorelines. Marine geology 416, 105979.

Reddering, J.S.V., Esterhuysen, K., Rust, I.C., 1981. Sedimentation in the Sundays estuary. University of Port Elizabeth.

Reinson, G.E., 1984. Facies models. Geol. Assoc. Canada.

Rogers, J., 1977. Sedimentation on the continental margin off the Orange River and the Namib Desert.

Roksandić, M., 1978. Seismic facies analysis concepts. Geophysical prospecting 26, 383-398.

Roy, P., 1984. New South Wales estuaries: their origin and evolution. Coastal geomorphology in Australia.

Runds, M.J., Bordy, E.M., Pether, J., 2019. Late Quaternary sedimentological history of a submerged gravel barrier beach complex, southern Namibia. Geo-Marine Letters 39, 469-491.

Sangree, J., Widmier, J., 1977. Seismic stratigraphy and global changes of sea level: Part 9. Seismic interpretation of clastic depositional facies: Section 2. Application of seismic reflection configuration to stratigraphic interpretation.

Sangree, J., Widmier, J., 1979. Interpretation of depositional facies from seismic data. Geophysics 44, 131-160.

Spaggiari, R., Bluck, B.J., Ward, J., 1999. Beaches, barriers and bars: sedimentary facies of Early Pleistocene diamondiferous deposits within the Orange River mouth, Namibia, Abstract Volume. The Environmental Background to Hominid Evolution, XV International Congress, International Union for Quaternary Research, pp. 3-11.

Spaggiari, R., Bluck, B.J., Ward, J., 2006. Characteristics of diamondiferous Plio-Pleistocene littoral deposits within the palaeo-Orange River mouth, Namibia. Ore Geology Reviews 28, 475-492.

Spaggiari, R., 2011. Sedimentology of the Plio-Pleistocene gravel barrier deposits in the Palaeo-Orange River Mouth, Namibia: depositional history and diamond mineralisation. Rhodes University.

Spaggiari, R., Bordy, E.M., 2023. Anatomy of a diamondiferous gravel barrier spit at the palaeo-Orange River mouth, south-western Namibia. Sedimentology 70, 1630-1654.

Storms, J.E., Weltje, G.J., Terra, G.J., Cattaneo, A., Trincardi, F., 2008. Coastal dynamics under conditions of rapid sea-level rise: Late Pleistocene to Early Holocene evolution of barrier–lagoon systems on the northern Adriatic shelf (Italy). Quaternary Science Reviews 27, 1107-1123.

Swift, D.J., 1968. Coastal erosion and transgressive stratigraphy. The Journal of Geology 76, 444-456.

Thomas, M.A., Anderson, J.B., 1994. Sea-level controls on the facies architecture of the Trinity/Sabine incised-valley system, Texas continental shelf.

Thorne, J., Swift, D., 1991. Sedimentation on continental margins: VI. A regime model for depositional sequences, their component systems tracts, and bounding surfaces, Shelf sand and sandstone bodies: Geometry, facies and sequence stratigraphy. International Association of Sedimentologists Special Publications, pp. 189-255.

Vail, P.R., 1987. Seismic stratigraphy interpretation using sequence stratigraphy: Part 1: Seismic stratigraphy interpretation procedure.

Van Wagoner, J., 1990. Siliciclastic sequence stratigraphy in well logs, cores, and outcrops. Amer. Assoc. Petrol. Geol. Methods in Exploration Ser. 7, 1-55.

Van Wagoner, J., Mitchum Jr, R., Posamentier, H., Vail, P., 1987. Seismic stratigraphy interpretation using sequence stratigraphy: Part 2: Key definitions of sequence stratigraphy.

Vousdoukas, M.I., Ranasinghe, R., Mentaschi, L., Plomaritis, T.A., Athanasiou, P., Luijendijk, A., Feyen, L., 2020. Sandy coastlines under threat of erosion. Nature climate change 10, 260-263.

Warren, J.D., Bartek, L.R., 2002. The sequence stratigraphy of the East China Sea: Where are the incised valleys?

Weber, N., Chaumillon, E., Tesson, M., Garlan, T., 2004. Architecture and morphology of the outer segment of a mixed tide and wave-dominated-incised valley, revealed by HR seismic reflection profiling: the paleo-Charente River, France. Marine geology 207, 17-38.

Wells, J.T., 1995. Tide-dominated estuaries and tidal rivers, Developments in sedimentology. Elsevier, pp. 179-205.

Zaitlin, B.A., Dalrymple, R.W., Boyd, R., 1994. The stratigraphic organization of incised-valley systems associated with relative sea-level change.

Zecchin, M., Catuneanu, O., Caffau, M., 2019. Wave-ravinement surfaces: classification and key characteristics. Earth-science reviews 188, 210-239.

Appendix 1

Publication entitled "Antecedent controls of bedrock and shelf width dictate multiple cycles of geological inheritance on the central continental shelf of Namibia" by, Green, A.N., Senna, W., Cooper, J.A.G., Heeralal, T. and Labuschagne, H., 2024.

Marine Geology 469 (2024) 107242

Contents lists available at ScienceDirect

Marine Geology

journal homepage: www.elsevier.com/locate/margo

Antecedent bedrock control on the sediment-starved continental shelf of south/central Namibia

A.N. Green [a,b,*], W. Senna [c], J.A.G. Cooper [b,a], T. Heeralal [a,d], H. Labuschagne [d]

[a] Geological Sciences, University of KwaZulu-Natal, Westville, Private Bag X54001, South Africa
[b] School of Geography and Environmental Sciences, Ulster University, Coleraine BT52 1SA, Northern Ireland, UK
[c] Department of Earth and Environmental Sciences, University of Milano-Bicocca, Milano, Italy
[d] Trans Hex Marine (Pty) Ltd, 19 Chain Avenue, Montague Gardens, Cape Town 7441, South Africa

ARTICLE INFO

Editor: Michele Rebesco

Keywords:
Antecedent setting
Geological control
Inner shelf morphology
Seismic stratigraphy
Namib Sand Sea
Orange Delta

ABSTRACT

The Namibian inner continental shelf immediately north of the Orange River delta is sediment-poor, dominated by outcrop of metamorphic basement with a scarcity of sandy cover. Using a combination of high and very-high resolution geophysical tools and drill cores, an examination of the evolution of the inner shelf stratigraphy and geomorphology shows persistent antecedent bedrock controls throughout the Pleistocene.

The bedrock of the inner shelf comprises schists, in places overlain by Eocene sandstones, over which a subaerial unconformity (H1) formed in the late Oligocene. H1 was repeatedly re-occupied during succeeding transgressive/regressive cycles, creating a backstop for erosion/sedimentation and creating a repeating topography on which transgressions took place. Apart from localised development of Miocene phosphatic limestones, little sediment has since accumulated. Large-scale karst weathering of the limestones reflects several periods of subaerial exposure most recently during the Quaternary lowstands of sea level including MIS 2 and 1.

Thin Quaternary cover, housed within depressions on the H1 surface is predominantly preserved in the lee of bedrock ridges, behind which shallow and occasionally hypersaline lagoonal conditions developed. These preserved back-barrier sedimentary sequences developed post-MIS 5 (previous phases were either eroded/weathered or not deposited). Dolomite precipitation occurred when sea-level stabilised at −75 m 37,000 cal BP and restricted lagoonal conditions prevailed.

Currently, there are very limited MIS 2/1 deposits preserved above H1. The absence of thick sand cover, adjacent to and downdrift of the Orange River delta, suggests that the onshore diversion of sand that currently supplies the Namib Sand Sea also operated during lower sea levels, related to the bedrock control and lack of accommodation in surface H1. This persistent onshore diversion of sediment throughout the Quaternary has implications for sediment source as well as budget calculations for the Namib Sand Sea.

1. Introduction

The inner shelf of Namibia comprises a broad and mostly planar swath of seafloor, that with increasing distance north of the Orange River and its subaqueous delta (the main sediment delivery point), displays a systematic series of changes in the shelf geology and morphology. In the south, adjacent to the river mouth, the inner shelf comprises a submerged wave-dominated delta with accumulations of sediment up to 60 m-thick (Kirkpatrick et al., 2019a). Underlying bedrock controls on the inner shelf morphology become increasingly evident to the north. This is especially pronounced where sandy material from the Orange River, entrained in the littoral zone, is diverted onshore near Lüderitz to form the modern Namib Sand Sea (Corbett, 1993; Spaggiari et al., 2006) (Fig. 1) which, in turn, blocks potential fluvial inputs along 350 km of shoreline behind substantial coastal dunes (Compton et al., 2001).

Deprived of littoral sediment, the Namibian inner shelf north of Lüderitz presents a unique opportunity to examine the controlling effects of antecedent geological framework on the stratigraphy and geomorphology of the shelf (e.g. Lentz and Hapke, 2011; Schwab et al., 2014; Kirkpatrick and Green, 2018). Although shelf evolution is intertwined with evolving sea levels and changing rates of sediment supply, the relative balance between the three drivers (sea level, sediment supply and geology) can be examined and the evolutionary trajectory of

* Corrresponding author.
E-mail address: greena1@ukzn.ac.za (A.N. Green).

https://doi.org/10.1016/j.margeo.2024.107242
Received 18 August 2022; Received in revised form 12 February 2024; Accepted 13 February 2024
Available online 15 February 2024

the shelf revealed based on underlying preconditioning factors. Exposed rock strongly influences energy dispersion during wave ravinement (Aleman et al., 2015), with the palaeo-bathymetry modifying the wave regime (Riggs et al., 1995) and in turn, the evolving stratigraphy of the nearshore coastal system as it is drowned during transgression.

Despite the acknowledged importance of the role of antecedent and geological conditioning on shelf development, it is not well illustrated from the literature. Notable exceptions include studies from the continental shelf and coast of southern Namibia (Kirkpatrick and Green, 2018), SE Africa (Engelbrecht et al., 2022), Virginia (Shawler et al., 2021), North Carolina (Riggs et al., 1995), New Jersey (Hapke et al., 2010), and the Outer Hebrides of Scotland (Cooper et al., 2012). Using a combination of ultra-high resolution sub-bottom profiles, multibeam bathymetry and backscatter, in addition to over 1300 boreholes, we examine the development of the inner shelf offshore Saddle Hill, directly seaward of the Namib Sand Sea (Fig. 1). These data were collected primarily for marine diamond exploration by Trans Hex Marine (Pty) Ltd., however their density, resolution and location provide significant insight into the morphological and stratigraphic evolution of continental shelves in the context of inheritance of antecedent morphology and geological framework.

2. Regional setting

2.1. Physiography and offshore regional stratigraphy

The Namibian continental margin is a passive volcanic margin (Clemson et al., 1997; Gladczenko et al., 1997) with a wide shelf that extends up to 230 km offshore and a shelf break as deep as 500 m below sea level (Rogers, 1977; Dingle et al., 1983). The margin may be divided into four distinct morphological regions from the coast to seaward. The shallow areas are marked by a nearshore rocky platform to ~30 m

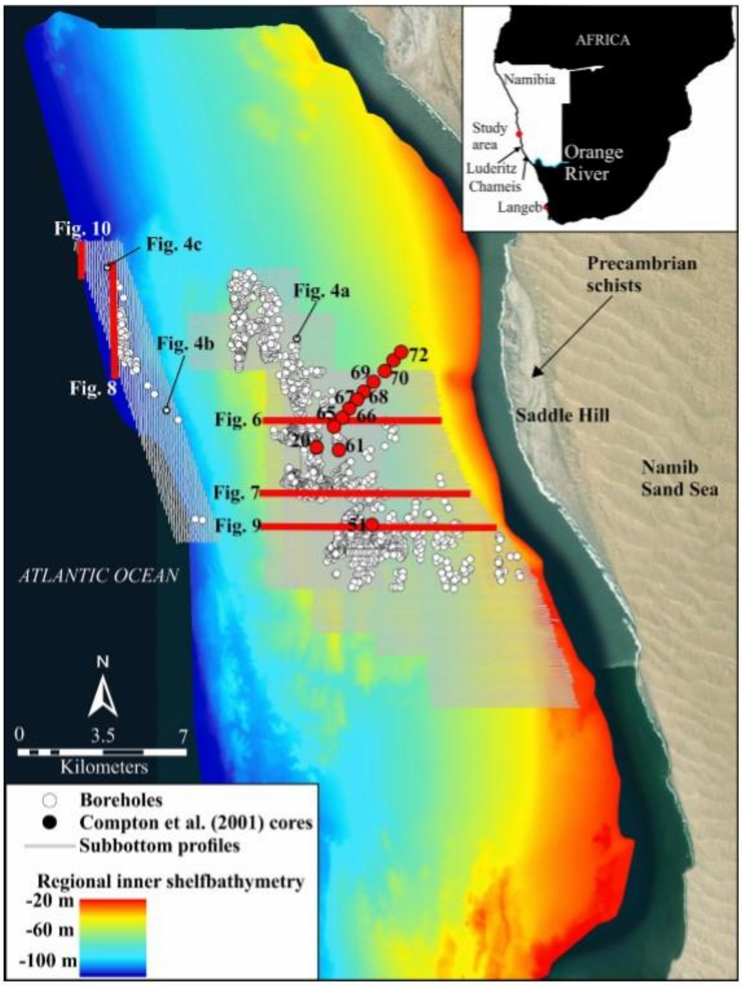

Fig. 1. Locality map of the study area offshore Saddle Hill, Namibia, outlining the regional bathymetry of the inner shelf. Grey lines denote the coverage by TOPAS sub-bottom profiles, white circles denote drill cores from this study, red circles denote vibracores from Compton et al. (2001). Red lines indicate specific seismic reflection profiles referred to in text. The locations of lithological samples in Fig. 4 are noted. In inset, Langeb. = Langebaan. (For interpretation of the references to colour in this figure legend, the reader is referred to the web version of this article.)

depth, with the inner shelf extending to an approximate depth of 130 m where a wave-cut terrace or notch marks the lowstand shoreline of the last glacial maximum (LGM) (Rogers, 1977). The outer shelf is a low gradient feature (<1°) that extends from depths of around 200 m to 500 m (Rogers, 1977; Bremner, 1978; Rogers and Rau, 2006). The inner shelf has a characteristic topographic profile marked by a step-like bedrock morphology, interpreted to represent wave-cut platforms and cliffs formed during sea-level still-stands (Hallam, 1964; Murray et al., 1970; Stocken, 1978; Jacob et al., 2006; Kirkpatrick and Green, 2021).

Precambrian basement schists of the Spencer Bay Formation are exposed in the nearshore and occasionally form the rocky headlands of large-scale crenulated coastal compartments. On the inner shelf these schists crop out, together with schists, phyllites and quartzites of the Gariep Belt, with a thin cover of Cenozoic successions to seaward. The latter are relatively thin, with only a few documented occurrences of Neogene-aged phosphatic limestones and stiff clays/claystones (Bremner, 1978; Compton and Bergh, 2016).

The Precambrian bedrock surface is marked by a gravel-rich basal bed that was formed by repeated reworking of shelf sediments as the shoreline migrated across the shelf in response to Cenozoic and Quaternary sea-level fluctuations (De Decker, 1986; Kirkpatrick et al., 2019a). Much of the shelf lacks a significant Quaternary cover, with occasional mud and sand depocenters up to 6 m-thick that overlie the bedrock or gravels (Compton et al., 2001).

2.2. *Sediment supply and coastal regime*

Since the break-up of Gondwana between ~180 and 130 Ma, several hundred thousand km^3 of rock were eroded from the Southern African sub-continent (Tinker et al., 2008; Guillocheau et al., 2012), with a maximum rate of accumulation in the Atlantic rift basin during the Upper Cretaceous (late Campanian), associated with a phase of hinterland uplift (Guillocheau et al., 2012) (Fig. 2a). Siesser and Dingle (1981) identified two further phases of hinterland uplift in the Lower Palaeocene and the Middle Oligocene (Fig. 2a). However, other authors recognise only one main pulse of uplift spanning 93.5 to 66.5 Ma that followed a phase of margin retrogradation 131–93.5 Ma (Baby et al., 2018). The shelf break, as reflected in the modern day, is a relic of the late Campanian uplift (Baby et al., 2018). This is superimposed by a late Oligocene unconformity formed by a less prominent phase of later uplift (Baby et al., 2018) within an overall prevailing phase of subsidence.

The Orange River, the principal conduit of sediment to the west coast of southern Africa, was established by the early Cretaceous (Dingle and Scrutton, 1974) and has drained the interior plateau of southern Africa since then (Dingle and Hendey, 1984; Aizawa et al., 2000; Bluck et al., 2007). Despite a reduction in the rate of sediment delivery to the margin in the Cenozoic (Guillocheau et al., 2012), the Orange River has continued to be the dominant sediment source to the southern Namibian coastline (Jacob, 2005). By the middle Eocene, it had entrenched its meandering form into the bedrock, fixing the mouth in approximately its present position (Jacob, 2005; Bluck et al., 2007; Kirkpatrick and Green, 2018) to form a subaqueous wave-dominated delta offshore the Orange River (Fig. 1).

At present, the river delivers a predominately finer-grained load to the inner shelf than in the past, comprising fine gravel, sand, silt, and clay (Bluck et al., 2007), the finer components supplying the littoral zone for over 1600 km to the north into southern Angola (Garzanti et al., 2018). Coarser materials are concentrated along the southern Namibian coast and shelf up to Chameis Bay (Spaggiari et al., 2006; Runds et al., 2019). Most sandy sediments are retained in the modern wave zone and directed towards the NW by a vigorous longshore drift and consistently high wave energy (Bluck et al., 2001, 2007) which has persisted since the middle to late Cenozoic (Spaggiari et al., 2006; Bluck et al., 2007). Wave refraction at headlands causes deposition of the sand in bays

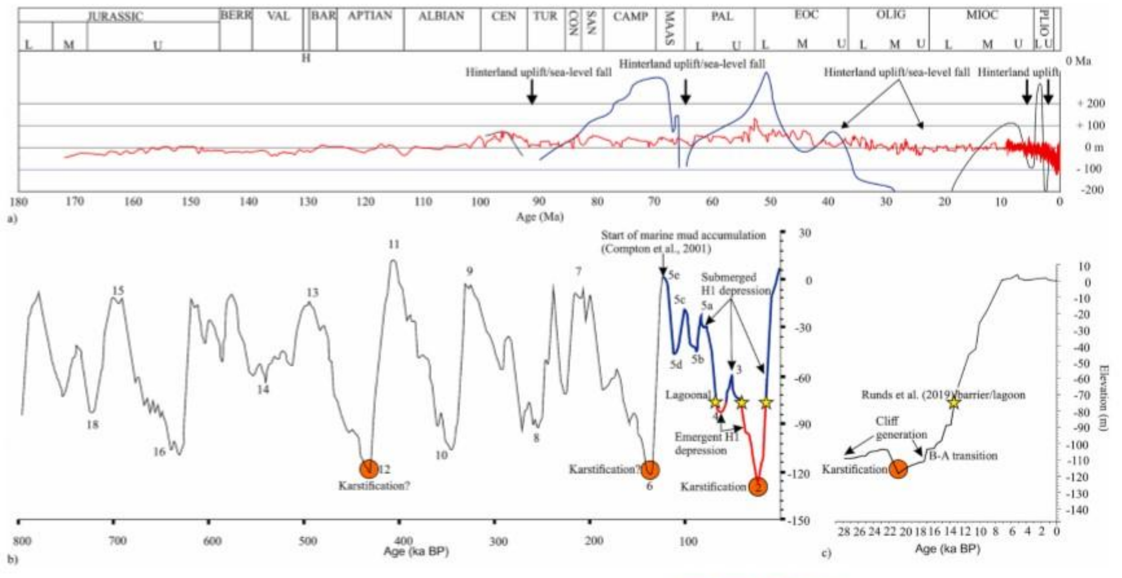

Fig. 2. Sea level curves a) the Middle Jurassic to present. Blue lines are sea level data presented by Siesser and Dingle (1981), detailing two phases of sea-level fall in the Lower Palaeocene and Oligocene. Phases of hinterland uplift and associated sea-level fall, as outlined by Baby et al. (2018), are marked by thick black arrows. The red line denotes the global sea level curve of Miller et al. (2015), however, little correlation exists between this and locally derived curves. b) the mid to late Pleistocene (from Spratt and Lisiecki, 2016), and b) the late Pleistocene to present (modified from Cooper et al., 2018 and Ishiwa et al., 2019). The curves in b) and c) outline periods of inner shelf exposure and possible karstification episodes (orange circles), together with submergence of the main erosional surface (H1) (blue lines) in the study area. Phases of lagoonal development are outlined by yellow stars. B-A = Bølling-Allerød. (For interpretation of the references to colour in this figure legend, the reader is referred to the web version of this article.)

(Corbett, 1993). At certain points associated with coastal inflection points, sand is returned onshore to contribute to the main Namib Desert Sand Sea (Lancaster and Ollier, 1983; Corbett, 1996; Bluck et al., 2007). The mud fraction delivered by the various rivers (most notably the Orange River), is transported by bottom waters to form an up to 15-m-thick Holocene-age mud belt along the inner to mid shelf between ~ − 50 m and − 140 m (Bremner, 1978; Compton and Bergh, 2016).

The gravel fraction conversely forms a series of Plio-Pleistocene-Holocene age narrow beaches, which in various forms, extend along the coast for thousands of kilometres north of the Orange River mouth (Bluck et al., 2001; Spaggiari et al., 2006) (Fig. 1). Raised diamondiferous gravel beaches are predominantly floored by siliciclastic rocks of the late Proterozoic that have been bevelled into a series of marine-cut platforms representative of various Quaternary high sea-level stands (Jacob et al., 2006; Kirkpatrick et al., 2019b).

2.3. Sea-level fluctuations

Throughout the Cretaceous period and up to the start of the Pleistocene, relative sea level was driven by tectonic processes (Siesser and Dingle, 1981). The pulses of hinterland uplift responsible for margin progradation (see sediment supply section) also contributed to relative sea-level lowstands (e.g. in the late Campanian-Baby et al., 2018) (Fig. 2a), though the magnitude of these is uncertain and not reflected in the global sea levels of Miller et al. (2005). Siesser and Dingle (1981) recognised phases of sea level fall in the Middle Oligocene, Upper Miocene and Upper Pliocene (Fig. 2a), and Baby et al. (2018) report an approximate 350 m sea level fall from the late Eocene highstand shoreline to seaward of the late Oligocene shelf break.

Sea-level fluctuations linked to glacio-eustasy have governed the prevailing energy over the shelf and have been the dominant controls on sediment distribution and stratigraphy for the past two million years (Pether et al., 2000; Rogers and Rau, 2006). During this time the inner shelf of the west coast of southern Africa has been influenced by multiple transgressive/regressive sea-level cycles (Fig. 2b). The most recent major sea-level low stand corresponds with the Last Glacial Maximum (LGM), when sea levels were ~ 120–130 m below those of the present ~22,000 BP (Spratt and Lisiecki, 2016). There is poor constraint on the timing of the shoreline occupation offshore Namibia and South Africa during the LGM; however, results from a similar far-field site, the Great Barrier Reef of Australia, indicate a shoreline occupation at ~100 m depth up to 21,900 cal BP, followed by a 20 m drop over the next 1400 years (Yokoyama et al., 2006) (Fig. 2b). This was followed by a rise in sea level to −104 m at 19000 cal BP.

Since the LGM, the postglacial sea-level rise has been episodic, with periods of slowly rising sea level interspersed with rapid rates of sea-level rise (Fig. 2c). Around the southern African coast, a regionally-developed palaeo-shoreline has been recognised at −100 m and has been linked to a still-stand during the Bølling-Allerød transition period ~14,500 yr BP (Salzmann et al., 2013; Green et al., 2014; Green et al., 2020) (Fig. 2b). Global records indicate this still-stand was followed by abrupt warming in the Northern Hemisphere at the Bølling transition ~14,650 yr BP. This coincided with accelerated melting of ice sheets and a spike in the rate of sea-level rise, termed Meltwater Pulse (MWP) 1 A (Fairbanks, 1989; Blanchon and Shaw, 1995). MWP 1 A was manifested by a rise in sea level of 12–14 m over ~340 yr at a rate of at least 4 cm yr-1 (Deschamps et al., 2012). This sudden rise in sea level was followed by relatively slower rates of sea-level rise (Blanchon and Shaw, 1995), notably the Younger Dryas interstadial (Abdul et al., 2016). During this period of relatively slowly rising sea levels, barrier shorelines formed along the southern Namibian coastline between 14,000 and 13,300 cal BP (Runds et al., 2019). These features were preserved by another spike in sea level associated with MWP-1B, where sea levels rose from −58 to −40 m between ~ 11,500 and 11,200 yr BP (Liu et al., 2004; Liu and Milliman, 2004). During the late Holocene (the past 6000 years), sea level reached its present level, with a highstand of ~3 m at 6280 cal BP, before dropping to present-day sea level ca. 3000 cal BP (Cooper et al., 2018).

3. Methods

3.1. Geophysical data

The study area was surveyed using a high-resolution Kongsberg EM 710 multibeam echosounder deployed off the MV DP Star in two different campaigns (March 2021 and September 2021). The data were positioned with a C-Nav 3050 DGPS and a Kongsberg Seapath 200 IMU, and sound velocity corrections were made using a Valeport Midas Mini Sound Velocity Profiler. These data span an area of ~170 km^2.

The bathymetry data were processed using QPS Qimera and the soundings reduced using the predicted tide charts for the area (Navy, 2021). The final bathymetry was gridded at a 0.5 m cell size to obtain the best possible resolution. Backscatter data were collected simultaneously and processed using the Geocoder utility in Qimera. Additional side scan sonar data were collected using a Klein 2000 digital side scan sonar, with the 500 kHz channel and a scan range of 75 m. The data were processed using the Klein SonarPro software, where the bottom was manually tracked, the data were filtered, time varied gains applied, the channels balanced for contrast, and the nadir zone removed for seamless mosaicking. The final backscatter and side scan sonar data set resolves to a mosaic pixel approximating 0.5 × 0.5 m.

The sub-bottom was examined using a TOPAS PS40 parametric sub-bottom profiler. The data were collected using a Chirp LFM pulse and match filtered using the Kongsberg SBP utility where transducer motion was also modelled using the inputs from the Kongsberg Seapath 200. The final RAW TOPAS files were exported as full waveform data to SEG-Y format with a resolution of <20 cm. The data were collected at a grid spacing of ~100 m with occasional closer spaced lines up to 50 m apart (Fig. 1).

The sub-bottom data were interpreted using Geosuite Allworks where the seabed was manually tracked. Gain, swell filtering, and water column muting were then applied. Multibeam bathymetry was acquired simultaneously to the sub-bottom data for the purposes of absolute depth correction of the sea floor and sub sea floor reflectors. The various stratigraphic horizons were converted from two-way travel time (TWT) to depth by using constant velocities of 1500 m/s for seawater and 1600 m/s for sediments. These were chosen based on standard published values for the shallow Namibian shelf stratigraphy (Kirkpatrick et al., 2019a).

3.2. Lithological data

Geological data were acquired from drill hole data recorded in the field for 1384 boreholes (Fig. 1). The boreholes were drilled following a 50 m grid pattern in some areas, dictated by the interpretation of previous seismic and bathymetric data. Samples were obtained using a 5 m^2 reverse circulation (RC) drilling apparatus capable of drilling to a maximum depth of 8 m. Drilling was limited to areas within the study site where the water column depth exceeded 30 m due to restrictions associated with the sampling vessel. Sub-sampling of materials for age dating was not possible due to the diamond content and restricted access to associated materials. Due to the nature of the drilling technique, samples are returned as chips, blocks or fragments as opposed to continuous core.

Additional legacy vibracore data were integrated into the geophysical interpretations. Lithological descriptions (Compton et al., 2001) were used to refine the upper 5 m of the unconsolidated sediment package in this study. The geochronology of the upper packages was further constrained by ^{14}C analyses (Compton et al., 2001).

4. Results

4.1. Seafloor geological framework

The acoustic facies of the study area (Fig. 3; Table 1) are dominated by a mixture of low-relief, low and even-toned backscatter and low-relief, high-backscatter seafloor (Fig. 3a). Two coast-parallel strips of low-relief, high backscatter areas are evident, with the landward portions slightly more irregular in tone, with multiple irregular coast-oblique ridges of higher backscatter (Fig. 3 inset i). To seaward, the higher backscatter facies lack the higher backscatter ridges and display a series of intersecting lineaments of low, even-toned backscatter (Fig. 3 inset ii). At the seaward edge of the study area, an area of even-toned high backscatter occurs in which polygonal areas of smooth homogenous low backscatter occur.

The main high backscatter areas are separated by areas of smooth, even-toned backscatter, and an extensive zone with mottled higher backscatter and rippled texture abutting areas of high backscatter (Fig. 3 inset iii). The outer portions of the study area are mostly dominated by low, even toned backscatter.

The high-backscatter zones with coast-oblique ridges represent the seaward extension of Precambrian schists of the Spencer Bay Formation that crop out along the coastline of the study area (Fig. 4a). To seaward, higher backscatter zones with intersecting lineaments represent outcrop of the Gariep Belt schists and quartzites (Fig. 4b). The seaward-most, high backscatter facies represents outcrop of phosphatic limestones (Fig. 4c).

The low, even toned backscatter represents recent shelf muds and sands that drape the low points of the hard rock features and fill fractures in the bedrock surfaces (the low backscatter lineaments). Pervasive, mottled backscatter seafloor represents coarser gravelly or sandy material that often occurs in association with the rocky seabed.

4.1.1. Seismic stratigraphy, lithostratigraphy and unit distribution

Two regional reflectors, Horizon 1 (H1) and WRS (Fig. 5) and five seismic units, A-E (Figs. 6–10), were identified in the study area (Table 1). Seismic units were defined by their internal reflection configurations, reflection amplitudes, termination patterns and bounding reflectors. Most units were also intersected by the various drill holes of the study area (Fig. 1), allowing the sub-bottom record to be reconciled with the regional lithostratigraphy described by Aizawa et al. (2000) and Stevenson and McMillan (2004). Isopachs of the various units, derived from a combination of core and sub-bottom data, are presented.

4.1.2. Regional reflector H1

H1 forms an erosional high amplitude reflector that truncates the lower portions of the stratigraphy (Figs. 6–10). The morphology of H1 reveals a N-S coast-elongate bedrock depression fringed by coast parallel ridges of bedrock that crop out at −40 m and − 50 m respectively (Fig. 5a). The H1 depression is up to 20 m in relief and is 4 km-long and 2.5 km-wide. The general pattern of post-H1 sediment thickness reflects a dearth of sediment to seaward of the western ridge (Fig. 5b). A thin (< 0.7 m) veneer of post H1 material drapes the outer portions of the inner shelf, out to the 120 m isobath (Fig. 5b). The thickest accumulations of

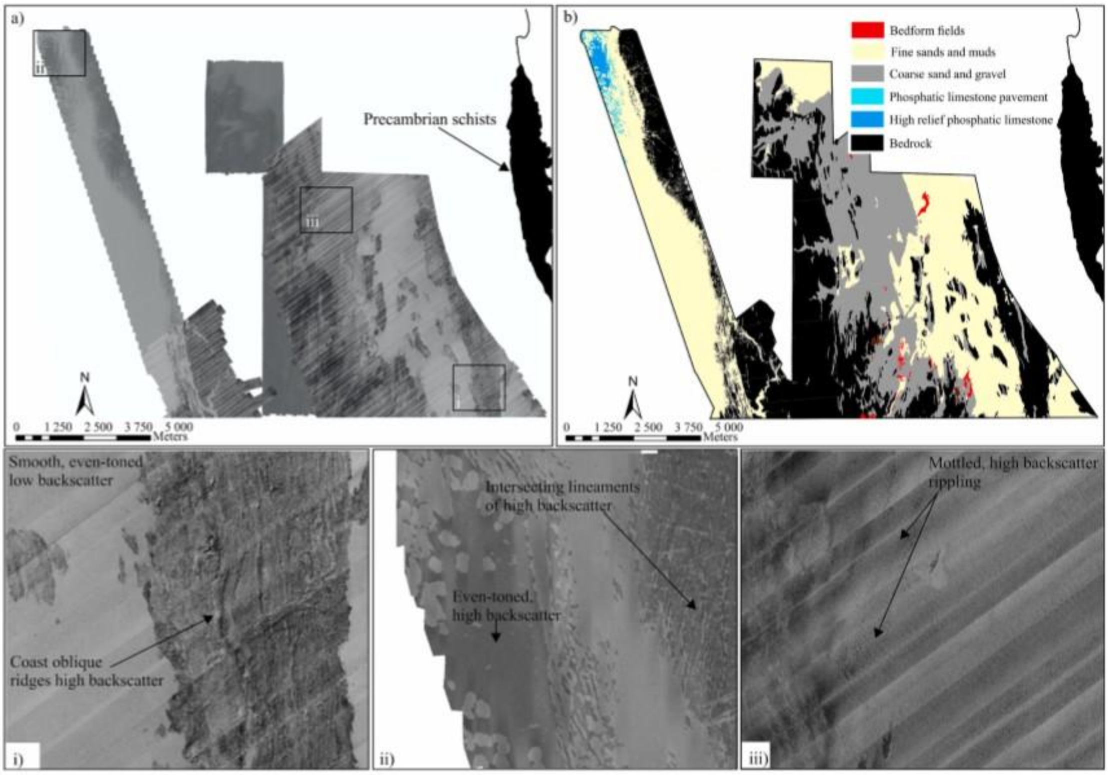

Fig. 3. a) Merged side scan sonar and backscatter mosaic of the study area. b) Seafloor geology of the area based on acoustic facies and drill core samples. Inset i) coast oblique, high relief ridges of high backscatter surrounded by even-toned, low backscatter. Inset ii) Even-toned high backscatter seafloor with polygonal shapes, and intersecting lineaments marked by high backscatter. iii) Mottled, high backscatter seafloor with rippled textures.

Table 1
Seismic stratigraphic units, description of seismic facies, intepreted depositional environment and age.

Unit/ Surface	Underlying Surface/Units	Description	Internal Reflection	Interpreted Depositional Environment	Primary Lithology	Age
Unit A	n/a	Rugged topography when exposed	High amplitudes and low - medium frequency,chaotic in character, limited penetration	Acoustic basement	Schists and quartzites	Precambrian / Proterozoic
	n/a	Thin (at resolution of the sub-bottom data)	Low amplitude and frequency, parallel to sub-parallel, indistinct	Chemical erosion and weathering	Saprolite	Palaeocene?
	n/a	Thin (at resolution of the sub-bottom data)	Low amplitude and frequency, parallel to sub-parallel, indistinct	Mechanical weathering, wave transport of residual weathered material	Clay	Palaeocene?
Unit B	n/a	Localised peaked bodies	Low - medium frequency, low to high amplitude, downlapping sets, sub-parallel	Marine, possibly shallow subtidal	Sandstone with *Diplochaetetes longitubus*	Eocene
H1	Units A and B	Continuous surface, forms depression	High amplitude	Subaerial unconformity/ incised valley	n/a	Early Eocene
Unit C	H1	Pinnacled upper surface forming polygonal depressions	Continuous surface	Marine	Phosphatic limestone	Miocene (Burdigalian)
Unit D	Units A, B, C, H1	Often forms basal layer in depressions of H1	High amplitude, low to medium frequency, chaotic	Lowstand gravel lag deposit / postglacial transgression	Gravel	early Miocene to late Quaternary
Unit E	Units A, B, C, H1	Capping stratigraphy	Alternating high and low amplitude, moderate frequency, aggradational, continuous parallel with minor wavy patterns, onlaps high points of H1		Mixed	Pleistocene to recent
Sub-unit E1	n/a		n/a	Shoreface	Lower sand, mud, dolomitised in places	Pleistocene
Sub-unit E2/ WRS	n/a		High amplitude, continuous, erosional truncation	Wave ravinement surface	Shell hash, *Turritela declivis, Fusinus ocelliferus, Phacoides saldanhae*	Pleistocene
Sub-unit E3	n/a		Low amplitude, continuous	Modern shelf regime	Mud and sand	Holocene

Fig. 4. a) Precambrian schists of the Spencer Bay Fm. b) Schists and quartzites of the Gariep Belt. c) Phosphatic limestone marked by *Trypanites sp* borings. See Fig. 1 for sample sites.

unconsolidated sediment occur in the main depression between the western and eastern ridges of outcropping rock. A distinct depocenter to the north is apparent, with a second depocenter with greater variations in sediment accumulation to the south. The southern depocenter comprises coast-parallel, linear to sinuous accumulations of sediment 1–4 m-thick (Fig. 5b). A sinuous feature occurs to the south of the northern depocenter, with ribbons of sediment >3 m-thick, and from 150 to 300 m-wide.

4.1.3. Regional reflector WRS (wave ravinement)

The regional reflector WRS has a moderate amplitude surface and spans the entire area (Figs. 6–10). The surface mostly mirrors the underlying H1 surface (Fig. 5c). Where bedrock crops out, the WRS steepens and often merges with H1 to form a composite erosional surface at the seabed (Figs. 6–10). The scattered material that overlies WRS is locally up to 3.5 m-thick, mostly associated with low points in the H1 and WRS elevations (Fig. 5d). Three main depocenters are recognised; a seaward depocenter that trends roughly coast parallel, a depocenter in the south formed in the H1 depression, and a northern depocenter associated with a bowl-shaped depression in H1 (Fig. 5b, d).

4.1.4. Unit A: schists, quartzites (acoustic basement) and weathering residues (saprolites and clays)

Unit A forms the acoustic basement and occurs throughout the study area (Figs. 6–10). It is represented by acoustically chaotic, high amplitude internal reflections, truncated by H1. Drilling reveals this unit to comprise micaceous schists (Fig. 4a) and quartzites of the Namaqua Metamorphic Complex and Gariep Belt, respectively. Overlying the acoustic basement are isolated patches of very thin saprolites and clays, derived as weathering residues from the schists. They are generally too thin to distinguish from the acoustic basement in sub-bottom profile and are more apparent from drill samples where they appear as <20 cm-thick horizons. These comprise clay-rich layers with remnant pieces of weathered schist still present (Fig. 11a). Clay layers occur as grey

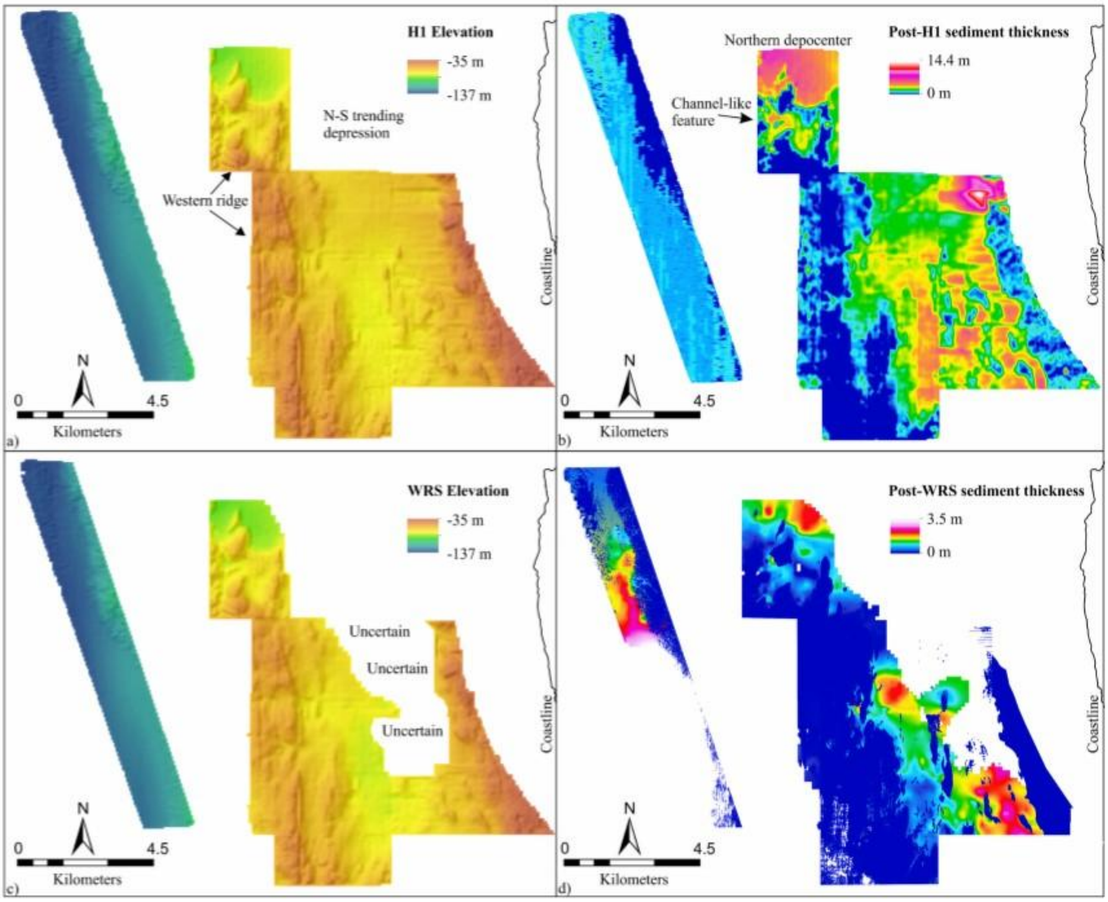

Fig. 5. a) Sunshaded relief image of the H1 surface elevation relative to mean sea level. Note the N-S trending depression in the bedrock, with an eastern and western bedrock high. b) Post-H1 sediment isopach map of the study area with a northern depocenter, and a southern depocenter of more irregular sediment cover. Note the lack of sediment seaward of the western ridge. c) Sunshaded relief image of WRS. A similar trend in morphology to H1 occurs. Due to the difficulty in mapping WRS from sub-bottom profiles alone, certain areas are not able to be reconstructed (marked uncertain). d) Post-WRS sediment isopach map (Unit E3), outlining the main post transgressive ravinement depocenters.

deposits without remnant rock pieces, are fossil-free and often form spherical to rod-shaped mudballs, associated with surface H1 (Fig. 11b).

Saprolite is distributed sporadically in isolated pockets within the H1 depression and exclusively to landward of the western ridge of outcropping schist (Fig. 12a). A maximum saprolite thickness of ~0.5 m is found in the northern depocenter in H1 (Fig. 12a). The weathered clay is found on the landward edge of the western ridge and to the westernmost extent of the area, forming deposits that are up to 40 cm-thick (Fig. 12b).

4.1.5. UNIT B: sandstone

Resting within the lows between basement highpoints are numerous patches of material comprising bodies of acoustically opaque to chaotic reflections. These often form localised peaks around which the overlying sediments onlap or drape over (Fig. 6 insets). Drilling reveals these to comprise sandstones (Fig. 11c) with abundant tubes of the early Eocene-age polychaete *Diplochaetetes longitubus* (Fig. 11d) (Pickford and Senut, 2002). Sandstones are mostly present in the landward (lee side) of the western ridge of Unit 1 and may reach 1.8 m-thick (Fig. 11c). The tops of these sandstones are truncated by H1.

4.1.6. UNIT C: phosphatic limestone and phosphorites

Unit C overlies H1 and rests atop the schists at a depth of 110–120 m at the seaward-most edge of the study area (Figs. 10). Its presence is marked by a pinnacled upper surface and subsurface topography, with high amplitude chaotic to wavy internal reflections that are distinct from the more complex, chaotic reflections of the schists beneath (Fig. 10). Each pinnacle of Unit C marks a near vertical surface, that separates bowl-shaped depressions. These depressions terminate on the boundary between Unit C and the schists (Fig. 10) and are filled with sediments of Unit E (see below) rich in pelletal phosphorites (*Bill Ludick pers. comm*). Boreholes reveal the material to comprise a *Trypanites* sp-bored, dense, black phosphatic limestone (Fig. 4c). The base of this unit is difficult to discern in the sub-bottom reflections, hence a detailed isopach was not created.

4.1.7. UNIT D: basal gravel bodies

Throughout the area, deposits comprising high amplitude, chaotic

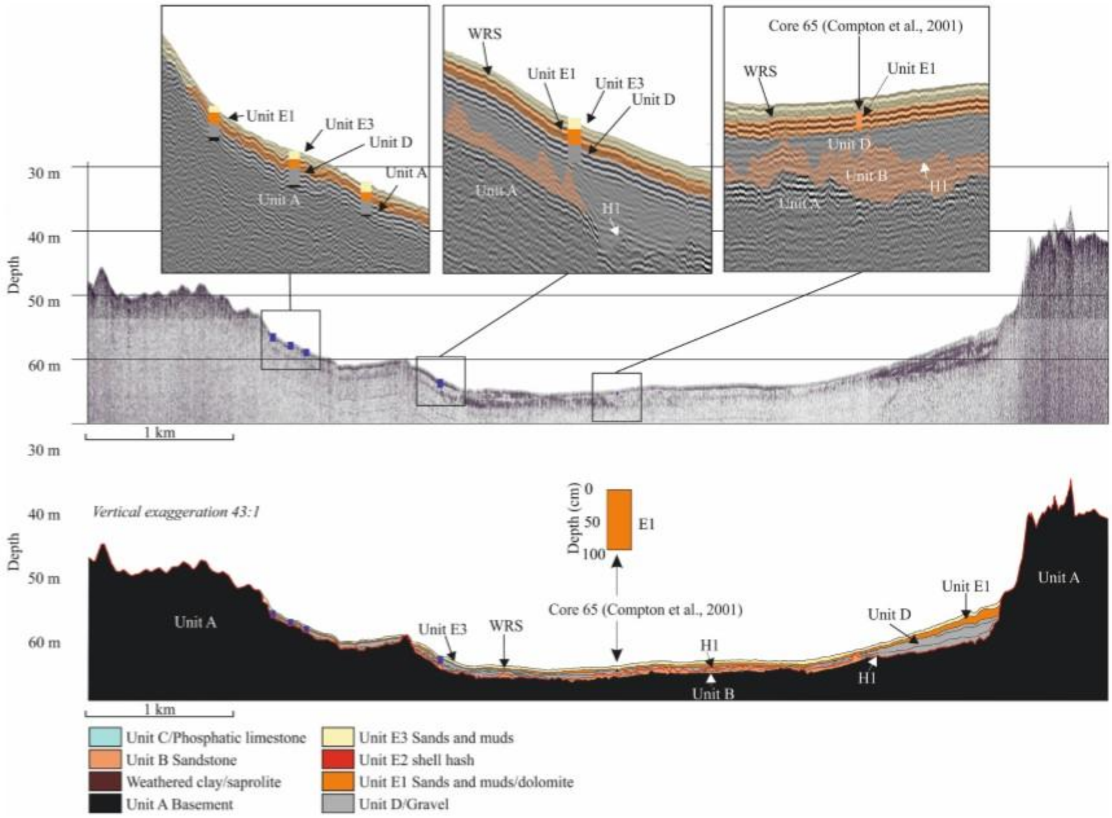

Fig. 6. Very high-resolution, coast perpendicular TOPAS sub-bottom profile (top-uninterpreted, bottom-interpreted) detailing the fill succession of the H1 depression. Insets show positions of cores relative to high resolution, full waveform enlarged sub-bottom data.

and occasionally transparent reflections, can be observed (Figs. 6–9). These occur in depressions and scours in the H1 horizon and take the form of several, metre-thick packages, or wedges trailing off high points in the acoustic basement and sandstones of Unit B.

Drill data reveal Unit D to be composed of gravel (Fig. 11e), with a variety of clast sizes and compositions including granules to large cobbles of schist, quartzite, phosphatic limestone, and volcanoclastic material. Unit D is in places truncated by WRS. These deposits are found in greatest thicknesses in the H1 depression at depths of 60–75 m and are often discontinuous along-strike forming small depocentres ~1 km^2 in extent (Fig. 12d). Though no dates could be assigned to this unit, various authors consider the regional scale gravel body that extends from the Orange River to be a multi-phase regressive/transgressive deposit that spans the early Miocene to late Quaternary (Compton et al., 2002; Lodewyks, 2010; Kirkpatrick et al., 2019a, 2019b).

4.1.8. UNIT E: younger unconsolidated and semi-consolidated sediments

Unit E caps the stratigraphy and comprises a seaward tapering wedge of horizontal-parallel, continuous, and at times sub-horizontal reflectors (Figs. 6–10).

Unit E is composed of sub-units E1, E2 and E3. Though not providing continuous core, the RC drill data reveal E1 to comprise a basal sand that occurs below the WRS, or in certain instances replaces it (Fig. 9). The basal sand unit reaches a maximum of 2.5 m-thick (Fig. 12e).

4.1.9. Legacy core data

Legacy vibracores described by Compton et al. (2001) reveal a more subtle sedimentary succession than what can be discerned from the sub-bottom data. These show an overlying calcareous muddy component to E1, with occasional dolomite-cemented sandy lenses (Fig. 9). Most vibracores terminate in the dolomitised sandy succession with some terminating in the gravels of Unit D.

Sub-unit E2 comprises bioclastic-rich gravels (shell hash) with valves of *Turritela declivis*, *Fusinus ocelliferus* and *Phacoides saldanhae*, in addition to pebbles of schist and quartzite (Fig. 11f). This upper gravel can be distinguished from the lower gravel (Unit D) by its high bioclastic content and finer grain size. The unit is unevenly distributed with marked variations in thickness (Fig. 12f).

Despite not being sampled by the vibracores, the succession is topped by a layer of soft sand or mud of sub-unit E3, characterised by initial sinking of the drill tool into the substrate (the post-WRS sediment). The thickest successions occur in the depression between the eastern and western ridges of Unit A, forming depocenters up to 3.5 m thick (Fig. 5d).

Radiocarbon dates indicate a Pleistocene age for most of the unconsolidated sediments (Fig. 9) (Compton et al., 2001). The shell hash of unit E2 (~ 70 m deep) was dated at 11000 ± 200 cal ka BP, and the underlying succession of dolomite-cemented calcareous sands at 37200 ± 140 cal ka BP, placing their cementation during MIS 2 (Fig. 9).

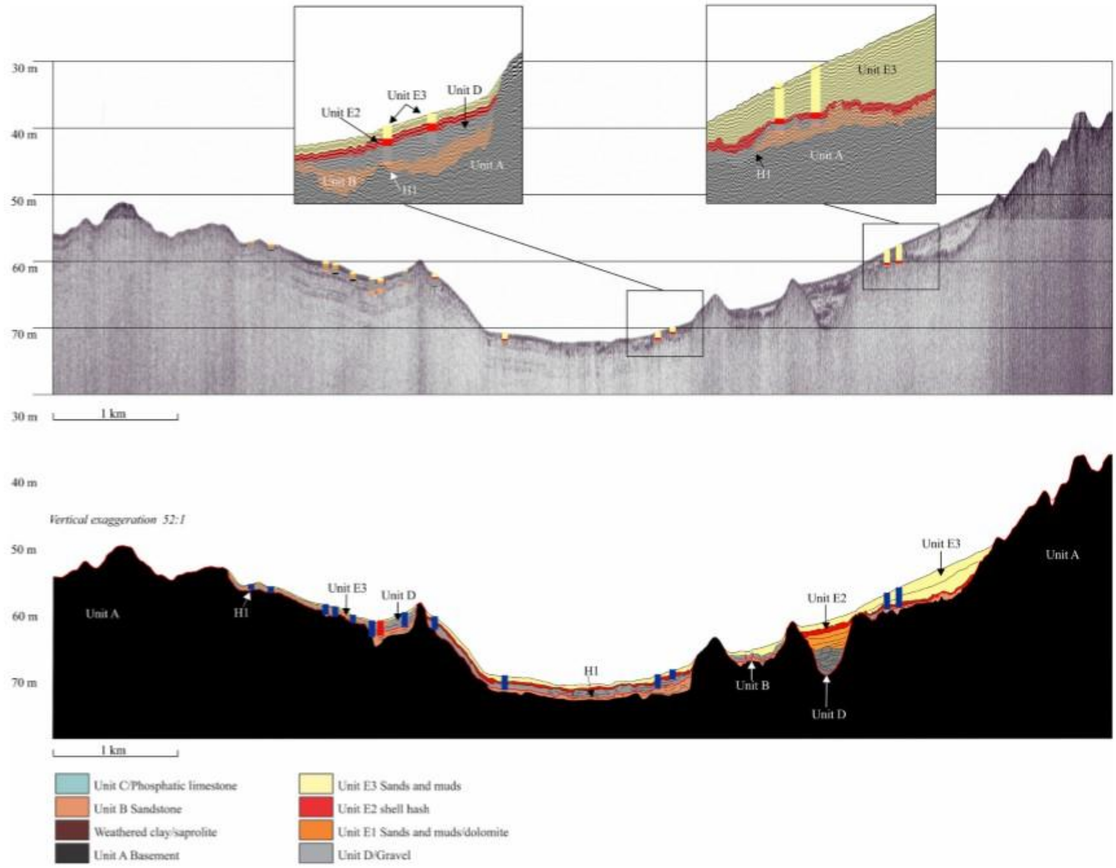

Fig. 7. Very high-resolution, coast perpendicular TOPAS sub-bottom profile (top-uninterpreted, bottom-interpreted) detailing the fill succession of the H1 depression. Insets show positions of cores relative to high resolution, full waveform enlarged sub-bottom data.

4.2. Seabed morphology

The landward-most portions of the mid-shelf are represented by mostly flat, low gradient sediment-draped seafloor, with occasional outcrop of the schists of Unit A (Fig. 13). A very well-defined, 850 m-wide, N-S trending outcrop of Unit A forms a high point on the seabed with smaller, isolated ridges of Unit A to seaward surrounded by flat seafloor. This flat seafloor is bordered to the west by a second ridge of Unit A. This ridge is up to 3 km-wide and marks the most seaward outcrop of the schist basement. The intervening seabed between the two ridges forms a broad, 20-m deep, N-S trending seafloor depression, the morphology of which mirrors the underlying palaeo-topography of H1 (Fig. 5a).

The seaward-most outcrop of Unit A terminates in a 1.5 m-high cliff, the NW-SE trend of which is similar in morphology to that of the modern coastline (Fig. 13). The cliff occurs at a depth of ~115 m and is fringed to seaward by a rock platform almost 400 m-wide, that rises above the seabed by 1–1.5 m. The upper surface of the platform is composed of Unit C and occurs at a depth of ~115 m, with the surface marked by several polygonal to circular depressions differing from each other in both shape and size. These are ~100 m-wide and 1 m-deep, with elongated axes arranged coast-parallel. Some have coalesced into larger features forming a coast-elongate depression (Fig. 13a inset i). Towards the north and south the platform surface is absent, except for the remnants of the raised rims of the polygonal depressions (Fig. 13a). The depressions are filled with sediments of Unit E (Figs. 3; Fig. 10).

5. Discussion

The stratigraphy offshore Saddle Hill reflects a complex mixture of Quaternary sand, gravel and mud deposited in bathymetric lows incised in weathered bedrock. This morphology is attributed to the combined effects of antecedent bedrock history and Pleistocene sea level fluctuations. Late Quaternary sedimentation has been confined to a rock-bound depression where accommodation space existed during successive periods of high sea level. The sequence preserved is, however, highly variable in thickness and spatial distribution and nowhere is a complete sedimentary succession preserved at a single location. This temporal variation in depositional loci reflects the interplay between available accommodation space and the effects of transgressive ravinement. The shelf also reveals geomorphological and sedimentological evidence for variable rates of sea-level rise during the postglacial transgressions from MIS 2 to MIS 1. Below we discuss the stratigraphic and geomorphological evolution of the inner shelf in this context.

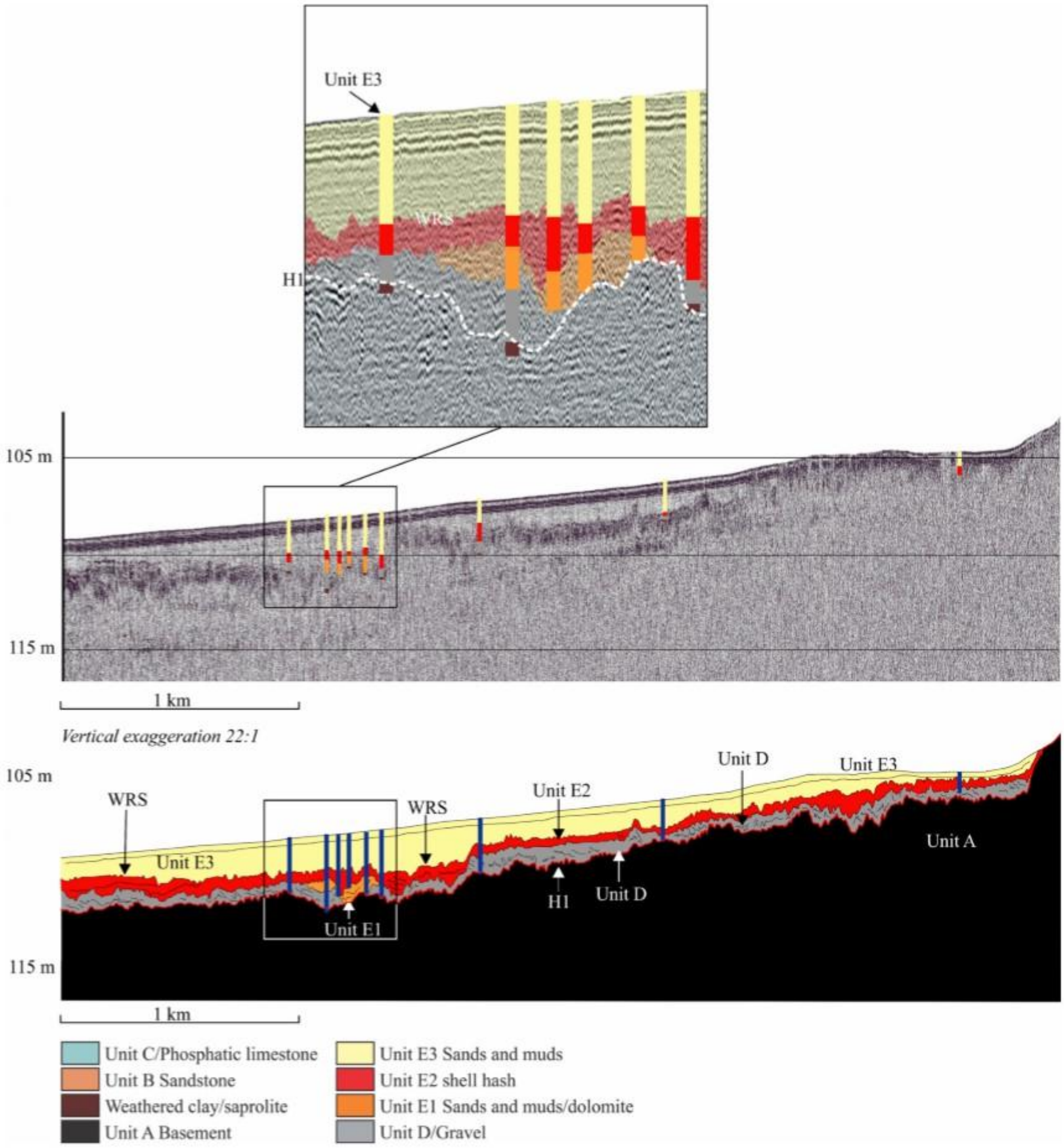

Fig. 8. Very high-resolution, coast parallel TOPAS sub-bottom profile (top-uninterpreted, bottom-interpreted) detailing the seismic stratigraphy of the more seaward parts of the inner shelf.

5.1. H1 as a repeatedly excavated and well-preserved palaeo-land surface

The acoustic basement (Unit A) of the shelf has been well-described by others (Stevenson and McMillan, 2004; Kirkpatrick and Green, 2018) and warrants no further discussion here. However, the surface that truncates the bedrock (H1), and the unusual platform of phosphatic limestone (Unit C) that rests atop the bedrock to seaward reflect a combination of processes that have acted to shape the geological framework in which the cover sediments have accumulated on the shelf.

H1 truncates the schists, quartzites and sandstones of the acoustic basement. The surface is also marked by saprolites and rolled mudballs, forming an erosional boundary between Units C, D and E and the acoustic basement. The presence of *Diplochaetetes longitubus* (Pickford and Senut, 2002) within the sandstones truncated by the subaerial unconformity constrains the age of H1 to early Eocene or younger.

The rounded nature of the mudballs where H1 has exposed the saprolites and clays above Unit A indicates the role of wave and/or tidal transport of eroded material in the surface's development (Tanner,

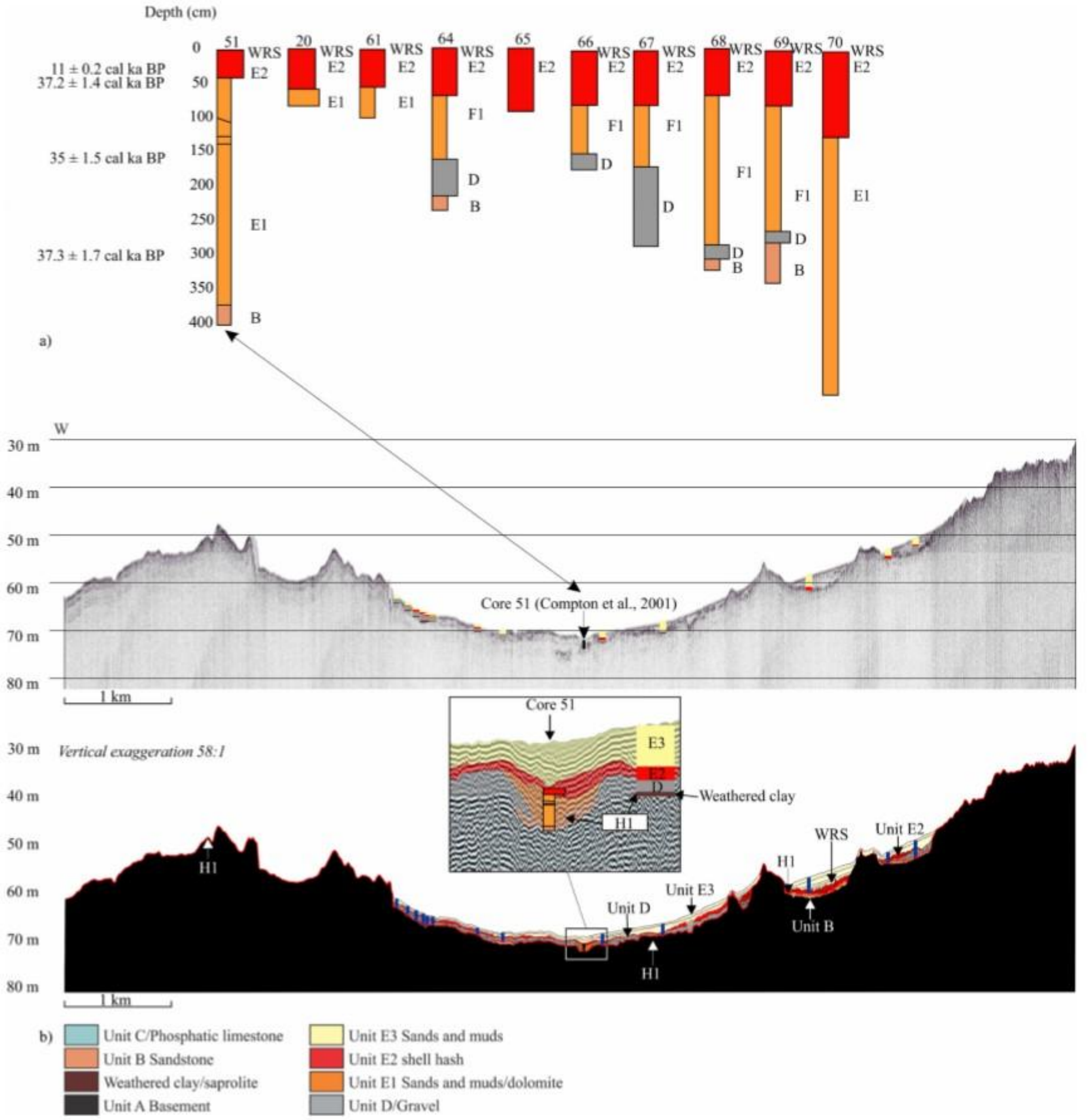

Fig. 9. a) Vibracores from the H1 depression, previously described by Compton (2001), outlining the main lithology of the cover succession and their seismic stratigraphic and geochronological context. b) Very high-resolution, coast perpendicular TOPAS sub-bottom profile (top-uninterpreted, bottom-interpreted) intersecting core 51 and outlining the seismic stratigraphy of the H1 depression. Note the MIS 3 age for Unit E1, the Holocene-age for the gravel Unit E2, and the absence of Unit E3 from the cores, yet present in the seismic section. The top of unit E2 is considered the wave ravinement surface (WRS).

1996; Mukhopadhyay et al., 2022). Unit A would have been initially exhumed and exposed to subaerial processes during lowstands of the lower Paleogene (Baby et al., 2018). We consider this surface to represent a subaerial unconformity that was further entrenched during later sea level regressions (likely late Oligocene-Fig. 2). The surface was later subject to wave processes during multiple regressive and transgressive cycles of the Quaternary.

A discontinuous phosphatic limestone pavement was observed north of Lüderitz, along the outer parts of the inner shelf, by Birch (1979) and Birch et al. (1983). A phosphatic limestone pavement was also recognised from similar depths on the southern Namibian and South African shelf by Dingle (1974), who dated it to the early Miocene (Burdigalian). We consider Unit C as part of this succession, formed in the early Miocene and with its upper surface later exposed to subaerial processes. Subaerial exposure possibly first occurred during the smaller Miocene and Pliocene sea-level falls (Siesser and Dingle, 1981).

In the more proximal areas of the shelf, the finer materials of Unit E that were deposited on H1 after the highstand of MIS 5 and lithified

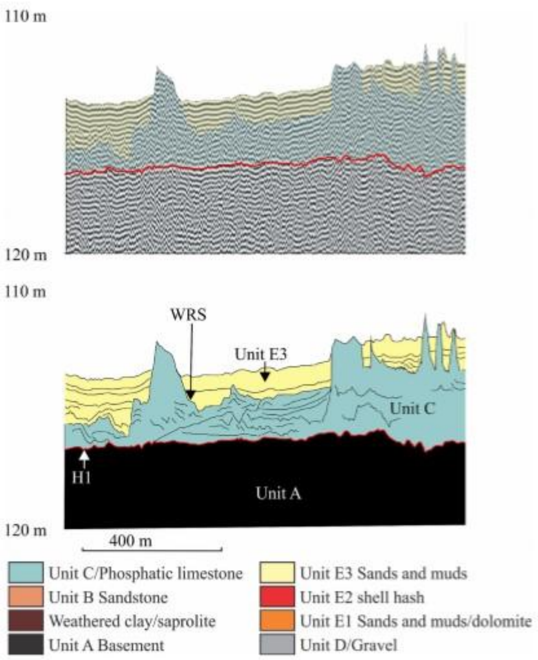

Fig. 10. Coast parallel, very high-resolution, full waveform TOPAS sub-bottom profile and interpretation (bottom) from the most seaward part of the inner shelf, showing Unit C overlying Unit A. Depressions in Unit C are filled by sediment of Unit E3.

during MIS 2 (~ 37,000 cal BP); their progressive dolomitisation is related to precipitation in hypersaline conditions (Compton et al., 2001) in a mixed seawater and groundwater environment, suggesting precipitation in an enclosed lagoonal or pan-type system (Compton et al., 2001). Their preservation above H1 indicates less severe subaerial erosion during the ensuing lowstand of MIS 4 and shelter from ravinement during subsequent transgressions.

The top of Unit E1 in the H1 depression likely marks the most recent subaerial unconformity associated with MIS 2 and the LGM. The deep shelf break (200–500 m), and relatively flat shelf profile preclude the upstream migration of topographic knickpoints and development of major incised valleys; sea level did not fall below the shelf break during the Pleistocene and erosion of the materials deposited on the shelf during lower than present sea levels was therefore hindered (e.g. Posamentier, 2001). Baby et al. (2018) considered the modern shelf break to have formed with the late Campanian uplift episode, and the Cretaceous drainage systems of SW Africa reactivated during the late Oligocene uplift. It is likely that this was the last stage where significant shelf incision was possible.

The deeper parts of H1 that crop out along the seabed represent the most recent lowstand unconformity of the LGM. This is merged with other older subaerial unconformities as they coalesce into one main surface of erosion, in keeping with the diachronous, seaward-younging and merging of these stratigraphic surfaces (Zecchin and Catuneanu, 2013).

The unusual surface texture manifest along the upper surface of Unit C bears a strong resemblance to karst surfaces formed in coastal carbonate sequences exposed to chemical weathering (Sweeting, 1973; Jennings, 1985; James and Choquette, 1988; Higgins and Coates, 1990; Ford and Williams, 2007). Some authors have considered karst features as a continuum that spans fluviokarst, where valley forms are sculpted, to polygonal karst, where the entire land surface is obscured by dolines with little to no trace of the previous valley form (Gunn, 2004; Kan et al., 2015). The unusual surface expression of unit C resembles the latter (Fig. 13a inset i), also called egg-box geomorphology (Day and Chenoweth, 2004; Kan et al., 2015). The depressions in the study area exhibit

Fig. 11. Disaggregated drill core material. a) Saprolite (upper Unit A). b) Elongate rods and sphere of clay (upper Unit A). c) Sandstone. d) *Diplochaetetes longitubus*. e) Pebbles and cobbles of angular to well-rounded schist and sandstone that form the gravel components of Unit D. f) Shell hash and finer gravels (granules and pebbles) of Unit E2.

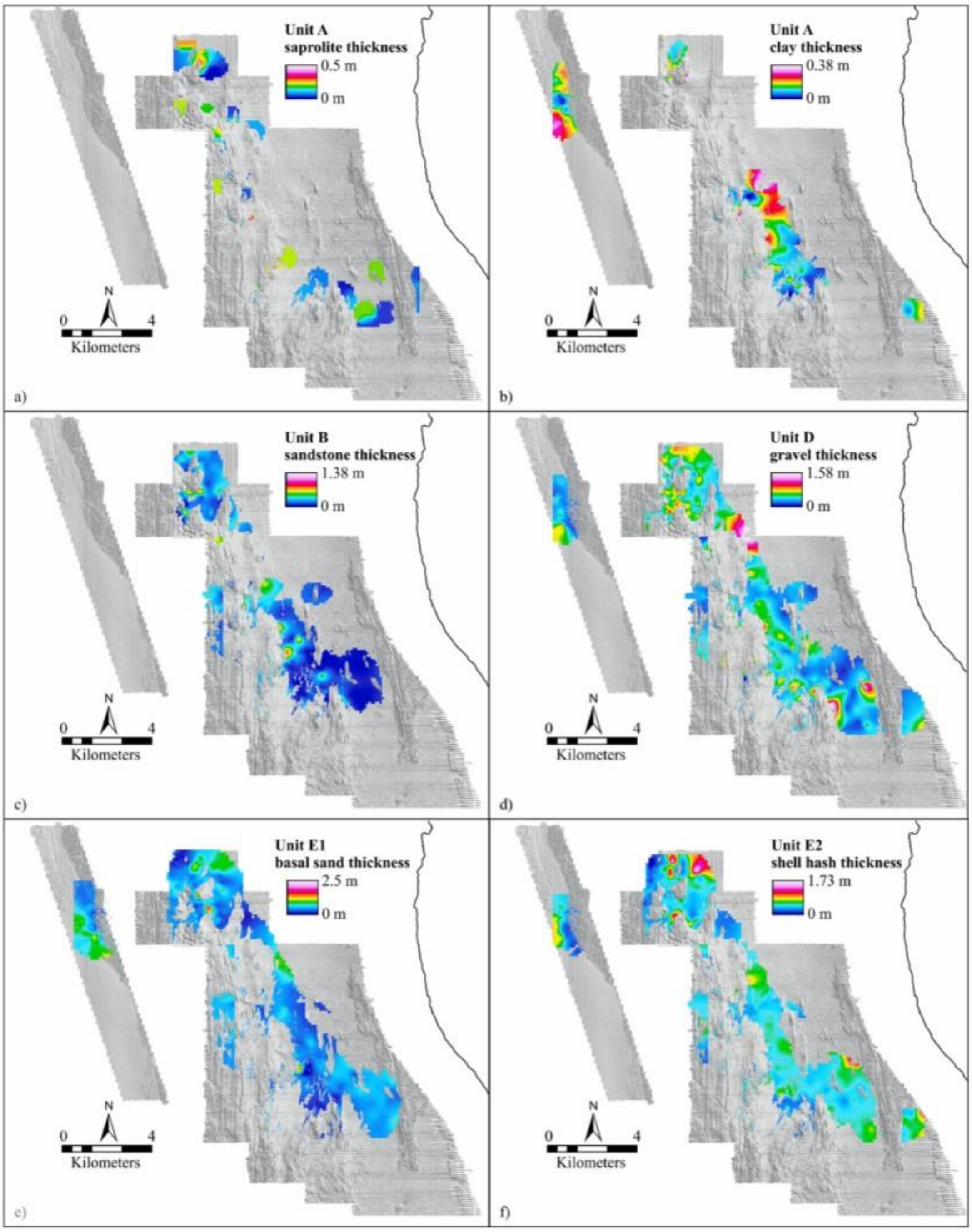

Fig. 12. Isopach maps for the various seismic and lithostratigraphic units. a) Saprolite (upper part of Unit A, reconstructed form core data). b) Clay (upper part of Unit A, reconstructed from core data). c) Sandstone of Unit B. d) Gravel of Unit D. e) Basal sand of Unit E1. f) Shell hash of Unit E2.

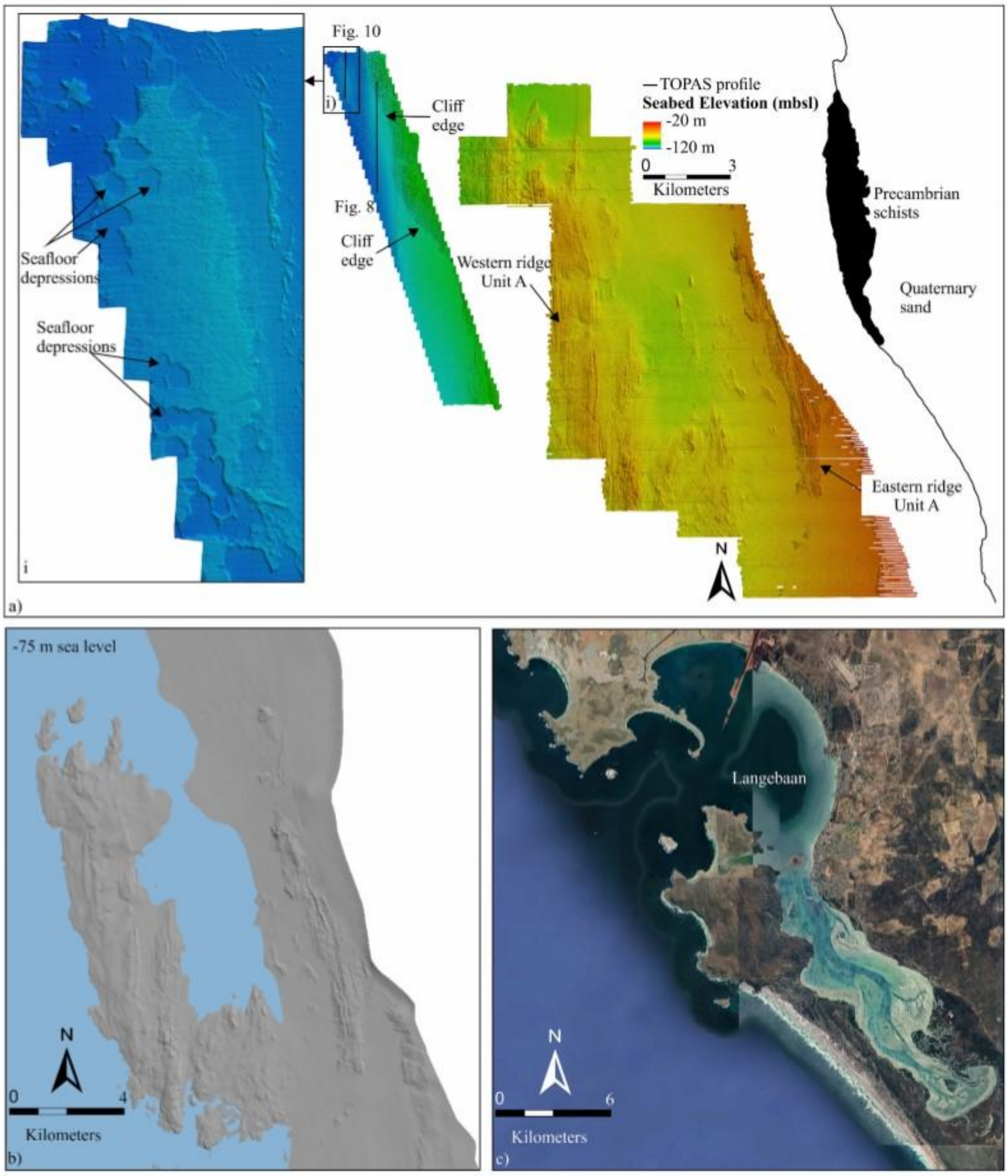

Fig. 13. a) Multibeam bathymetry of the study area showing the main bedrock ridges that form the H1 depression, and a cliff edge at −100 m. Note the similarity in seafloor morphology to that of H1 in Fig. 5a. Inset i shows polygonal seafloor depressions located along the seaward edge of a raised and flat platform of Unit C. b) Reconstructed palaeo-sea level at −75 m, superimposed on the bathymetry showing a lagoon-like water body. c) Comparison to Langebaan lagoon on the west coast of South Africa showing a similar morphology, with a rock-bound inlet.

bowl-shaped forms with vertical walls (Fig. 10), and with sizes that correspond to those of general karst dolines, typically tens to hundreds of meters in diameter and with depths of a few meters to tens of meters (Fig. 10a) (Williams, 2004). Their sizes are also similar to submerged dolines that have been recognised in Ha Long Bay, Vietnam (Waltham and Hamilton-Smith, 2004); Phang Nga Bay in Thailand (Kiernan, 1994); Dweyra Bay and the Blue Grotto in Malta (Paskoff, 2005); Rock Island in Palau (Dieter, 1991); Marseille (Collina-Girard, 1996); on the Adriatic Coast of Croatia (Suric, 2002); near Lesbos Island and along the Argolid Peninsula in Greece (Scheffers et al., 2012); and in Nagura Bay, Japan (Kan et al., 2015).

The karstification of the Miocene-age phosphatic limestones could have occurred during the ensuing lowstands of the Pliocene (Fig. 2a), and during at least three periods of subaerial exposure during the

Pleistocene (Fig. 2b), when sea level fell below 120 m. Based on the late Pleistocene sea level stack of Spratt and Lisiecki (2016), we identify possible exposures during MIS 12 and MIS 6. Evidence from offshore the Orange River shows that the LGM sea levels also reached at least 125–130 m below present (Rogers, 1977), and as such, this was certainly a period of platform exposure.

The exceptional preservation of the karst landscape can be related to several factors. Firstly, the depth (110–120 m) at which the limestone occurs confined periods of subaerial weathering to only a few intervals of very low sea level (Fig. 2). Some material has certainly been eroded; however, a thick-enough body of limestone remained in which karst could form without complete platform degradation. Secondly, the platform experienced rapid submergence after each phase of karstification. This would have protected the platform from further chemical weathering during MIS 12–11, MIS 6-5e and the last postglacial transgression (Fig. 2) (e.g. Cooper and Green, 2016; Cooper et al., 2019).

5.2. Lagoons and pans during the Pleistocene and geological inheritance

The filling of the H1 depression (Fig. 5a) is related to the sporadic development of a shallow, hypersaline lagoon in the same position during several periods. In Fig. 2, we show the general trends in Pleistocene sea level that would facilitate the mixed groundwater-seawater precipitation of dolomite in a restricted water body formed in the depression (cf. Compton et al., 2001). Most modern dolomite forms in hypersaline coastal environments (Arvidson and Mackenzie, 1999; Qiu et al., 2017). Such conditions would have been initiated when sea level was at ca. -75 m, at which point the western ridge of Unit 1 would have been breached and the H1 depression progressively inundated. Connection between the restricted water body and the ocean could have been maintained through an opening to the north and a larger, coast-parallel bedrock-framed strait adjacent to this channel (Fig. 13b). This coastal configuration would have occurred during MIS 4 and again during the fall in sea level from MIS 3 when the shoreline would have once again coincided with the 75 m isobath (Compton et al., 2001).

A further period of lagoonal development would also have been possible after MIS 2. Runds et al. (2019) described a palaeo-lagoon and gravel barrier at −75 m on the southern Namibian shelf, ~ 250 km to the south of the study area. They linked the barrier's development to multiple regressive-transgressive phases, with initial flooding of the lagoon during a sea-level slowstand at −75 m, between 14,000 and 13,300 cal. BP (Runds et al., 2019). Given a protracted shoreline occupation at −75 m, a bedrock-bound lagoon would have once more developed in the study area (Fig. 13b).

We acknowledge that there have been many times prior to MIS 4 when the conditions would have been met to produce a lagoon (Fig. 2b), however only lagoonal sediments postdating MIS 4 have been preserved. The lack of preservation may be due to subaerial erosion during lowstands prior to and including MIS 6, though based on the sea level curves of Spratt and Lisiecki (2016), these appear to be of a lesser magnitude when compared to the LGM lowstand which did not erode the materials in H1. Conversely, sea-level rise during the transgressions prior to MIS 3 may have been slower, resulting in more effective wave ravinement processes eroding materials. Lastly, the stillstands or slowstands required to produce planform equilibrium features like lagoons may not have coincided with the depth of the H1 depression as serendipitously as it has done in MIS 4, 3 and 1, thus conditions may not have been met to produce the hypersaline conditions and later dolomitisation that would increase preservation potential. Unfortunately, without a more detailed sea level history for this coastline, these arguments remain speculative.

In contrast to other locations where the development of lagoons is dependent on barrier-building during sea-level still-stands (e.g. Murakoshi and Masuda, 1992; Stattegger et al., 2006; Green et al., 2013; Runds et al., 2019), this lagoon's development is facilitated by the rocky promontory to seaward that acts as a geological barrier and the lagoon that forms in its lee resembles the rock-bounded lagoons of Mexico (Lankford, 1977), Langebaan in South Africa (Flemming, 1977) (Fig. 13c), or the bedrock-confined incised valley systems of South Africa (Cooper, 1993; Dladla et al., 2019). This sheltering effect facilitated dolomite precipitation by creation of shallow and tranquil environments, thus increasing the preservation potential of the early filling materials of Unit E. As Compton et al. (2001) recognised, the rocky promontory also sheltered the incipient fills from wave ravinement during transgression. The accommodation in the lagoon was progressively reduced by successive phases of dolomite formation including the partially indurated fill at its base. Thus the potential for development of subsequent postglacial fill was much reduced, in contrast to deeper back-barrier systems of comparable size from elsewhere (e.g. Wright et al., 2000; Dladla et al., 2022). In this case, the wave ravinement surface mantles the older, MIS 2 material of Unit E1 ~ 37,000 cal. BP, as opposed to the more recent MIS 2/1 transgressive systems tract.

5.3. Holocene material and postglacial wave ravinement

Sub-bottom profiles reveal a distinct layer of low amplitude material capping the higher amplitude shell hashes and gravels of Unit E2 (Fig. 8). Given the shelly nature and Holocene age of the gravels (Compton et al., 2001), we consider these to be related to the Holocene wave ravinement surface (e.g. Zecchin et al., 2019). The discontinuous and sporadic nature of Unit E2 can be related to variable availability of coarse material during the ravinement process. The cores of Compton et al. (2001) do not include the capping material above the wave ravinement that are apparent in sub-bottom profiles (Fig. 8) and the gravel at the top of the recovered cores is not exposed on the seabed (Fig. 11). This likely reflects the fine, "soupy" nature of the upper Holocene package, which resembles a nepheloid layer (e.g. Rogers and Li, 2002; Inthorn et al., 2006) that was not sampled by either vibracore or RC drilling due to poor cohesion.

On the seaward edge of the western ridge, the post LGM surface shows the development of a cliff line cut into the competent schists (Fig. 13). This scarp can be linked to wave erosion during periods of shoreline stability at −110 m, at least one of which preceded the last glacial maximum at ~28,000 cal BP (Ishiwa et al., 2019). The cliff was reworked during the relatively slower transgression from the LGM, between 21,000 and 17,500 cal BP (Ishiwa et al., 2019). This cliff was then preserved in situ by a prompt rise in sea level from −96 m to −84 m (e.g. Zecchin et al., 2011) that is associated with MWP-1 A.

Post-ravinement, modern sediment distribution patterns show a strong correlation between coarser sand distribution and gully formation in the bedrock schists. Likewise, sand concentrates in the karst features of the phosphatic limestones and in the immediate landward lee of the western bedrock ridge. We interpret these sandy sediments as relict shoreface sediment, left behind during the transgression and modified by turbulent winnowing as the shoreface translated over the rough bedrock surface and antecedent geological framework (e.g. Pretorius et al., 2018). The coarse sandy and gravelly materials on the landward margin of the western ridge likely formed through development of a turbulent leading edge of the transgressing shoreline, where wave (especially storm-induced) winnowing focused on a narrow zone immediately in the zone of flow attachment landward of the flow obstacle (McMullen et al., 2015; Pretorius et al., 2018; Collinson, 2019). With distance from either the western ridge or the gullies in the bedrock, the seabed becomes increasingly finer reflecting less turbulence.

5.4. Where does the bulk of the sandy sediment go if not on the inner shelf?

The evidence above shows that during the lowstand periods of the Pleistocene, and probably since the late Oligocene, the inner shelf has served as a sediment bypass system for material. Given the long-lived longshore transport system that feeds gravel and sand-sized sediment northward from the Orange River (Bluck et al., 2007), the lack of sediment on the shelf seems surprising. The strong geological controls outlined above that restricted accommodation space in part explain the dearth of sediment and very thin shelf cover.

Nonetheless, although it was not deposited and preserved in the geological record on the shelf, Orange River-derived sediment was still supplied to the region. The fate of that sediment is not immediately clear. It did not accumulate on the outer shelf and the nearest site for deposition is onshore in the Namib Sand Sea (Corbett, 1993) into which sediment has been diverted via vigorous wave and aeolian transport at the coastal offset at Luderitz. Multiple authors have argued that the Orange River is the source of sediment for the extensive sandy dune fields that characterise the sand sea (Corbett, 1993; Lancaster and Ollier, 1983) but the sediment transport path has been unclear. Garzanti et al. (2018) identified an ultra-long littoral cell that extends from the Orange River into southern Angola, indicating that sediment has passed northward through or around the study area. The Namib Sand Sea thus seems to serve as a terrestrial sector of this northward-directed coastal sedimentary system (Cooper and Green, 2023). Luminescence dates from the sand sea indicate three broad grouping of dates in deposition, MIS 5, the LGM and the Holocene (Stone, 2013), with the LGM date confirming lowstand sediment bypassing along the shelf and to the sand sea.

5.5. Evolutionary model

Below and in Fig. 14, we provide an evolutionary model for the inner shelf in the study area.

1. Initial subaerial erosion of the inner shelf took place in the lower Palaeocene to form the proto H1 surface (Fig. 14a).
2. Protracted chemical weathering formed saprolites and clays which were reworked by transgressive/regressive processes (especially wave activity) to form mudballs (Fig. 14b).
3. An early Eocene sea level high caused shallow marine flooding of the H1 depression. Sandstones formed, composed of the reef-building tubeworm *Diplochaetetes longitubus* (Fig. 14c).
4. A late Oligocene sea level fall caused further excavation of the palaeo-shelf and full development of the H1 surface (Fig. 14d).
5. An early Miocene sea level high caused deposition of the Burdigalian-age phosphatic limestones along inner shelf edge (Fig. 14e).
6. Lowstands of the Miocene to Pleistocene began to karstify the limestone, forming the polygonal karst features. During this time gravels began to be supplied to the shelf by the Orange River and became concentrated with repeated regressive/transgressive cycles over the Pleistocene. The shelf had begun to operate as a bypass system across lowstand cycles and sand was not stored on the inner shelf but transported to Namib Sand Sea. (Fig. 14f)
7. During MIS5e, muds and sands accumulated as a thin veneer in H1. A regression to −75 m with a stillstand produced a hypersaline, rock-bound lagoon where dolomite had precipitated, aiding in the cementation and preservation of the H1 fill (Figs. 14 g and h).
8. A further phase of karstification ensued during the LGM (Fig. 14i) A still stand during the post-LGM sea-level rise cut a cliff into the seaward edge of the schists and quartzites at −100 m (Fig. 14j). Further stepped sea-level rise in the Holocene caused the re-occupation of the lagoon. With a rise in sea level to modern day, the WRS developed across the shelf and some sandy material was preserved in H1 due to overstepping (Fig. 14k).

5.6. Stratigraphic significance

The long-lived antecedent geological framework that existed since the late Oligocene has controlled the distribution and preservation of Miocene and later cover sequences deposited atop H1, and especially those in the H1 depression. The extent of the thin post-Oligocene sedimentary cover in this depression is clearly bedrock-controlled (via accommodation and shelter from erosion) and, although it records several million years of deposition, reaches a maximum thickness of <14 m. The sequence is also spatially variable and the presence/absence of a particular unit at any given location is a function of the availability of accommodation space at the time of deposition, and the extent of subsequent erosion during subaerial weathering and/or transgressive ravinement. This situation is in marked contrast to shallow shelves, such as the SE African margin (Green et al., 2013), the SW Spanish margin (Rodero et al., 1999) and the NE Brazilian margin (Aquinio Da Silva et al., 2016) where typically Pleistocene sediments of appreciable thickness have survived subaerial erosion and later ravinement. In the case of deep shelves, especially those with flat bathymetries, knickpoint migration and shelf erosion is subdued (Posamentier, 2001).

On the Namibian inner shelf there is a significant alongshore component of sediment transfer and accumulation during lowstands, driven in part by the geological controls that were set in place several million years prior. These include the deep shelf break, together with the long-prevailing rocky outcrop that hinders off-shelf sediment transfer and erosion. When coupled to the vigorous wave climate, alongshore sediment dispersal and entrainment into the terrestrial dune cordons has arisen as opposed to a thick shelf, or relatively young cover, sequence. The thin cover sequence of the shelf represents a condensed sequence. Condensed sequences are typically represented by authigenically cemented shell debris, and are associated with transgression, occurring above the wave ravinement surface (Zecchin et al., 2017). In contrast, the condensed sequence from the inner shelf of Hottentot's Bay reflects multiple sea level cycles and is only partly cemented (dolomitised). The surface it rests on is a long-lived, multi-phase subaerial unconformity that has amalgamated with several transgressive ravinement surfaces. Such a stratigraphic architecture may be characteristic of passive margins with wide and deep shelves.

6. Conclusions

Using a high-resolution geophysical approach, and strengthened by evidence from multiple cores of different types, we reveal strong geological control on the evolution of the inner shelf of Namibia offshore Hottentot's Bay. This involves the long-lived inheritance of the same palaeo-land surface (H1) from at least the late Oligocene, with phases of subaerial exposure of the inner shelf during MIS 12, 6 and 1.

On most of the inner shelf, there is limited sediment accumulation, and a notable absence of incised valley fills. Given the wide and deep antecedent shelf morphology that provided suitable accommodation space, the absence of sediment must relate to persistent sediment bypass and suggests that the contemporary onshore diversion of sediment into the Namib Sand Sea may also have been active during lower sea levels with the strong alongshore sediment transport regime.

Where sediment is abundant (> 2 m-thick), most of it is carbonate that accumulated atop the subaerial unconformity in a bedrock-hosted lagoon, sheltered from ravinement by a bedrock sill to seaward. Deposition occurred during MIS 4 and 3, contemporaneous with cementation by dolomite. This in situ binding of sediment further limited accommodation and filling of the H1 depression during more recent phases of transgression e.g. MIS 1.

Condensed sequences, such as this are expected to characterise passive margins with wide and deep shelves. This is especially the case where the shelf break is substantially lower than the lowstands of the Pleistocene, and where there are few topographic irregularities to act as knickpoints along the inner shelf profile.

CRediT authorship contribution statement

A.N. Green: Formal analysis, Funding acquisition, Investigation, Methodology, Project administration, Resources, Software, Supervision, Writing – original draft. **W. Senna:** Formal analysis, Writing – original draft. **J.A.G. Cooper:** Formal analysis, Writing – original draft. **T.**

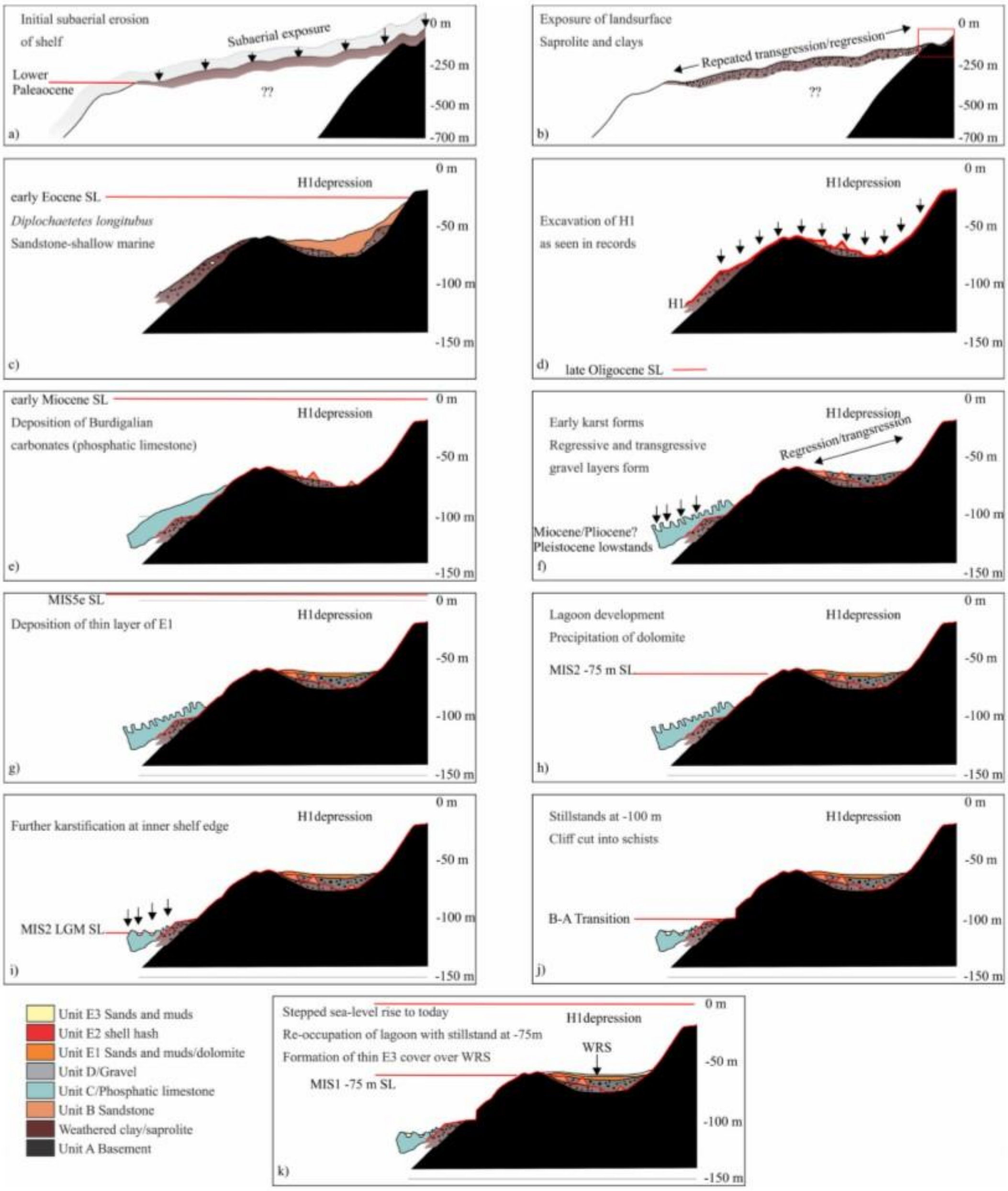

Fig. 14. Evolutionary model of the inner shelf offshore Saddle Hill. a) Regional shelf section showing initial subaerial erosion of the lower Palaeocene. b) development of saprolites and clays, reworking by transgressive/regressive processes notably waves to form mudballs. c) Early Eocene sea level high causing shallow marine flooding of H1 depression, formation of sandstones with reef-building *Diplochaetetes longitubus*. d) Late Oligocene sea level fall causes further excavation of palaeo-shelf and development of the H1 surface. e) Early Miocene sea level high with deposition of Burdigalian phosphatic limestones along inner shelf edge. f) Miocene to Pleistocene lowstands begin to karstify limestone, gravels appear are supplied and are concentrated with repeated regressive/transgressive cycles. At this point, shelf bypass is operating across lowstand cycles and sand is not stored on the inner shelf but transported to Namib Sand Sea. g) During MIS5e, muds and sands accumulate as thin veneer in H1. h) Regression to −75 m with stillstand produces hypersaline, rock-bound lagoon, precipitation of dolomite ensues. i) Further karstification of limestone ensues at LGM. j) A still stand at 100 m forms a cliff into the seaward edge of the schists and quartzites. k) Stepped sea-level rise in the Holocene causes a re-occupation of the lagoon. WRS develops across shelf and some sandy material is preserved due to stepped rises in sea level.

Heeralal: Formal analysis, Investigation, Methodology, Writing – original draft, Writing – review & editing. **H. Labuschagne:** Data curation, Funding acquisition, Project administration, Resources, Supervision, Writing – review & editing.

Declaration of competing interest

The authors declare that they have no known competing financial interests or personal relationships that could have appeared to influence the work reported in this paper.

Data availability

Data are proprietary to Trans Hex Pty Ltd. Due to their sensitive and economic nature, they are not available for public distribution. Queries may be directed to info@transhex.co.za.

Acknowledgements

We are grateful to Trans Hex Marine Pty Ltd. for their logistical and financial support, especially for their permission to publish the data herein. We thank the master, crew and colleagues aboard the MV DP Star during the data collection, especially Kurt Dennis who collected the data and assisted in multibeam processing. Prof. John Compton is thanked for his friendly and helpful discussions surrounding the core set published in 2001. John Pether further assisted with discussions on fossil ages. We especially thank Drs. John Goff, Samuel Johnson and two anonymous reviewers for their helpful and constructive feedback which helped benefit the paper significantly. WS acknowledges an Erasmus Mundus mobility grant to South Africa for his MSc, of which this paper forms part of. This paper forms a contribution to the EU-H2020 funded project iAtlantic Grant agreement No. 818123.

References

Abdul, N.A., Mortlock, R.A., Wright, J.D., Fairbanks, R.G., 2016. Younger Dryas Sea level and meltwater pulse 1B recorded in Barbados reef crest coral Acropora palmata. Paleoceanography 31, 330–344.

Aizawa, M., Bluck, B.J., Cartwright, J., Milner, S., Swart, R., Ward, J., 2000. Constraints on the geomorphological evolution of Namibia from the offshore stratigraphic record. Commun. Geol. Surv. Namibia 12, 337–346.

Aleman, N., Robin, N., Certain, R., Anthony, E.J., Barusseau, J.P., 2015. Longshore variability of beach states and bar types in a microtidal, storm-influenced, low-energy environment. Geomorphology 241, 175–191.

Aquinio Da Silva, A.G., Stattegger, K., Schwarzer, K., Vital, H., 2016. Seismic stratigraphy as indicator of late Pleistocene and Holocene Sea level changes on the NE Brazilian continental shelf. J. S. Am. Earth Sci. 70, 188–197.

Arvidson, R.S., Mackenzie, F.T., 1999. The dolomite problem; control of precipitation kinetics by temperature and saturation state. Am. J. Sci. 299 (4), 257–288.

Baby, G., Guillocheau, F., Morin, J., Ressouche, J., Robin, C., Broucke, O., Dall'Asta, M., 2018. Post-rift stratigraphic evolution of the Atlantic margin of Namibia and South Africa: Implications for the vertical movements of the margin and the uplift history of the South African Plateau. Mar. Pet. Geol. 97, 169–191.

Birch, G.F., 1979. Phosphatic rocks on the western margin of South Africa. J. Sediment. Res. 49 (1), 93–110.

Birch, G.F., Thomson, J., McArthur, J.M., Burnett, W.C., 1983. Pleistocene phosphorites off the west coast of South Africa. Nature 302 (5909), 601–603.

Blanchon, P., Shaw, J., 1995. Reef drowning during the last deglaciation: evidence for catastrophic sea-level rise and ice-sheet collapse. Geology 23 (1), 4–8.

Bluck, B.J., Ward, J.D., Spaggiari, R.I., 2001. Gravel beaches of southern Namibia. Ecol. Geomorpholo. Coast. Shingle. Westbury, Otley 56, 76.

Bluck, B.J., Ward, J.D., Cartwright, J., Swart, R., 2007. The Orange River, southern Africa: an extreme of a wave-dominated sediment dispersal system in the South Atlantic Ocean. J. Geol. Soc. Lond. 164 (2), 341–351.

Bremner, J.M., 1978. Sediments on the Continental Margin off South West Africa between Latitudes 17° and 25° S. PhD Thesis.. University of Cape, Town, Cape Town.

Clemson, W.C., Cartwright, J., Booth, J., 1997. Structural Segmentation and the influence of Basement Structure on the Namibian Passive margin. J. Geol. Soc. Lond. 154 (3), 477–482.

Collina-Girard, J., 1996. Préhistoire et karst littoral: la grotte Cosquer et les Calanques Marseillaises (Bouches-du-Rhone, France). Karstologia 27 (1), 27–40.

Collinson, J., 2019. Sedimentary Structures. Dunedin Academic Press Ltd.

Compton, J.S., Bergh, E.W., 2016. Phosphorite deposits on the Namibian shelf. Mar. Geol. 380, 290–314.

Compton, J.S., Harris, C., Thompson, S., 2001. Pleistocene dolomite from the Namibian shelf: High $^{87}Sr/^{86}Sr$ and $\delta^{18}O$ values indicate an evaporate, mixed water origin. J. Sediment. Res. 71 (5), 800–808.

Compton, J.S., Mulabisana, J., McMillan, I.K., 2002. Origin and age of phosphorite from the last Glacial Maximum to Holocene transgressive succession off the Orange River, South Africa. Mar. Geol. 186, 243–261.

Cooper, J.A.G., 1993. Sedimentation in the cliff-bound, microtidal Mtamvuna Estuary, South Africa. Marine Geol. 112 (1–4), 237–256.

Cooper, J.A.G., Green, A.N., 2016. Geomorphology and preservation potential of coastal and submerged aeolianite: examples from KwaZulu-Natal, South Africa. Geomorphology 271, 1–12.

Cooper, J.A.G., Green, A.N., 2023. Southern African sandy coasts in the context of near-future sea-level rise. Transact. Roy. Soc. South Af. 78, 149–166.

Cooper, J.A.G., Green, A.N., Vital, H., Lima-Filho, F.P., 2019. Geomorphology and clast assemblages of intertidal beachrock: Implications for submerged shoreline preservation. Geomorphology 343, 106–118.

Cooper, J.A.G., Jackson, D.W.T., Dawson, A.G., Dawson, S., Bates, C.R., Ritchie, W., 2012. Barrier islands on bedrock: a new landform type demonstrating the role of antecedent topography on barrier form and evolution. Geology 40 (10), 923–926.

Cooper, J.A.G., Green, A.N., Compton, J.S., 2018. Sea-level change in southern Africa since the last Glacial Maximum. Quat. Sci. Rev. 201, 303–318.

Corbett, I.B., 1993. The modern and ancient pattern of sand flow through the southern Namib deflation basin. Int. Assoc. Sedimentol. Spec. Publ. 16, 45–60.

Corbett, I.B., 1996. A review of diamondiferous marine deposits of western southern Africa. Africa Geosci. Rev. 3, 157–174.

Day, M., Chenoweth, S., 2004. Cockpit Country cone karst, Jamaica. In: Gunn, J. (Ed.), Encyclopedia of Caves and Karst Science. Fitzroy Dearborn, NewYork, pp. 233–235.

De Decker, R.H., 1986. The Geological Setting of Diamondiferous Deposits on the Inner Shelf between the Orange River and Wreck Point, Namaqualand (Master's thesis). University of Cape Town.

Deschamps, P., Durand, N., Bard, E., Hamelin, B., Camoin, G., Thomas, A.L., Henderson, G.M., Okuno, J., Yokoyama, Y., 2012. Ice- sheet collapse and sea-level rise at the Bolling warming 14,600 years ago. Nature 483 (7391), 559–564.

Dieter, K., 1991. Main trends of Palau Islands' coastal evolution, identified by air and ground trothing. Geojournal 24 (1), 77–85.

Dingle, R.V., 1974. Agulhas Bank phosphorites: a review of 100 years of investigation. S. Afr. J. Geol. 77 (3), 261–264.

Dingle, R.V., Hendey, Q.B., 1984. Late Mesozoic and Tertiary sediment supply to the eastern Cape Basin (SE Atlantic) and paleo-drainage systems in south western Africa. Mar. Geol. 56 (1–4), 13–26.

Dingle, R.V., Scrutton, R.A., 1974. Continental breakup and the development of post-Paleozoic sedimentary basins around Southern Africa. Geol. Soc. Am. Bull. 85 (9), 1467–1474.

Dingle, R.V., Sessier, W.G., Newton, A.R., Balkema, A.A., 1983. Mesozoic and Tertiary Geology of Southern Africa, p. 375.

Dladla, N.N., Green, A.N., Cooper, J.A.G., Humphries, M.S., 2019. Geological inheritance and its role in the geomorphological and sedimentological evolution of bedrock-hosted incised valleys, lake St Lucia, South Africa. Estuar. Coast. Shelf Sci. 222, 154–167.

Dladla, N.N., Green, A.N., Humphries, M.S., Cooper, J.A.G., Godfrey, M., Wright, C.I., 2022. Back-barrier evolution and along-strike variations in infilling of the Kosi Bay lake system, South Africa. Estuar. Coast. Shelf Sci. 272, 107877.

Engelbrecht, L.D., Green, A.N., Cooper, J.A.G., Mackay, C.F., 2022. Antecedent geological control on transgressive delta and shoreline preservation: Examples from the SE African shelf. Marine Geol. 454, 106934.

Fairbanks, R.G., 1989. A 17,000-year glacio-eustatic sea level record: influence of glacial meltin rates on the Younger Dryas event and deep-ocean circulation. Nature 342 (6250), 637–642.

Flemming, B.W., 1977. Langebaan Lagoon: a mixed carbonate-siliciclastic tidal environment in a semi-arid climate. Sediment. Geol. 18 (1–3), 61–95.

Ford, D., Williams, P., 2007. Introduction to karst. Karst Hydrogeol. Geomorphol. 1–8.

Garzanti, E., Dinis, P., Vermeesch, P., Andò, S., Hahn, A., Huvi, J., Limonta, M., Padoan, M., Resentini, A., Rittner, M., Vezzoli, G., 2018. Sedimentary processes controlling ultralong cells of littoral transport: Placer formation and termination of the Orange sand highway in southern Angola. Sedimentology 65, 431–460.

Gladczenko, T.P., Hinz, K., Eldholm, O., Meyer, H., Neben, S., Skogseid, J., 1997. South Atlantic volcanic margins. J. Geol. Soc. Lond. 154 (3), 465–470.

Green, A.N., Cooper, J.A.G., Leuci, R., Thackeray, Z., 2013. Formation and preservation of an overstepped segmented lagoon complex on a high-energy continental shelf. Sedimentology 60 (7), 1755–1768.

Green, A.N., Cooper, J.A.G., Salzmann, L., 2014. Geomorphic and stratigraphic signals of postglacial meltwater pulses on continental shelves. Geology 42, 151–154.

Green, A.N., Cooper, J.A.G., Dlamini, N.P., Dladla, N.N., Parker, D., Kerwath, S.E., 2020. Relict and contemporary influences on the postglacial geomorphology and evolution of a current swept shelf: the Eastern Cape Coast, South Africa. Mar. Geol. 427, 106230.

Guillocheau, F., Rouby, D., Robin, C., Helm, C., 2012. Quantification and causes of the terrigeneous sediment budget at the scale of a continent margin: a new method applied to the Namibia-South Africa margin. Basin Res. 24, 3–30.

Gunn, J., 2004. Encyclopedia of Caves and Karst Science. Taylor and Francis, 2004.

Hallam, C.D., 1964. The geology of the coastal diamond deposits of southern Africa (1959). The Geology of some Ore Deposits of Southern Africa. Geol. Soc. South Afr. Johannesburg 2, 671–728.

Hapke, C.J., Lentz, E.E., Gayes, P.T., McCoy, C.A., Hehre, R., Schwab, W.C., Williams, S. J., 2010. A review of sediment budget imbalances along Fire Island, New York: can nearshore geologic framework and patterns of shoreline change explain the deficit? J. Coast. Res. 26 (3), 510–522.

Higgins, C.G., Coates, D.R., 1990. Groundwater Geomorphology: The Role of Subsurface Water in Earth-Surface Processes and Landforms. Geological Society of America, p. 252.

Inthorn, M., Mohrholz, V., Zabel, M., 2006. Nepheloid layer distribution in the Benguela upwelling area offshore Namibia. Deep-Sea Res. I Oceanogr. Res. Pap. 53 (8), 1423–1438.

Ishiwa, T., Yokoyama, Y., Okuno, J.I., Obrochta, S., Uehara, K., Ikehara, M., Miyairi, Y., 2019. A sea-level plateau preceding the Marine Isotope Stage 2 minima revealed by Australian sediments. Sci. Rep. 9 (1), 1–8.

Jacob, J., 2005. The Erosional and Cenozoic Depositional History of the Lower Orange River, Southwestern Africa (Doctoral dissertation). University of Glasgow.

Jacob, J., Ward, J.D., Bluck, B.J., Scholz, R.A., Frimmel, H.E., 2006. Some observations on the diamondiferous bedrock gully trapsites on late Cainozoic, marine cut-platforms of the Sperrgebiet, Namibia. Ore Geol. Rev. 28 (4), 493–506.

James, N.P., Choquette, P.W., 1988. Paleokarst. Springer-Verlag, New York.

Jennings, J.N., 1985. 1985. Karst Geomorphology. Basil Blackwell Inc., New York, p. 293.

Kan, H., Urata, K., Nagao, M., Hori, N., Fujita, K., Yokoyama, Y., Nakashima, Y., Ohashi, T., Goto, K., Suzuki, A., 2015. Submerged karst landforms observed by multibeam bathymetric survey in Nagura Bay, Ishigaki Island, southwestern Japan. Geomorphology 229, 112–124.

Kiernan, K., 1994. The coastal tower karst of Phang Nga Bay. In: International Symposium on the Exploitation and Protection of Karst and Cave Scenic Tourist Resources (pp. 9-21).

Kirkpatrick, L.H., Green, A.N., 2018. Antecedent geologic control on nearshore morphological development: the wave dominated high sediment supply shoreface of southern Namibia. Mar. Geol. 403, 34–47.

Kirkpatrick, L.H., Green, A.N., 2021. Mapping diamondiferous palaeo-shorelines in complicated terrain: seismic and GIS-based methods from the inner shelf of southern Namibia. Geo-Mar. Lett. 41 (3), 1–18.

Kirkpatrick, L.H., Green, A.N., Pether, J., 2019a. The seismic stratigraphy of the inner shelf of southern Namibia: the development of unusual nearshore shelf stratigraphy. Mar. Geol. 408, 18–35.

Kirkpatrick, L.H., Jacob, J., Green, A.N., 2019b. Beaches and bedrock: how geological framework controls coastal morphology and the relative grade of a Southern Namibian diamond placer deposit. Ore Geol. Rev. 107, 853–862.

Lancaster, N., Ollier, C.D., 1983. Sources of sand for the Namib sand sea. Z. Geomorphol. 45, 75–83.

Lankford, R.R., 1977. Coastal lagoons of Mexico and their origin and classification. In: Wiley, M. (Ed.), Estuarine Processes, vol. 2. Academic Press, New York, pp. 182–215.

Lentz, E.E., Hapke, C.J., 2011. Geologic framework influences on the geomorphology of an anthropogenically modified barrier island: assessment of dune/beach changes at Fire Island, New York. Geomorphology 126 (1–2), 82–96.

Liu, J.P., Milliman, J.D., 2004. Reconsidering melt-water pulses 1A and 1B: global impacts of rapid sea-level rise. J. Ocean Univ. China 3 (2), 183–190.

Liu, J.P., Milliman, J.D., Gao, S., Cheng, P., 2004. Holocene development of the Yellow River's subaqueous delta, North Yellow Sea. Mar. Geol. 209 (1–4), 45–67.

Lodewyks, T., 2010. Seismic Stratigraphy of Upper Pleistocene Gravel and Holocene Mudbelt Deposits Between Wreck Point and the Kamma River on the Western Shelf of South Africa. University of Cape Town (Unpublished MSc).

McMullen, K.Y., Poppe, L.J., Parker, C.E., 2015. Character, distribution, and ecological significance of storm wave-induced scour in Rhode Island Sound, USA. Geo-Mar. Lett. 35 (2), 135–144.

Miller, K.G., Kominz, M.A., Browning, J.V., Wright, J.D., Mountain, G.S., Katz, M.E., Sugarman, P.J., Cramer, B.S., Christie-Blick, N., Pekar, S.F., 2005. The Phanerozoic record of global sea-level change. Science 310, 1293–1298.

Mukhopadhyay, S., Sen, A., Koley, A., Samanta, P., 2022. Evaluating the formative and shape-controlled dispersive mechanisms of mud balls in a low-energy coastal setting: New insights. Geol. J. 57 (3), 925–949.

Murakoshi, N., Masuda, F., 1992. Estuarine, barrier-island to strand-plain sequence and related ravinement surface developed during the last interglacial in the Pale-Tokyo Bay, Japan. Sediment. Geol. 80 (3–4), 167–184.

Murray, L.G., Joynt, R.H., O'Shea, D.O.C., Foster, R.W., Kleinjan, L., 1970. The Geological Environment of some Diamond Deposits off the Coast of South West Africa. HM Stationery Office.

Navy, SA, 2021. 2021 South African tide tables. South African Hydrographic Office.

Paskoff, R.P., 2005. Karst coasts. In: Schwartz, M.L. (Ed.), Encyclopedia of Coastal Science. Springer, Dordrecht, pp. 581–586.

Pether, J., Roberts, D.L., Ward, J.D., 2000. Deposits on the West Coast. Oxf. Monogr. Geol. Geophys. 40, 33–54.

Pickford, M., Senut, B., 2002. The Fossil Record of Namibia. Geological Survey of Namibia, Windhoek, Namprint, pp. 39–pp.

Posamentier, H.W., 2001. Lowstand alluvial bypass systems: incised vs. unincised. AAPG Bull. 85 (10), 1771–1793.

Pretorius, L., Green, A.N., Cooper, J.A.G., 2018. Submerged beachrock preservation in the context of wave ravinement. Geo-Mar. Lett. 38 (1), 19–32.

Qiu, X., Wang, H., Yao, Y., Duan, Y., 2017. High salinity facilitates dolomite precipitation mediated by Haloferax volcanii DS52. Earth Planet. Sci. Lett. 472, 197–205.

Riggs, S.R., Cleary, W.J., Snyder, S.W., 1995. Influence of inherited geologic framework on barrier shoreface morphology and dynamics. Mar. Geol. 126 (1–4), 213–234.

Rodero, J., Pallarés, L., Maldonado, A., 1999. Late Quaternary seismic facies of the Gulf of Cadiz Spanish margin: depositional processes influenced by sea-level change and tectonic controls. Mar. Geol. 155 (1–2), 131–156.

Rogers, J., 1977. Sedimentation on the Continental Margin off the Orange River and the Namib Desert (Unpubl PhD. thesis). University of Cape Town.

Rogers, J., Li, X.C., 2002. Environmental impact of diamond mining on continental shelf sediments off southern Namibia. Quat. Int. 92 (1), 101–112.

Rogers, J., Rau, A.J., 2006. Surficial sediments of the wave-dominated Orange River Delta and the adjacent continental margin off South-Western Africa. Afr. J. Mar. Sci. 28 (3–4), 511–524.

Runds, M.J., Bordy, E.M., Pether, J., 2019. Late Quaternary sedimentological history of a submerged gravel barrier beach complex, southern Namibia. Geo-Mar. Lett. 39 (6), 469–491.

Salzmann, L., Green, A.N., Cooper, J.A.G., 2013. Submerged barrier shoreline sequences on a high energy, steep and narrow shelf. Mar. Geol. 346, 366–374.

Scheffers, A.M., Scheffers, S.R., Kelletat, D.H., 2012. The Coastlines of the World with Google Earth. Springer, Dordrecht, p. 293p.

Schwab, W.C., Baldwin, W.E., Denny, J.F., Hapke, C.J., Gayes, P.T., List, J.H., Warner, J. C., 2014. Modification of the Quaternary stratigraphic framework of the inner-continental shelf by Holocene marine transgression: an example offshore of Fire Island, New York. Mar. Geol. 355, 346–360.

Shawler, J.L., Ciarletta, D.J., Connell, J.E., Boggs, B.Q., Lorenzo-Trueba, J., Hein, C.J., 2021. Relative influence of antecedent topography and sea-level rise on barrier-island migration. Sedimentology 68, 639–669.

Siesser, W.G., Dingle, R.V., 1981. Tertiary Sea-level movements around southern Africa. J. Geol. 89, 523–536.

Spaggiari, R.I., Bluck, B.J., Ward, J.D., 2006. Characteristics of diamondiferous Plio-Pleistocene littoral deposits within the paleo-Orange River mouth, Namibia. Ore Geol. Rev. 28 (4), 475–492.

Spratt, R.M., Lisiecki, L.E., 2016. A late Pleistocene sea level stack. Clim. Past Discuss. 11 (4), 3699–3728.

Stattegger, K., de O. Caldas, L.H., Vital, H., 2006. Holocene coastal evolution of the northern Rio Grande do Norte Coast, NE Brazil. J. Coast. Res. 151–156.

Stevenson, I.R., McMillan, I.K., 2004. Incised valley fill stratigraphy of the Upper cretaceous succession, proximal Orange Basin, Atlantic margin of southern Africa. J. Geol. Soc. Lond. 161 (2), 185–208.

Stocken, C.G., 1978. A Review of the Later Mesozoic and Cenozoic Deposits of the Sperrgebiet (COM Geological Department internal report). Namdeb Diamond comproration(Pty) Ltd., Oranjemund, Namibia.

Stone, A.E.C., 2013. Age and dynamics of the Namib Sand Sea: A review of chronological evidence and possible landscape development models. J. Af. Earth Sci. 82, 70–87.

Suric, M., 2002. Submarine karst of Croatia – evidence of former lower sea levels. Acta Carsol. 31 (3), 89–98.

Sweeting, M.M., 1973. Karst Landforms and limestones. S. Afr. Geogr. J. 55 (1), 81–88.

Tanner, L., 1996. Armoured mud balls revisited. Atl. Geol. 32 (2), 123–125.

Tinker, J., De Wit, M., Brown, R., 2008. Linking source and sink: evaluating the balance between onshore erosion and offshore sediment accumulation since Gondwana break-up, South Africa. Tectonophysics 455 (1–4), 94–103.

Waltham, T., Hamilton-Smith, E., 2004. Ha Long Bay, Vietnam. In: Gunn, J. (Ed.), Encyclopedia of Caves and Karst Science, pp. 413–414.

Williams, P., 2004. Dolines. In: Gunn, J. (Ed.), Encyclopedia of Caves and Karst Science, pp. 304–310.

Wright, C.I., Miller, W.R., Cooper, J.A.G., 2000. The late Cenozoic evolution of coastal water bodies in Northern KwaZulu-Natal, South Africa. Mar. Geol. 167 (3–4), 207–229.

Yokoyama, T., Purcell, A., Marshall, J.F., Lambeck, K., 2006. Sea-level during the early deglaciation period in the Great Barrier Reef, Australia. Glob. Planet. Chang. 53 (1–2), 147–153.

Zecchin, M., Catuneanu, O., 2013. High-resolution sequence stratigraphy of clastic shelves I: units and bounding surfaces. Mar. Pet. Geol. 39, 1–25.

Zecchin, M., Ceramicola, S., Gordini, E., Deponte, M., Critelli, S., 2011. Cliff overstep model and variability in the geometry of transgressive erosional surfaces in high-gradient shelves: the case of the Ionian Calabrian margin (southern Italy). Mar. Geol. 281 (1–4), 43–58.

Zecchin, M., Catuneanu, O., Caffau, M., 2017. High-resolution sequence stratigraphy of clastic shelves V: criteria to discriminate between stratigraphic sequences and sedimentological cycles. Mar. Pet. Geol. 85, 259–271.

Zecchin, M., Catuneanu, O., Cafau, M., 2019. Wave-ravinement surfaces: classification and key characteristics. Earth Sci. Rev. 188, 210–239.

Appendix 2

Publication in review titled "Anatomy and stratigraphic evolution of a shelf bypass valley system" by, Green, A.N., Meltzer, L., Cooper, J.A.G., Heeralal, T., Labuschagne, H.

Anatomy and stratigraphic evolution of a shelf bypass valley system

Andrew Green[1,2], Liam Meltzer[1], Andrew Cooper[1,2], Herman Labuschagne[3], Tamera Heeralal[1,3]

[1]*Geological Sciences, University of KwaZulu-Natal, Private Bag X54001, Durban, South Africa*

[2]*School of Geography and Environmental Science, Ulster University, Cromore Road, Coleraine Northern Ireland, BT52 1SA, United Kingdom*

[3]*Trans Hex Marine, 19 Chain Avenue, Montague Gardens, Cape Town, 7441, South Africa*

ABSTRACT

The stratigraphic architecture and evolution of a bypass alluvial valley system on the wide and deep Namibian shelf is investigated using a dense, pseudo-3D grid of ultra high-resolution sub-bottom profiler data, high-resolution multibeam and backscatter data, and more than 4900 cores, is used to investigate. The channel morphology is defined by changes in terrain slope, with steeper slopes hosting more sinuous and narrower channels. It does not conform to existing morphodynamic channel classification schemes. Nine seismic units were identified in the < 10 m-thick fill. Acoustic basement of the area comprises Precambrian gneisses and schists of the Namaqua Metamorphic province, and schists, phyllites and quartzites of the Gariep belt. These crop out on the shelf and form the framework within which the valley is located. A subaerial unconformity developed during an episode of Late Campanian hinterland uplift during which the channel system was initiated.

The basal fills of the channels (Units B and C) comprise weathered and reworked derivatives of Unit A, namely saprolites and balls of mudrock that were reworked by tidal and wave processes. These represent a long-term hiatus (weathering episode and landscape exposure of the Lower Palaeocene), followed by the transgressive flooding and filling of the channels during surfzone migration. After a subsequent hiatus shallow marine sandstones were deposited during the Early Eocene. The remaining valley fill comprises unconsolidated sediment of varying size classes. A gravel body (granules to boulders) dominates this fill, and represents initial fluvial deposition, followed by reworking during multiple phases of transgression and regression up to and including the Holocene. The capping succession of sands and muds represents the modern sediments of the shoreface and shelf, however, these are constrained to the original valley form and reflect strong geological control and lack of accommodation on the valley interfluves.

The fill succession and architecture of this shelf bypass valley contrast markedly with incised valley fills, where multiple regressive transgressive cycles form compound valleys. It developed over a much longer period of geologic time, is dominated by transgressive sediments and stratigraphic surfaces, is exceptionally thin and lacks multiple incisions. The lack of connection to a terrestrial drainage system for at least the past million years has contributed to the lack of incision and scour of accumulated sediment during lowstands.

Such a sequence in the geologic record could easily be misinterpreted if the overall valley depositional setting was not recognised. Given the occurrence of many contemporary low gradient and deep shelves along passive margins globally, as well as in the geologic record, such systems are probably more common than presently thought.

INTRODUCTION

The conditions required for incised valleys to form relate to three main variables. The first is associated with a decline in base level or sea level, whereby the palaeo-shelf is exposed to subaerial processes of erosion (Allen and Posamentier, 1993; Zaitlin et al., 1994). If the palaeo-shelf gradient is considerably steeper than the adjacent palaeo-alluvial plain, valley incision will commence (Posamentier, 2001). This invariably relates to the crossing of a topographic threshold, where a knickpoint is formed and upslope erosion of the valley can begin (Schumm, 1988). Valley incision will not take place if the shoreline trajectories migrate over palaeo-surfaces where the gradient is lower or equivalent to that of the palaeo-alluvial plain (Posamentier, 2001) and no knick-point is present. In such instances, lowstand alluvial systems will develop, however, most of the fluvial sediment load bypasses the shelf and non-incised bypass systems will form (Posamentier, 2001). In such systems the relationships between incision, available accommodation, and infilling that mark simple (single-incision) or complex (multi-incision) systems preclude the development of typical tripartite facies models of incised valley fills (sensu Zaitlin et al., 1994). Unlike traditional incised valleys, that can extend from submarine canyon heads to highstand shorelines, these systems are typically confined to the inner shelf as the drop in sea level does not reach the shelf edge, resulting in re-incision (Posamentier, 2001).

A second factor, independent of shelf gradient, involves tectonic mechanisms such as hinterland tilting or uplift (Humphrey and Conrad, 2000). This may increase stream flows, and also cause valley incision, though these are uncommon in sites where the predominant changes to base level are driven by glacio-eustasy over the Pleistocene. The third factor involves underfit streams where a small channel settles over a previously larger channel formed during higher fluvial discharges (e.g. Blum, 1990; 1993; Blum and Valastro (1989). The result is a river occupying a valley with characteristics of incision extending across the entire valley (Posamentier, 2001). These may relate to changes to climate and the regional rainfall patterns of an area. Of these three mechanisms, the first is most common on passive margins, and of those examples, almost all valleys are considered to fall into the 'incised' as opposed to 'bypass' category.

Conditions for formation of bypass valleys are likely to have existed through geologic time and the recognition and correct interpretation of such systems requires the documentation of modern analogues of which there are few. Here we discuss a valley preserved on the wide and deep Namibian shelf (Fig. 1) and examine its stratigraphic architecture and evolution in high spatial resolution. The remarkable depth of the shelf break (~ 500 m) means that it was not intersected during the sea level falls of the Pleistocene, and instead, bypassing conditions prevailed over multiple highstand and lowstand periods. This provides a unique opportunity to examine the stratigraphy of such a bypass system in detail, and to provide comparisons to valley incision models.

REGIONAL SETTING

The study area is located on the inner continental shelf offshore Hottentot's Bay, ~ 55 km north of Luderitz, Namibia (Fig. 1). Here, the volcanic continental margin of Namibia has one of the widest and most extensive shelves in the world, with a shelf break below 500 m and located ~ 230 km offshore (Kirkpatrick et al., 2019). The shelf geology consists of Late Jurassic to Early Cretaceous syn-rifted siliciclastic and volcanic sequences underlain by Proterozoic rifted continental basement. These are overlain by a clastic, post-rifted sediment wedge 3-5 km thick (Aizawa et al., 2000) that thins landward. Prolonged rifting during the Permo-Triassic formed the main basins of SW Africa, with the northward break up of Gondwana in the Early Cretaceous developing the continental margin (Maslanyj et al., 1992). Crustal extension of the South Atlantic lead to the development of three post-rift depocenters (the Orange, Luderitz and Walvis Basins) elongated to the west and parallel to the continental margin (Bluck et al., 2007; Maslanyj et al., 1992). These basins become inverted during the Late Cretaceous to Early Cenozoic (Bluck et al., 2007), associated with phases of hinterland uplift in the Late Campanian (Guillocheau et al., 2012) (Fig. 2a), the Lower Palaeocene and the Middle Oligocene (Fig. 2a). Some authors consider these to comprise one main pulse of uplift spanning 93.5 to 66.5 Ma that followed a phase of margin retrogradation 131–93.5 Ma (Baby et al., 2018). The shelf break, as reflected in the modern day, is a relic of the Late Campanian uplift (Baby et al., 2018), superimposed by a Late Oligocene unconformity formed by a less prominent phase of hinterland uplift (Baby et al., 2018). The modern shelf is now characterised by a shallow inner shelf, up to 130 m depth, with a low gradient outer shelf terminating at -500 m.

The local geology of the inner shelf comprises Precambrian-age outcrops of gneisses and schists of the Namaqua Metamorphic Complex (Compton et al., 2001) and schists, phyllites and quartzites of the Gariep Belt. These are overlain by a thin unconsolidated cover sequence of Pleistocene to Holocene sandstones, gravels, sands and muds (Rau, 2003). In some places, reworked clays and saprolites, derived from weathering of the two metamorphic units, are apparent in subcrop (Senna et al., in press). The geology relates to repeated regression and transgression cycles that reworked and redeposited these materials on top of the shallow Precambrian basement

(Senna et al., in press). Sea levels, initially driven by tectono-eustatic mechanisms, and then later by glacio-eustatic processes, ranged from ~ 180 m above current sea levels during an Eocene high to ~ 120 m below current sea levels during the Pleistocene lowstands, including the Last Glacial Maximum (LGM) (Fig. 2b and c) (Kirkpatrick et al., 2021). The most recent transgression is characterised by a step-wise pattern of still or slow stand, interspersed with rapid pulses of sea-level rise, termed meltwater pulses (MWPs-Fig. 2c) (Cooper et al., 2018; Runds et al., 2019). Evidence for both MWP1A and MWP1B exist in the area (Cooper et al., 2018; Runds et al., 2019; Senna et al., in press), with overstepped barriers, incised valleys, lagoons and cliff features marking palaeo-shorelines that were preserved during periods of rapid sea-level rise.

Now, as in the past, the drainage system of the Orange - Vaal river system has been the main conduit of sediment from southern Africa, draining the interior plateau of the region (Bremner et al. 1990). During Cretaceous times and associated with hinterland uplift, the lower section of the Orange River incised deeply into the landscape and has delivered vast quantities of sediment to the SW African margin. Despite a reduction in the rate of sediment delivery to the margin in the Cenozoic (Guillocheau et al., 2012), the Orange River has continued to be the dominant sediment source to the southern Namibian coastline (Jacob, 2005). By the middle Eocene, it had entrenched its meandering form into the bedrock, fixing the mouth in approximately its present position (Jacob, 2005; Bluck et al, 2007; Kirkpatrick and Green, 2018) to form a subaqueous wave-dominated delta offshore Oranjemund, 320 km to the south. Unlike the Orange River, little is known of the smaller fluvial systems that drained the escarpment since the margin formed. This is especially complicated in areas such as Hottentot's Bay, where the adjacent coast and alluvial plain are blanketed by the Namib Desert Sand Sea (Fig. 1), a vast accumulation of unconsolidated sand that has obscured the underlying geomorphology from Luderitz to Walvis Bay (Lancaster and Ollier, 1983; Corbett, 1996; Bluck et al, 2007).

The hydrodynamics of the coast are characterised by a microtidal regime (1.8 m range) and year-round high wave energies (Hay and Brock, 1992). Short period waves that range between 0.75 - 3.25 m develop from strong SE winds and superimpose on the South Atlantic SW swell at a height of > 3 m (Kirkpatrick et al., 2019b). The wave base averages a depth of ~ 40 m but can extend to ~ 110 m under storm conditions (Kirkpatrick et al., 2019b). This hydrodynamic regime has persisted since at least Eocene times (Bluck et al., 2007).

Sediment transported into the system is distributed by several oceanic currents and longshore drift systems along the northward and westward sections of the coastline (Bluck et al., 2007). Since the truncation and uplift of southern Africa during the late Cretaceous to early Cenozoic era, sand, gravel and mud have each had separate distribution routes into the ocean at different rates depending on the time period (Bluck et al., 2007). Most of the sandy material is distributed northwards and alongshore by oblique waves. In some instances, sand is transported onshore to feed the Namib Sand Sea and smaller dune fields (Corbett, 1996; Kirkpatrick et al., 2021). Mud is more extensively distributed along the north, south and west sections of the continental shelf, driven by slow-moving oceanic currents, while gravel was accumulated for over 300 km north of the Orange River mouth due to direct onshore wave reworking of the coarsest littoral components (Bluck et al., 2007; Spaggiari and Bordy, 2023).

METHODS

Bathymetry, backscatter and sub-bottom profiling

Ultra-high-resolution sub-bottom data and high-resolution multibeam bathymetry were collected aboard the MV DP Star during a single survey campaign in January and February 2018. A high-resolution Kongsberg EM 710 multibeam echosounder coupled to a Kongsberg Seapath 200 IMU and C-Nav 3050 DGPS were used to collect the bathymetry and backscatter data described in this paper. Sound velocity variations in the water column were corrected using a Valeport Midas Mini Sound Velocity Profiler.

Sub-bottom data were recorded using a TOPAS PS120 parametric sub-bottom profiler triggered in CW burst mode with a frequency between 2 and 8 kHz. The data were bandpass filtered using the Kongsberg SBP utility and exported as SEGY format for further processing and interpretation in Allworks Geosuite. The grid distance between each recorded line was spaced on average 100 m apart, with the majority of lines separated by a distance of 50 m or less.

A total of 132 North-South and 504 East-West orientated sub-bottom profiles were incorporated into the Geosuite project where they were bottom tracked. Trace mixing, time varied gain, and swell filtering were applied to each line. Where possible, each significant seismic stratigraphic horizon was digitised using a sound velocity of 1500 $m.s^{-1}$ for seawater and 1600 $m.s^{-1}$ for sediments. The sediment isopach and bedrock terrain models were constructed from the digitized data and gridded in Golden Surfer 12 and combined with the bathymetry where rock was seen to crop out using Global Mapper.

Lithological data

To reconcile the seismic stratigraphy with the regional lithostratigraphy, core logs of lithological wells drilled between 2017 and 2021 were incorporated into Geosuite. A total of 4908 drill holes were integrated with the seismic stratigraphy. Each well was drilled using a subsea reverse circulation (RC) 5 m^2 drill tool capable of operating to -180 m water depth and reaching penetration depths up to 12 m into the seabed. Due to the often-sporadic nature of the various seismic units observed, and the occasional poor data resolution due to rough sea conditions, the individual lithological unit distribution and thickness were used to produce the isopach maps of the main seismo-lithologic units. The data were gridded in Golden Surfer 12 together with the seismic stratigraphic picks.

RESULTS

Seafloor geology

The acoustic facies of the study area are dominated by areas of high-relief, high-backscatter seafloor (Fig. 3). The landward portions are slightly more irregular in backscatter tone, with multiple irregular coast-oblique ridges of high backscatter (Fig. 3a). These are intersected by linear features composed of low backscatter. To seaward, the higher backscatter facies have ridges that are less pronounced than the former high relief facies and which are orientated coast-parallel, with a series of intersecting lineaments of low, even-toned backscatter (Fig. 3b).

The high backscatter areas are separated by areas of smooth, even-toned backscatter, with occasional zones of mottled higher backscatter and rippled texture (Fig. 3a). Occasionally interspersed within the smooth even-toned areas, and between areas of high backscatter, are moderate backscatter, high-relief features that create linear seafloor features (Fig. 3c).

The shallower more landward, high-backscatter zones represent the seaward extension of the schists, quartzites and gneisses of the Namaqua Metamorphic Complex basement that crops out along the coastline of the study area (Geological Map of Namibia 1:250 000 sheet 2615 and 2514). The more seaward, higher backscatter zones relate to outcrop of schists, phyllites and quartzites of the Gariep Belt. Both materials form the pre-valley basement to the study in which the valley system now lies. The low, even toned backscatter represents recent shelf muds and sands that drape the low points of the hard rock basement and fill fractures in the bedrock surfaces (the low backscatter lineaments). The occasional mottled backscatter represents coarser gravelly or sandy material that often occurs in association with the rocky seabed. Based on drill samples, the moderate backscatter and high relief features are interpreted as sandstones that crop out between the main bedrock outcrop. The outline of the valley is thus represented clearly by the distribution of the lower backscatter facies that is indicative of soft sediment.

Seismic and lithostratigraphic units

Table 1 is a summary of the acoustic properties (surfaces-Fig. 4; units Figs. 5-9) and lithologies (Fig. 10) of the seismic units identified in the area. A total of 9 units (A-I) were identified. Figure 11 details the seismic and lithological unit distributions.

Surface 1

Surface 1 represents the main unconformity surface in the area and marks the division between the mostly unconsolidated sediments and underlying harder rock geology and derivatives thereof. Figure 4 illustrates the overall framework of the underlying valley surfaces formed in Surface 1, together with the overlying packages of sediment (Fig. 4b). Surface 1 forms a dendritic valley system that increases in relief to landward (Fig. 4d), with the main trunk directed to the south at its most seaward extent. The channels of the valley system are mostly narrow and shallow, up to 800 m wide and ≤ 15 m deep (Table 1); their interfluves and floors comprise exposed bedrock of both Namaqua Metamorphic Complex schists and gneisses, and the schists of the Gariep Belt (Fig. 4d). The interfluves are rugged, with steep sides (up to 10°), that contrast with the flat (~ 1°) valley floors (Fig. 4c). The valley is best developed in schists in water depths of 50 m to 100 m, where the valley form is more deeply incised and narrow (Fig. 4d). The system widens to seaward, becoming less incised at a bedrock knickpoint at -100 m, which marks the contact between Gariep Belt outcrop to seaward and Namaqua Metamorphic Complex outcrop to landward (Fig. 3; 4d). The main channel trunks range in sinuosity from 1.2 (winding) to 1.8 (meandering), with the more sinuous features hosted in schists (Table 1). The ratio of channel width to depth averages 0.01, with higher ratios observed from the schist-hosted channels.

Pre-valley geology (Unit A)

Unit A is the lowermost unit observed in the seismic data. The internal reflections are high amplitude and chaotic, though the strong return by the upper surface of the unit masks the underlying stratigraphic architecture (Figs. 5-9). Unit A comprises Namaqua Metamorphic Complex schists (Fig. 10a), represented by the high-relief, high backscatter seafloor facies (Fig. 3).

Despite being discernible from its surface characteristics (see figure 3), the schists and quartzites of the Gariep Belt (Fig. 10b) are indistinguishable in seismic reflection from the Namaqua Natal Complex varieties. They are thus consolidated with Unit A in terms of seismic stratigraphy.

Post incision geology

Unit B and C (Saprolite and reworked mudstone). Overlying the schists and mudstones, two distinct units of weathering residue occur along the valley floors, the thicknesses of which are at the very limits of the seismic resolution (~ 20 cm). The weathering residues comprise saprolites (Unit B) and muddy material (Unit C). Both have indistinct, low amplitude flat-lying reflections (Figs. 5-9). In the landward portions of the area, the muddy materials are disaggregated and comprise subangular light grey pebble-sized blocks of firm clay (Fig. 10c), together with rounded cobble sized clasts of light brown kaolinite clay that co-occur with schist fragment-embedded saprolite (Fig. 10d). Both deposits may form rods through to spheres. To the west of the area, the weathering residues are exclusively cobble to pebble-sized, light grey rounded balls of clay (Fig. 10e). Both saprolites and clays occur throughout the study area in a widespread fashion (Fig. 11b).

Unit D (Sandstone). Unit D is characterised by low to medium frequency, low amplitude, continuous reflections that downlap surface 1. The internal reflection configuration is sub-parallel and its overall geometry varies significantly with a peaked, higher relief upper surface (Fig. 5). The unit is confined to the western and south-western offshore portions of the study area (Fig. 11c), where drill cores reveal it to comprise a fossiliferous sandstone containing abundant tubes of the polychaete *Diplochaetetes longitubus* and bored by *Trypanites sp* (Fig. 10f).

Unit E (Lower sand). Unit E is dominated by low amplitude, medium to high frequency reflections. This package may comprise sub-parallel continuous packages of reflections or small-scale hummocky clinoform patterns concordant to the underlying surface 1 or 2. The unit thins seaward from a maximum thickness of 0.7 m and throughout the valley system (Fig. 11d). Core data reveal this to comprise a sandy unit with occasional shell debris. The surface separating Unit E and F is indistinct in the sub-bottom data and most often can be identified as a weakly reflective, low amplitude low relief reflector (Fig. 5-9).

Unit F (Gravel). Unit F is found throughout the study area, forming a continuous package of low to medium frequency and higher amplitude chaotic reflections (Figs. 5-9). The unit thins to landward, with the thickest accumulations found at the confluences of tributaries and along the outer bends of well-developed meanders (Fig. 11e). Where the trunk is directed coast-parallel, a set of deposits $\leq$ 2.5 m-thick occur.

The unit comprises a variety of gravel-sized materials, including cobbles, pebbles and granules. These are commonly composed of quartz and/or quartzites, along with a variety of gemstones such as jasper and agate (Fig. 10g). Towards the east, there is a notable increase in the bioclastic component of the deposit (Fig. 10h).

It is not possible to differentiate between the size classes from the seismic reflection alone, however, their distributions can be assessed from the dense core data. Gravel deposits of all size classes thicken to seaward with localised small pockets of thicker accumulation (Fig. 11f-h).

Unit G and Unit H (Shell hash, upper sand and mud). The upper boundary of the gravels is marked by WRS, a low to moderate amplitude erosional surface. This surface corresponds to a sporadic shell hash of whole and broken *Phacoides saldanhae* bivalves and fragmented *Lugubrilaria lugubris* gastropods. This shell hash occurs throughout the valley system (Fig. 10i) and forms localised accumulations up to 1.5 m-thick (Fig. 11i). The shell hash is overlain by Unit G, a sub-parallel to wavy package of moderate amplitude reflections that can form shingled mounds in the stratigraphy (Fig. 8). This unit corresponds to a sand layer sporadically distributed throughout the valley system (Fig. 11j), over which the alternating high and low amplitude, parallel reflections of Unit H are deposited. Unit H represents relatively fine-grained deposits of sand and mud, as reflected in the modern sediment distribution of the seafloor (Fig. 3). The upper sand unit is mostly restricted to the seaward parts of the inner shelf, in the coast-parallel valley trunk (Fig. 11k). The mixed sand/mud of the uppermost sediment package forms an up to 4 m-thick package that caps the valley fill and is restricted to the valley itself. In the main valley tributaries this unit thickens landwards.

DISCUSSION

Overview

The data reveal a broad and shallow palaeo-valley cut in Namaqua Metamorphic Complex gneisses and schists (and those of Gariep Belt to seaward), with a thin fill component. This fill comprises weathered materials at the base, that are successively overlain by sand, a gravel-rich sediment body, and a capping of sand and mud. The valley is best developed in the Namaqua Metamorphic Complex schists and gneisses in water depths >50 m, where it is more deeply incised and narrower. The valley system then widens and becomes less incised at a bedrock knickpoint at -100 m, which marks the junction between Gariep Belt outcrop to seaward and Namaqua Metamorphic Complex outcrop to landward. These occupy small zones of accommodation created by the transition from the two units in the outer shelf, where bedrock control is less significant i.e. softer substrate with lower relief surfaces and flatter interfluves.

Channel morphology

The morphology of the valley is defined by two separate bedrock terrains; a steeper, more rugged Namaqua Metamorphic Complex terrain to landward, and a gentler-sloped lower relief terrain to seaward, the influence of which impacts on valley morphology and fill character. The junction between the two terrains is marked by a gradient knickpoint at a depth of 100 m, a depth that coincides with several lowstands in Southern Hemispheric sea level prior to and post the LGM period (Yokoyama et al., 2018; Ishiwa et al., 2019, Fig. 2), during the Bølling-Allerød (B-A) transition period (Green et al., 2014) and possibly during MIS 4 and 6 (Cawthra et al., 2016; Green et al., 2023). The repeated occupation of the shoreline at this depth during these time periods likely exacerbated the relief differences between the two terrains by the preferential bevelling of the less competent Gariep material into a flatter surface. The change in bedrock gradient has allowed channels of the valley system to widen substantially.

In contrast to other geologically-controlled incised valleys where low bedrock gradients cause pronounced meandering (e.g. Dladla et al., 2019), these valleys are narrower, more sinuous, and of greater relief where they incise schists of steeper hosting terrain with steeper gradient, (Table 2).. Overall, the channels are substantially more sinuous (average sinuosity of 1.5) and steeper than those of comparable middle to outer incised valley segments from less geologically-constrained settings where the valleys are not fringed by competent bedrock along their interfluves (e.g. Nordfjord et al., 2005).

In alluvial river channel classification schemes (Schumm, 1977; 1985), the channels offshore Hottentot's Bay correspond to the bed-load river category where channel width to depth ratios exceed 40, however, their sinuosity (> 1.3 and < 2) is closer to that of mixed-load rivers and a comparison of slope % vs sinuosity (Schumm and Khan, 1972) places them in the braided river category. Application of Rosgen's (1994) classification of natural rivers provides a mixed outcome. Width to depth ratios identify the channels as Stream type D "braided channel with longitudinal bars and transverse bars". However, the channels are far steeper than the minimum of 0.04° and are more closely related to the Aa+ category of deeply entrenched debris transport streams with slopes > 0.1°. When sinuosity is included, they approximate type C low gradient meandering systems.

There is thus no clear fit between model classifications and the channels observed in this study. When compared to channels incised into similar rock types (high grade metamorphic or granitic rocks), the average channel width to depth in our study exceeds that of channels with gravel-rich substrates such as those observed here (Fig. 11e) (Finnegan et al., 2004). Finnegan et al. (2004) show that water tends to flow faster through steeper reaches and occupies smaller channels, which accords with the steeper areas of our study hosting narrower channels. However, channel depth varies dramatically and appears to be more closely related to the hosting geology (Table 1). Channel form thus appears to be divorced from any one specific genetic mechanism (e.g. substrate type, stream power) as proposed by the above schemes.

Timing and genesis of channel/fill development

The valley system reported here is currently disconnected from any comparable feature to landward. Instead, it is bordered by the Namib Desert Sand Sea (Fig. 1), that is more than 1 million years old (Vermeesch et al., 2010; Stone, 2013). It thus appears that although this channel system has been disconnected from any significant fluvial source throughout most of the Pleistocene it has maintained a surface expression despite being repeatedly transgressed and subaerially exposed during several lowstand and highstand periods over that time frame. The valley does not continue past the inner shelf, where it terminates in a coast-parallel channel associated with flatter gradients at depths of 100-120 m.

The channel was incised into Precambrian rocks, with its basal-most fill comprising the weathered derivatives of the Gariep and Namaqua Natal Complexes. Baby et al. (2018) consider the modern shelf break to have formed during a period of Late Campanian uplift, and these original Cretaceous drainage systems of SW Africa were possibly reactivated during Late Oligocene uplift (Fig. 2). It is likely that this was the last stage where significant shelf incision was possible and the age of the channels can thus be constrained to Late Cretaceous (e.g. Stevenson and McMillan, 2004) with some additional reworking during the Middle to Upper Oligocene. The weathering of the hard-rock substrate was likely accomplished during the protracted tectono-lowstands of the Lower Palaeocene (Baby et al., 2018) (Fig. 2).

The weathered deposits that line the valley base have been reworked by combined tide and wave activity in the surfzone, as evidenced by the well-rounded appearance of the materials, and their rod and sphere-like shapes (e.g. Tanner, 1996). They thus record the first deposits preserved in the valleys and are representative of transgressive flooding and filling of the channels during surfzone migration, as opposed to bayline migration (sensu Zaitlin et al., 1994). The initial transgressive fill was in turn overlain by sandstones characterised by *Diplochaetetes longitubus*. Pickford and Sanut (2002) consider these part of a shallow marine, Early Eocene-age fossil association. The presence of the trace fossil *Trypanites sp* indicates these were likely exposed as a hardground for a significant period of time, thus marking another hiatus in the sedimentary fill. The sandstone is entirely located in the coast-parallel channel where the gradient knickpoint between the Gariep Belt and Namaqua Metamorphic Complex occurs (Fig. 11c). It is likely that this was the only suitable accommodation for the preservation of open shelf deposits, with the prominent-relief schists restricting accommodation to landward.

The remaining sediment that fills the various channels comprises unconsolidated sediment of varying size classes. The exact age of deposition of all of the various packages is difficult to constrain. Several authors have dated the submerged gravel-rich bodies associated with incised valleys of the southern Namibian shelf, placing these as late Pleistocene to early Holocene in age (Kirkpatrick et al., 2019; Runds et al., 2019). Compton et al. (2001) found the shell hash that overlies the main gravel body, (our WRS), to be early Holocene in age. Where the main gravel body is absent, the underlying sandy materials date to MIS 3 (Compton et al., 2001). Kirkpatrick et al. (2019) considered the gravel body from the Oranjemund shelf to represent deposition during combined transgressions and regressions since the Miocene, with matching gravel deposits elevated along the modern shoreline of Plio-Pleistocene age (Spaggiari et al., 2006; Spaggiari and Bordy, 2023). It thus seems likely that the valley fill unit up to WRS is a similarly composite feature, spanning various ages of deposition with discontinuous reworking by the long-lived and vigorous wave climate.

The lowermost sand unit thickens to landward (Fig. 11d) in contrast to the various gravel fractions which all form seaward-thickening bodies (Fig. 11e-h), despite the seaward reduction in channel depth and relief. The uppermost sandy/muddy unit that caps the fill corresponds to modern sediments of the shoreface and shelf. Their position is, however, constrained by the original channel (Fig. 3; 11k) form, and thus are in direct contrast to most mid to outer segments of typical incised valleys, where the capping shoreface material forms a thick cover sequence and the valley form is not recognizable in the modern bathymetry. Several examples exist where underfilled incised valleys are currently exposed at the seabed (e.g. Payenberg et al., 2006; Simms et al., 2006;

Pretorius et al., 2019; Neto et al., 2021; Manikam et al., 2022), however, these relate to reduced sediment supply, current scouring or overstepping of the outer valley by meltwater pulses. We consider the lack of a blanketing cover sequence in our example to be the result of the strong geological control and lack of accommodation that results from the prominent and steep interfluves of schist.

Comparison with incised valley fills

Given the longevity of the southern Namibian coast's high energy coastal regime (since Eocene times), the fill characteristics of the channels observed offshore Hottentot's Bay must be assessed in the context of wave-dominated incised valley fills. Wherever relevant, we further compare to mixed wave and tide dominated systems (Table 3). It is important to note that these channels are Cretaceous in age, and the valley fills themselves have been deposited and preserved over multiple Tertiary and Quaternary transgressive/regressive cycles. This stands in contrast to most incised valley fills on modern shelves that seldom record more than a single transgressive cycle (e.g. Nordfjord et al., 2006).

The basal unit of the fill succession is composed of reworked weathered materials (clays and saprolites) that represent a flooding phase of the channels, with a mixture of tidal and wave-ravinement processes operating along the subaerial unconformity. These underlie any form of sand or gravel bodies, despite the abundance of materials along the valley walls, interfluves and catchment that could produce such material. This contrasts with typical incised valley systems, where the basal facies usually comprises lowstand fluvial gravels overlain by muddy central basin fills or inner estuary deposits (Zaitlin et al., 1994; Allen and Posamentier, 1993; 1994; Fenies et al., 2010). The lack of fluvial and central basin fill material is indicative of either erosion or non-deposition during the intervening lowstand periods between incision (late Campanian) and the earliest point in time when the weathering products developed (Lower Palaeocene). Given the occurrence of intact saprolite in the landward sectors of the channels, it is thus unlikely that all these materials are reworked and transported by wave or tide currents and there are still portions of the basal fill that have not been eroded. We thus favour a situation of prevailing non-deposition as opposed to erosion during the lowstand periods prior to deposition of the transgressive wave-rolled facies.

The juxtaposition of shallow marine sandstones with the shallower, surfzone and estuary mouth facies of Units B and C suggests continued deepening in the valley, with the unconformity between the two representing a ravinement surface (wave or tide, or a combination of both) that separates coastal (Unit B and C) and shelf (Unit D) facies. An exceptionally limited amount of this transgressive material is hosted between the subaerial unconformity and the uppermost ravinement surface (<1.3 m) in contrast to most incised valley systems (e.g. Zaitlin et al., 1994; de Falco et al., 2022). The sandstones mark a long hiatus, during which boring by molluscs occurred to form the *Trypanites sp* ichnofacies. We consider this unit and its upper surface to represent a maximum flooding surface *sensu* Zecchin et al. (2021; 2022).

Incised valley fills are classified as 'simple' or 'compound' depending on whether polycyclic episodes of incision and related sequence boundaries are preserved (Zaitlin et al., 1994; Burger et al., 2001; De Falco et al., 2022). Although the system reported here has affinities with the compound category, it has developed over a much longer period of geologic time and is dominated by transgressive sediments and stratigraphic surfaces. It is also exceptionally thin and lacks the multiple incisions of compound incised valleys. The lack of connection to a terrestrial drainage system for at least the past million years has contributed to a lack of incision and scour of accumulated sediment during lowstands. It has also contributed to generally low rates of terrestrial sediment supply during the Quaternary.

The transgressive fills deposited in the accommodation space provided by the valley comprise mainly coarse-reworked material that has been preserved from complete erosion during transgressive ravinement by virtue of the shelter provided in the lower topography of the valley. They thus provide a preferential preservation of transgressive marine deposits whose development and preservation is restricted on the higher topography and more exposed conditions of the interfluves. The unconsolidated cover sequence is mostly constrained by the palaeo-topography of the valley system. Typical incised valley systems, especially in their mid to outer segments, have a capping unit of shoreface sediments that totally obscure the underlying channels (Zaitlin et al., 1994; Dalrymple et al., 2006). However, in the case of the bypass system described here, the strong geological control and low rates of Quaternary terrigenous sediment have limited deposition to the more accessible accommodation sites of the underfilled bypass channels.

CONCLUSIONS

The bypass valley is a major dendritic fluvial system incised during Cretaceous times and containing sediments of Cretaceous, Tertiary and Quaternary age, the latter of which define the shape and extent of the valley form. The valley morphology is related to the differential gradient of the inner and outer shelf and does not fit easily in any contemporary fluvial channel classification. The initial channels were cut during lowered sea level relative to a palaeo-shelf break in the Cretaceous. Since that time, subsequent lowstands did not extend below a shelf knickpoint, thus the rivers did not incise, but likely modified their form by lateral grading, overprinting the original river morphodynamic framework. This accounts for the departure from traditional channel morphodynamic classification schemes.

The original valley has been disconnected from any contemporary fluvial input for at least the past million years and its fill is dominated by a thin sequence of coarse-grained transgressive marine sediments separated by erosional unconformities that developed in former marine embayments rather than estuarine settings. These are preferentially preserved in the accommodation space provided by the valley compared to the high-relief interfluves where they are absent due to non-deposition and/or transgressive ravinement. Such a sequence in the geologic record could easily be misinterpreted as straightforward open marine deposits if the overall valley depositional setting was not recognised. This lies in stark contrast to models of incised valley fills incised at the timescale of glacial/interglacial cycles, in which clear packages of transgressive fill relate to a single, or occasionally several phases of transgressive filling deposited during the latest transgressive phases of these cycles. Although bypass valleys have seldom been identified or studied on modern continental shelves, given the occurrence of many low gradient and deep shelves along passive margins globally, we expect to see similar systems develop, especially where local hinterland uplift occurred in the early stages of the valley development. Such conditions undoubtedly occurred in the geologic past and these observations present a modern analogue for the identification and interpretation of such features.

ACKNOWLEDGMENTS

We wish to thank the master, crew and scientists that collected the various data from the MV DP Star, most notably Kurt Denis. We also thank Trans Hex Marine for permission to publish these data, and for their interest in supporting academic pursuits. Funding for software licenses and student support came from the European Union's Horizon 2020 iAtlantic project (Grant Agreement No. 818123), for which we are extremely grateful. We are especially indebted to John Pether for discussions surrounding various fossils and age relationships.

REFERENCES CITED

Aizawa, M., Bluck, B.J., Cartwright, J., Milner, S., Swart, R., and Ward, J., 2000, Constraints on the geomorphological evolution of Namibia from the offshore stratigraphic record: Communications of the Geological Survey of Namibia, v. 12, p. 337-346.

Allen, G.P., and Posamentier, H.W., 1993, Sequence stratigraphy and facies model of an incised valley fill: the Gironde estuary, France: Journal of Sedimentary Petrology, v. 63, p. 378-391, doi.org/10.1306/D4267B09-2B26-11D7-8648000102C1865D.

Allen, G.P., and Posamentier, H.W., 1994, Transgressive Facies and Sequence Architecture in Mixed Tide- and Wave-Dominated Incised Valleys: Example from the Gironde Estuary, France, *in* Dalrymple, R,W., Boyd, R., and Zaitlin, B,A., eds., Incised-Valley Systems :

Origin and Sedimentary Sequences: Society for Sedimentary Geology, Oklahoma, Special Publication 51, p. 395-401, doi.org/10.2110/pec.94.12.0225.

Baby, G., Guillocheau, F., Morin, J., Ressouche, J., Robin, C., Broucke, O., and Dall'Asta, M., 2018, Post-rift stratigraphy evolution of the Atlantic margin of Namibia and South Africa : Implications for the vertical movements of the margins and the uplift history of the South African Plateau: Marine and Petroleum Geology, v. 97, p. 169-191. doi.org/10.1016/j.marpetgeo.2018.06.030

Bluck, B.J., Ward, J.D., Cartwright, J., and Swart, R., 2007, The Orange River, southern Africa: an extreme of a wave-dominated sediment dispersal system in the South Atlantic Ocean: Journal of the Geological Society, v. 164, p. 341-351, doi.org/10.1144/0016-76492005-189.

Blum, M.D., 1990, Climatic and eustatic controls on Gulf Coastal Plain fluvial sedimentation: an example from the Late Quaternary of the Colorado River, Texas, *in* Armentrout, J.M., and Perkins, B.F., eds., Sequence Stratigraphy as an Exploration Tool : Concepts and Practices in the Gulf Coast Gulf Coast: Society of Economic Palaeontologists and Mineralogists Foundation, Texas, GCSSEPM Foundation, p. 71– 83, doi.org/10.5724/gcs.90.11.0071.

Blum, M.D., 1993, Genesis and Architecture of Incised Valley fill Sequences: A Late Quaternary Example from the Colorado River, Gulf Coastal Plain of Texas, *in* Weimer, P., and

Posamentier, H.W., eds., Siliciclastic Sequences Stratigraphy: Recent Developments and Applications: Memoir American Association of Petroleum Geologists, v. 58, p. 259-283, doi.org/10.1306/M58581C10.

Blum, M.D., and Valastro, S., 1989, Response of the Pedernales River of central Texas to late Holocene climate change: Annals of the Association of American Geographers, v. 79, p. 435-456, doi.org/10.1111/j.1467-8306.1989.tb00271.x.

Bremner, J. M., Rogers, J., and Willis, J. P., 1990, Sedimentological aspects of the 1988 Orange river floods: Transactions of the Royal Society of South Africa, v. 47, p. 247-294, doi.org/10.1080/00359199009520243.

Burger, R.L., Fulthorpe, C.S., and Austin Jr, J.A., 2001, Late Pleistocene channel incisions in the southern Eel River Basin, northern California: implications for tectonic vs. eustatic influences on shelf sedimentation patterns: Marine Geology, v. 177, p. 317-330, doi.org/10.1016/S0025-3227(01)00166-9.

Cawthra, H.C., Compton, J.S., Fisher, E.C., MacHutchon, M.R., and Marean, C.W., 2016, Submerged shorelines and landscape features offshore of Mossel Bay, South Africa: Geological Society London Special Publications 411, p. 219-233, doi.org/10.1144/SP411.11.

Compton, J., Harris, C., and Thompson, S., 2001, Pleistocene Dolomites from the Namibian shelf: High $^{87}Sr/^{86}Sr$ and $\delta^{18}O$ values indicate an evaporative, mixed-water origin: Journal of Sedimentary Research, vol. 71, p. 800-808, doi.org/10.1306/2DC40969-0E47-11D7-8643000102C1865D.

Cooper, J.A.G., Green, A.N., and Compton, J.S., 2018, Sea-level change in southern Africa since the Last Glacial Maximum: Quaternary Science Reviews, v. 201, p. 303-318, doi.org/10.1016/j.quascirev.2018.10.013.

Corbett, I.B., 1996, A review of diamondiferous marine deposits of western southern Africa. Africa Geoscience Review, v. 3, p. 157-174.

De Falco, G., Carannante, A., Del Vais, C., Gasperini, L., Pascucci, V., Sanna, I., Simeone, S. and Conforti, A., 2022, Evolution of a single incised valley related to inherited geology, sea level rise and climate changes during the Holocene (Tirso river, Sardinia, western Mediterranean Sea): Marine Geology, v. 451, p.106885, doi.org/10.1016/j.margeo.2022.106885.

Dladla, N.N., Green, A.N., Cooper, J.A.G., and Humphries, M.S., 2019, Geological inheritance and its role in the geomorphological and sedimentological evolution of bedrock-hosted incised valleys, lake St Lucia, South Africa: Estuarine, Coastal and Shelf Science, v. 222, p.154-167, doi.org/10.1016/j.ecss.2019.04.013.

Fenies, H., Lericolais, G., and Posamentier, H.W., 2010, Comparison of wave-and tide-dominated incised valleys: specific processes controlling systems tract architecture and reservoir geometry: Bulletin de la Société géologique de France, v. 181, p. 171-181, doi.org/10.2113/gssgfbull.181.2.171.

Finnegan, N.J., Roe, G., Montgomery, D.R., and Hallet, B., 2004, A New Approach to Scaling Channel Width in Bedrock Rivers and its Implications for Modeling Fluvial Incision: American Geophysical Union, p. 1824-1886.

Green, A., Hastie, W., Cooper, A., and Lightfoot, D., 2023, Anomalously large marine potholes on a submerged relict shore platform: The Eastern Cape shelf of SE Africa: Geomorphology, v. 430, p. 1-14, doi.org/10.1016/j.geomorph.2023.108673.

Green, A.N., Cooper, J.A.G., and Salzmann, L., 2014, Geomorphic and stratigraphic signals of postglacial meltwater pulses on continental shelves: Geology, v. 42, p.151-154, doi.org/10.1130/G35052.1.

Guillocheau, F., Rouby, D., Robin, C., Helm, C., Rolland, N., Le Carlier de Veslud, C., and Braun, J., 2012, Quantification and causes of the terrigeneous sediment budget at the scale of a continental margin: a new method applied to the Namibia-South African margin: Basin Research, v. 24, p. 3-30, doi.org/10.1111/j.1365-2117.2011.00511.x.

Hay, W.W., and Brock, J.C., 1992, Temporal variation in intensity of upwelling off southwest Africa, *in*: Summerhays, C.P., Prell, W.L., and Emeis, K.C. eds., Upwelling Systems: Evolution since the Early Miocene: Geological Society, London, Special Publication 63, p. 463-497, doi.org/10.1144/GSL.SP.1992.064.01.31.

Humphrey, N.F., and Konrad, S.K., 2000, River incision or diversion in response to bedrock uplift: Geology, v. 28, p. 43-46, https://doi.org/10.1130/0091-7613(2000)28%3C43:RIODIR%3E2.0.CO;2.

Ishiwa, T., Yokoyama, Y., Okuno, J., Obrochta, S., Uehara, K., Ikehara, M., and Miyari, Y., 2019, A sea-level plateau preceding the Marine Isotope Stage 2 minima revealed by Australian sediments: Scientific Reports 9, p. 1-8, doi.org/10.1038/s41598-019-42573-4.

Jacobs, R.J., 2005, The erosional and Cainozoic depositional history of the Lower Orange River, southwestern Africa [PhD Thesis]: University of Glasgow, p. 175-181.

Kirkpatrick, L.H., and Green, A.N., 2018, Antecedent geologic control on nearshore morphological development: the wave dominated high sediment supply shoreface of southern Namibia: Marine Geology, v. 403, p. 34-47 .doi.org/10.1016/j.margeo.2018.05.003.

Kirkpatrick, L.H., and Green, A.N., 2021. Mapping diamondiferous palaeo-shorelines in complicated terrain: seismic and GIS-based methods from the inner shelf of southern

Namibia: Geo-Marine Letters, v. 41, p. 1-18, https://doi.org/10.1007/s00367-021-00711-w.

Kirkpatrick, L.H., Jacob, J., and Green, A.N., 2019, Beaches and bedrock: How geological framework controls coastal morphology and the relative grade of a Southern Namibian diamond placer deposit: Ore Geology Review, v. 107, p. 853-862, doi.org/10.1016/j.oregeorev.2019.03.029.

Lancaster, N., and Ollier, C.D., 1983, Sources of sand for the Namib sand sea: Zeitschrift für Geomorphology Supplement Band, v. 45, pp. 71-83.

Manikam, S.L., Green, A.N., Cooper, A., Deacon, G., and Flemming, B., 2022, Development and preservation of transgressive sandy versus rocky shorelines: Observations from the SE African shelf: Geomorphology, v. 419, p. 1-18, doi.org/10.1016/j.geomorph.2022.108485.

Maslanyi, M.P., Light, M.P.R., Greenwood, R.J., and Banks, N.L., 1992, Extensive tectonic offshore Namibia and evidence for passive rifting in the South Atlantic: Marine and Petroleum Geolog, v. 9, p. 590-601, doi:10.1016/0264-8172(92)90032-A.

Miller, K.G., Kominz, M.A., Browning, J.V., Wright, J.D., Mountain, G.S., Katz, M.E., Sugarman, P.J., Cramer, B.S., Christie-Blick, N., and Pekar, S.F., 2005, The

Phanerozoic record of global sea-level change: Science, v. 310, p. 1293-1298, doi.org/10.1126/science.1116412.

Neto, A.R., Pessoa, P.R.S., Pinheiro, L.D.S., and de Morais, J.O., 2021, Seismic stratigraphy of a partially filled incised valley on a semi-arid continental shelf, Northeast Brazil: Geo-Marine Letters, v. 41, p. 1-15, doi.10.1007/s00367-021-00687-7.

Nordfjord, S., Goff, J.A., Austin Jr, J.A., and Sommerfield, C.K., 2005, Seismic geomorphology of buried channel systems on the New Jersey outer shelf: assessing past environmental conditions: Marine Geology, v. 214, p. 339-364, doi.org/10.1016/j.margeo.2004.10.035.

Payenberg, T.H., Boyd, R., Beaudoin, J., Ruming, K., Davies, S., Roberts, J., and Lang, S.C., 2006, The filling of an incised valley by shelf dunes—an example from Hervey Bay, east coast of Australia: SEPM Society of Sedimentary geology, v. 35, p. 87-98, doi.org/10.2110/pec.06.85.0087.

Pickford, M., and Senut, B., 2002, The fossil record of Namibia: Geological Survey of Namibia: Windhoek, v. 39. p. 2-5.

Posamentier, H.W., 2001, Lowstand alluvial bypass systems: incised vs. unincised: AAPG Bulletin, v. 85, p. 1771-1793, doi.org/10.1306/8626D06D-173B-11D7-8645000102C1865D.

Pretorius, L., Green, A.N., Cooper, J.A.G., Hahn, A., and Zabel, M., 2019, Outer-to inner-shelf response to stepped sea-level rise: Insights from incised valleys and submerged shorelines: Marine Geology, v. 416, p. 1-14, doi.org/10.1016/j.margeo.2019.105979.

Rosgen's, D.L., 1994. A classification of natural rivers. Catena (Elsevier), v. 22, p. 169-199.

Runds, M.J., Bordy, E.M., and Pether, J., 2019, Late Quaternary sedimentological history of a submerged gravel barrier beach complex, southern Namibia: Geo-Marine Letters, v. 39, p. 469-491, doi.10.1007/s00367-019-00590-2.

Schumm, S.A., 1977, The Fluvial Systems. A Wiley-Interscience, New York, p. 1-338.

Schumm, S.A., 1985, Patterns of alluvial rivers: Annual Review of Earth and Planetary Sciences, v. 13, p. 5-27.

Schumm, S.A., 1998, To interpret the earth: ten ways to be wrong: Cambridge University Press. p. 10-30.

Schumm, S.A., and Khan, H.R., 1972, Experimental study of channel patterns: Geological Society of America Bulletin, v. 83, p. 1755-1770.

Senna, W., Green, A.N., Cooper, J.A.G., and Heeralal, T., (in press), Antecedent bedrock control on the sediment-starved continental shelf of south/central Namibia: Marine Geology, (in press).

Siesser, W.G., and Dingle, R.V., 1981, Tertiary sea-level movement around southern Africa: Journal of Geology, v. 89, p. 83-96.

Simms, A.R., Anderson, J.B., Blum, M., 2006, Barrier-island aggradation via inlet migration : Mustang Island, Texas: Sedimentary geology, v. 187, p. 105-125, doi.org/10.1016/j.sedgeo.2005.12.023.

Spaggiari, R., and Bordy, E.M., 2023, Anatomy of a diamondiferous gravel barrier spit at the palaeo-Orange River mouth, south-western Namibia: Sedimentology, pp. 1-25, doi.org/10.1111/sed.13090.

Spaggiari, R.I., Bluck, B.J., and Ward, J.D., 2006, Characteristics of diamondiferous Plio-Pleistocene littoral deposits within the palaeo-Orange River mouth, Namibia: Ore Geology Reviews, v. 28, p. 475-492, doi.org/10.1016/j.oregeorev.2005.03.011.

Spratt, R.M., and Lisiecki, L.E., 2016, A Late Pleistocene sea level stack: Climate of the Past, v. 12, p. 1079-1092, doi.org/10.5194/cp-12-1079-2016.

Stevenson, I.R., and McMillan, I.K., 2004, Incised valley fill stratigraphy of the Upper Cretaceous succession, proximal Orange Basin, Atlantic margin of southern Africa: Journal of the Geological Society, v. 161, p. 185-208, doi.org/10.1144/0016-764902-003.

Stone, A.E.C., 2013, Age and dynamics of the Namib Sand Sea: A review of chronological evidence and possible landscape development models: Journal of African Earth Sciences, v. 82, p. 70-87, doi.org/10.1016/j.jafrearsci.2013.02.003.

Tanner, L.H., 1996, Armoured mud balls revisited: Atlantic Geology, v. 32, p. 123-125.

Vermeesch, P., Fenton, C.R., Kober, F., Wiggs, G.F.S., Bristow, C.S., and Xu, S., 2010. Sand residence times of one million years in the Namib Sand Sea from cosmogenic nuclides: Nature Geoscience, v. 3, p. 862-865, doi.10.1038/NGEO985.

Yokoyama, Y., Esat, T.M., Thompson, W.G., Thomas, A.L., Webster, J.M., Miyairi, Y., Sawada, C., Aze, T., Matsuzaki, H., Okuno, J.I., and Fallon, S., 2018, Rapid glaciation and a two-step sea level plunge into the Last Glacial Maximum: Nature, v. 559, p. 603-607, doi.10.1038/s41586-018-0335-4.

Zaitlin, B.A., Dalrymple, R.W., and Boyd, R., 1994, The stratigraphic organization of incised-valley systems associated with relative sea-level change, *in* Dalrymple, R. W., Boyd, R. and Zaitlin, B. A. eds., Incised-valley systems: origin and sedimentary sequences: Society of Economic Palaeontologists and Mineralogists, Oklahoma, Special Publication 51, p. 45-60, doi.org/10.2110/pec.94.12.0045.

Zecchin, M., Busetti, M., Donda, F., Dal Cin, M., Zgur, F., and Brancatelli, G., 2022, Plio-Quaternary sequences and tectonic events in the northern Adriatic Sea (Northern Italy): Marine and Petroleum Geology, v. 142, p. 1-15, doi.org/10.1016/j.marpetgeo.2022.105745.

Zecchin, M., Caffau, M., and Catuneanu, O., 2021, Recognizing maximum flooding surfaces in shallow-water deposits: An integrated sedimentological and micropaleontological approach (Crotone Basin, southern Italy): Marine and Petroleum Geology, v. 133, p. 1-30, doi.org/10.1016/j.marpetgeo.2021.105225.

FIGURE CAPTIONS

Figure 1. Locality map of the study area offshore Hottentot's Bay, Namibia. a) regional overview of the shelf bathymetry with the average Pleistocene lowstand shoreline level depicted. The seaward limit of the data marks the shelf break at -500 m (source Gebco, 2023). b) The high resolution regional inner shelf bathymetry with the incised valley system highlighted in white. c) high resolution multibeam bathymetry of the local study site, with representative sub-bottom profiles discussed in text highlighted. White dots denote core localities (n = 4908) targeting the incised valley system of the area.

Figure 2. Sea level trends in the basin since a) the Jurassic (Miller et al., 2005; Siesser and Dingle, 1981; Guillocheau et al., 2012), b) the Pleistocene (Spratt and Lisieki, 2016) and c) The Holocene (Cooper et al., 2018; Yokoyama et al., 2018). Red boxes denote MWPs.

Figure 3. Backscatter mosaic and interpreted seafloor acoustic facies. Bedrock is defined as hard rocky outcrop, irrespective of the rock type. The seafloor is mostly rocky outcrop-dominated, with fine sand and mud forming a veneer. Localised occurrences of low-relief rock, sandstones and gravel patches are evident. The fine sand-mud distribution marks the position of the valley system.

Figure 4. a) Surface 1/bedrock elevation model for the study area (cell size 25 x 25 m). Note the incisions into surface 1/the bedrock surface marking the valley network and the contact between the Gariep and Namaqua Metamorphic Complexes. b) Thickness ($\leq$ 6 m) of the unconsolidated sediment fill within the valley network. Thicknesses reduce seaward, with the thickest distribution of unconsolidated sediment in the western limb of the system, orientated coast parallel, N-S. c) Bedrock slope, highlighting the steep and rugged interfluve edges and the flat valley floors. Note the change in slope character between the seaward Gariep Belt schists and the landward Namaqua Metamorphic Complex gneisses and schists, marked by a gradient knickpoint at -100 m. d) Main drainage units (1-5) and the host rock of the incised valley system. Lines a-i are representative cross sections through the main channels, shown in the inset.

Figure 5. Uninterpreted and interpreted sub-bottom profile oriented west to east, representing the seismic stratigraphy of the landward portion of the study area. Units A, B, D – H are present with drill core 1558, 1359, 879 and 50. Mining furrow is present.

Figure 6. Uninterpreted and interpreted sub-bottom profile oriented west to east, representing the seismic stratigraphy of the seaward portion of the study area. Units A, C, D – H are present with drill cores 2809, 1439 and 210. Mining furrow is present.

Figure 7. Uninterpreted and interpreted sub-bottom profile oriented west to east, representing the seismic stratigraphy of the seaward portion of the study area. Units A – B, D – H are present with drill core 1633 and 1079.

Figure 8. Uninterpreted and interpreted sub-bottom profile oriented north to south, representing the seismic stratigraphy of the seaward portion of the study area. Units A, D – H present with numerous drill cores 1904, 1822, 1810, 1794, 1701, 1558, 1554 and 1553.

Figure 9. Uninterpreted and interpreted sub-bottom profile oriented north to south, representing the seismic stratigraphy of the landward portion of the study area. Units A – C, E – H present with drill cores 1119, 864, 703, 123, 50 and 28. Wave-ravinement surface (WRS) is present.

Figure 10. Samples retrieved from cores. a) Schist (SCH) fragments of the Namaqua Metamorphic Complex (Unit A). b) Schist and quartzite (QTZITE) fragments from the Gariep Complex. c) Rolled balls of reworked clay (CLY) derived from the weathered products (Unit B) of the underlying acoustic basement. Note the dominance of discs and rods. d) Kaolinite-rich saprolite (SPL) with fragments of schist (Unit C). e) cobble to pebble-sized balls of clay (Unit C). f) Sandstone (Unit D) with reef-building *Diplochaetes longitubus*, borings of *Trypanites sp.* g) Gravels (well-rounded) with quartzite (QTZITE), quartz fragments, jasper (JSP) and schist (Unit F). h) Sample with increased shelly content, including whole *Turritela declivis* and *Fusinus ocelliferus* shells. i) Shell hash with minor granule content, comprising abundant *Phacoides saldanhae* valves.

Figure 11. Unit distribution and sediment thickness. a) Unit B saprolite. B) Unit C clay. C) Unit D sandstone. D) Unit E lower sand. E) Unit F total gravel. F) Cobbles. g) Pebbles. H) Granules. i) Shell hash/WRS. J) Unit G upper sand. J) Unit H mixed sand and mud.

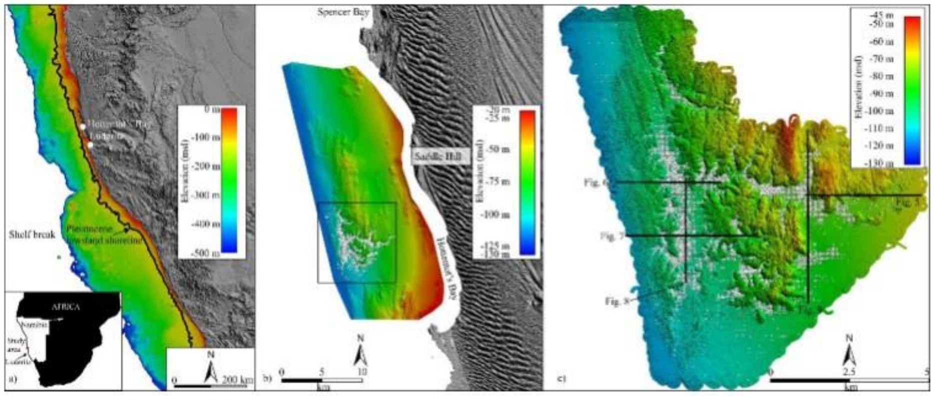

Figure. 1

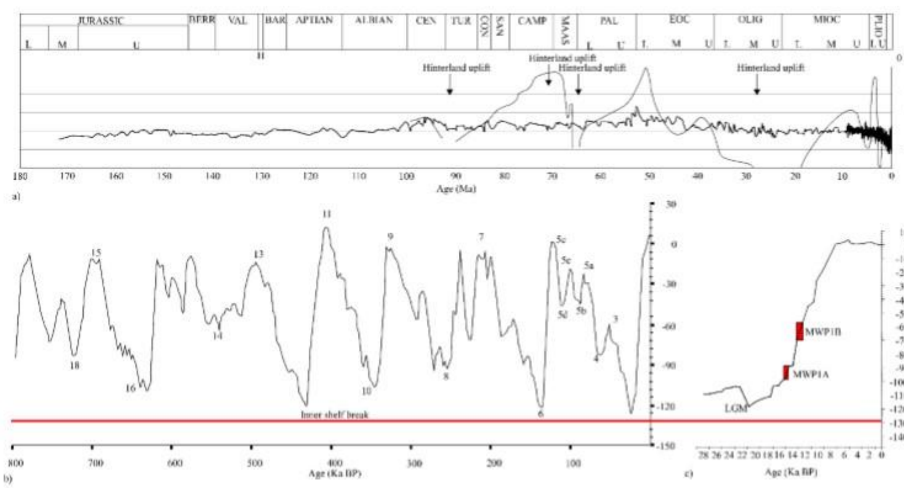

Figure. 2

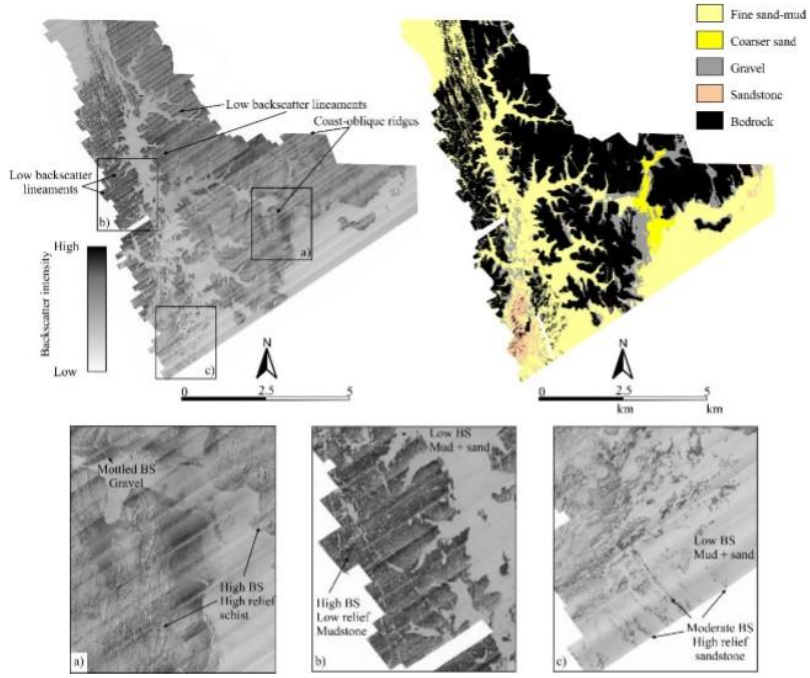
Low backscatter lineaments
Coast-oblique ridges
Low backscatter lineaments
b)
a)
c)
Backscatter intensity
High
Low
N
0
2.5
5
Fine sand-mud
Coarser sand
Gravel
Sandstone
Bedrock
N
0
2.5
km
5
km
Mottled BS
Gravel
High BS
High relief
schist
a)
Low BS
Mud + sand
High BS
Low relief
Mudstone
b)
Low BS
Mud + sand
Moderate BS
High relief
sandstone
c)

Figure. 3

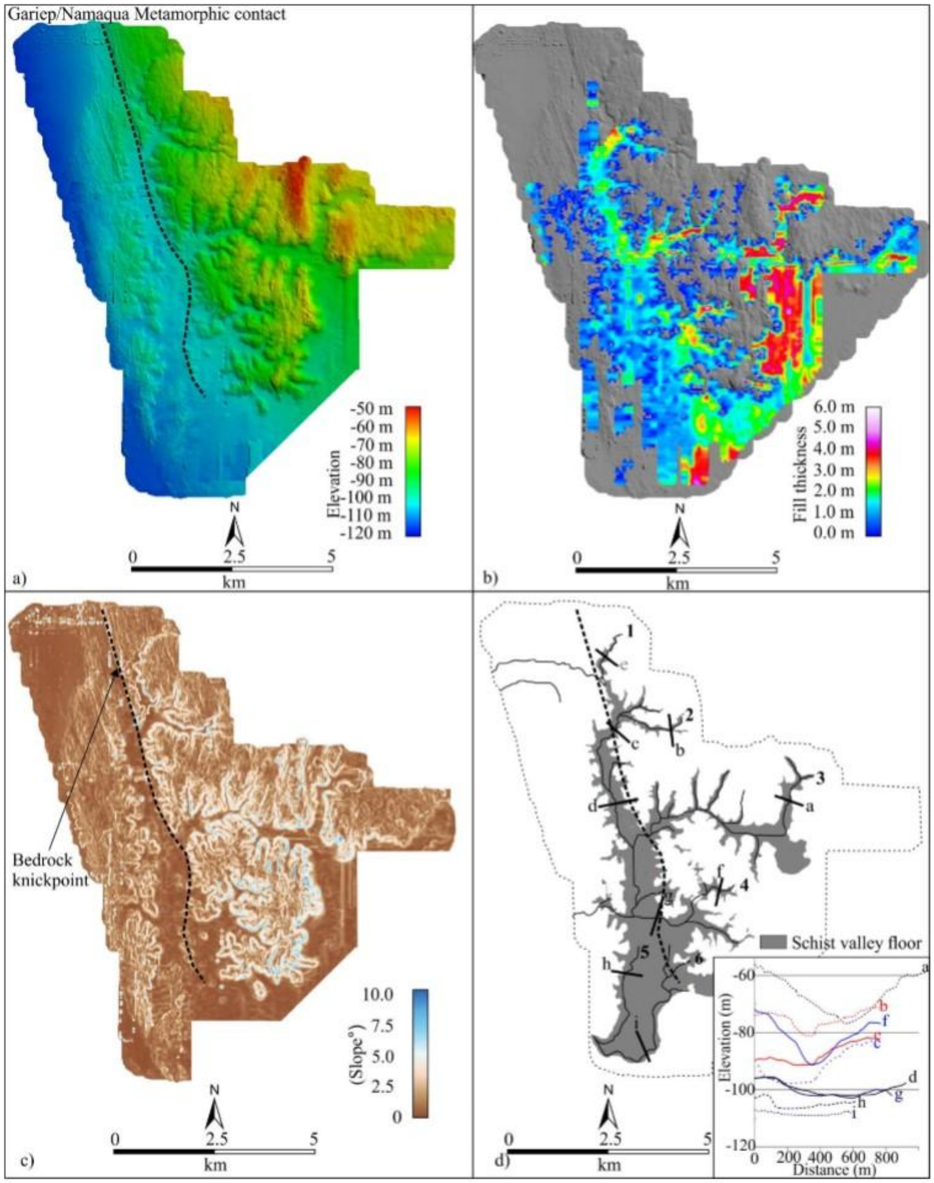

Gariep/Namaqua Metamorphic contact
Elevation
-50 m
-60 m
-70 m
-80 m
-90 m
-100 m
-110 m
-120 m
a)
Fill thickness
6.0 m
5.0 m
4.0 m
3.0 m
2.0 m
1.0 m
0.0 m
b)
Bedrock knickpoint
(Slope°)
10.0
7.5
5.0
2.5
0
c)
Schist valley floor
Elevation (m)
Distance (m)
d)
km

Figure. 4

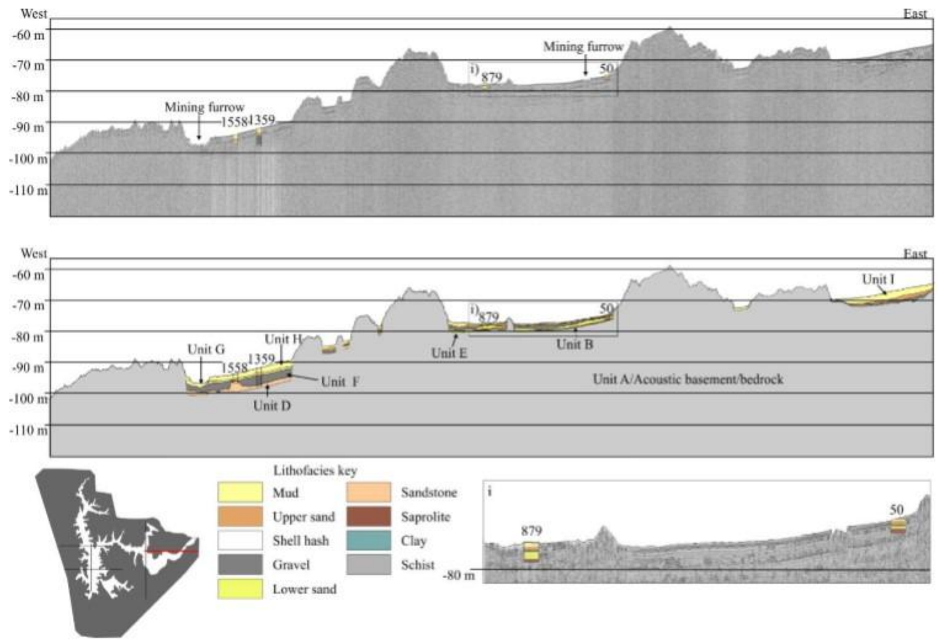

West
East
-60 m
-70 m
-80 m
-90 m
-100 m
-110 m
Mining furrow
1558
1359
i) 879
50
Unit G
Unit H
Unit F
Unit D
Unit E
Unit B
Unit I
Unit A/Acoustic basement/bedrock
Lithofacies key
Mud
Upper sand
Shell hash
Gravel
Lower sand
Sandstone
Saprolite
Clay
Schist
i
-80 m

Figure. 5

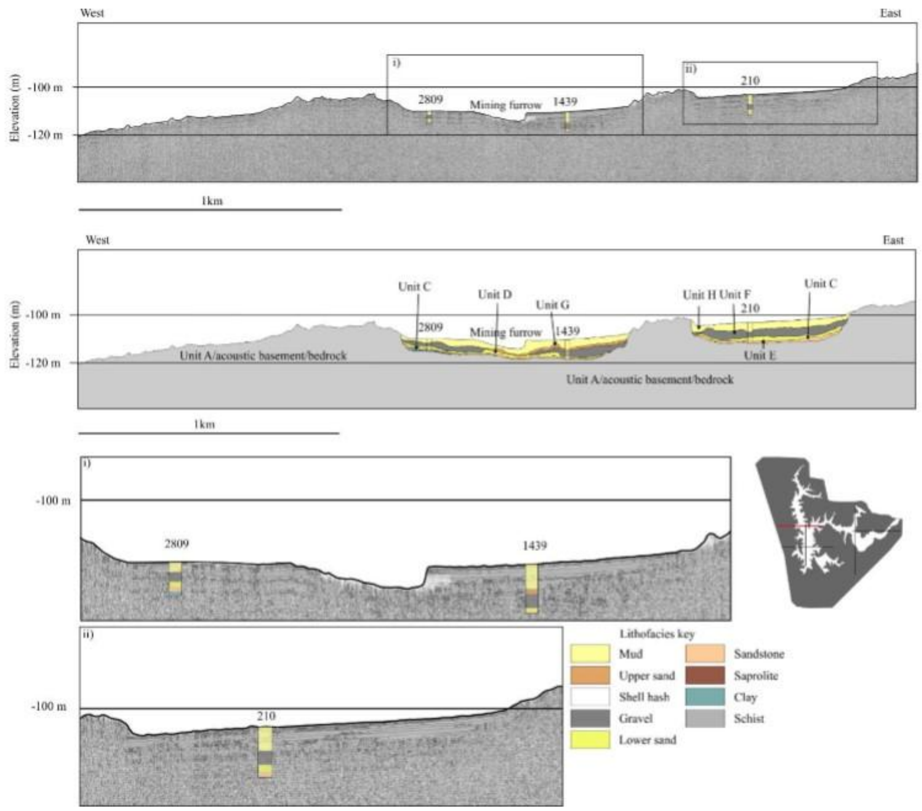
West
East
Elevation (m)
-100 m
-120 m
i)
ii)
2809
Mining furrow
1439
210
1km
Unit C
Unit D
Unit G
Unit H
Unit F
Unit E
Unit A/acoustic basement/bedrock
Lithofacies key
Mud
Upper sand
Shell hash
Gravel
Lower sand
Sandstone
Saprolite
Clay
Schist

Figure. 6

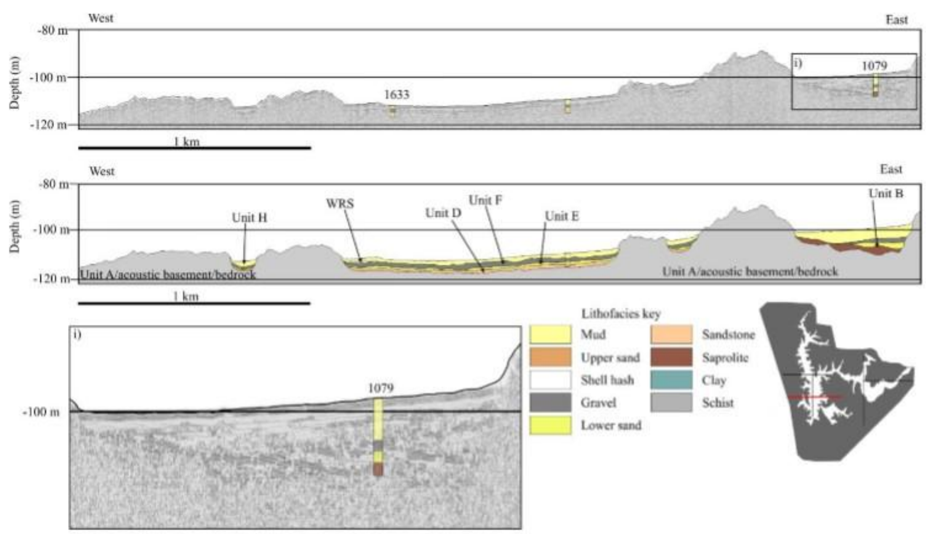
West
East
Depth (m)
-80 m
-100 m
-120 m
1633
i)
1079
1 km
Unit H
WRS
Unit D
Unit F
Unit E
Unit B
Unit A/acoustic basement/bedrock
Lithofacies key
Mud
Upper sand
Shell hash
Gravel
Lower sand
Sandstone
Saprolite
Clay
Schist

Figure. 7

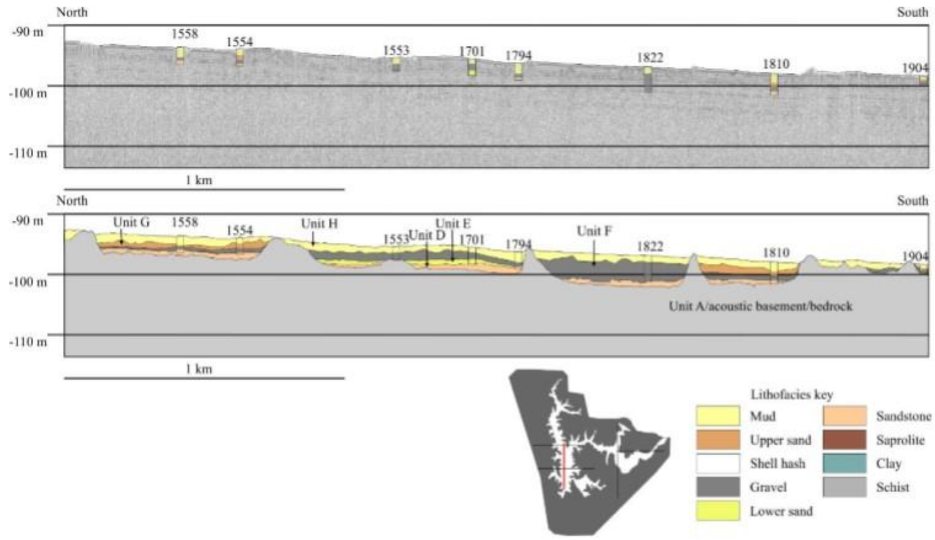

Figure. 8

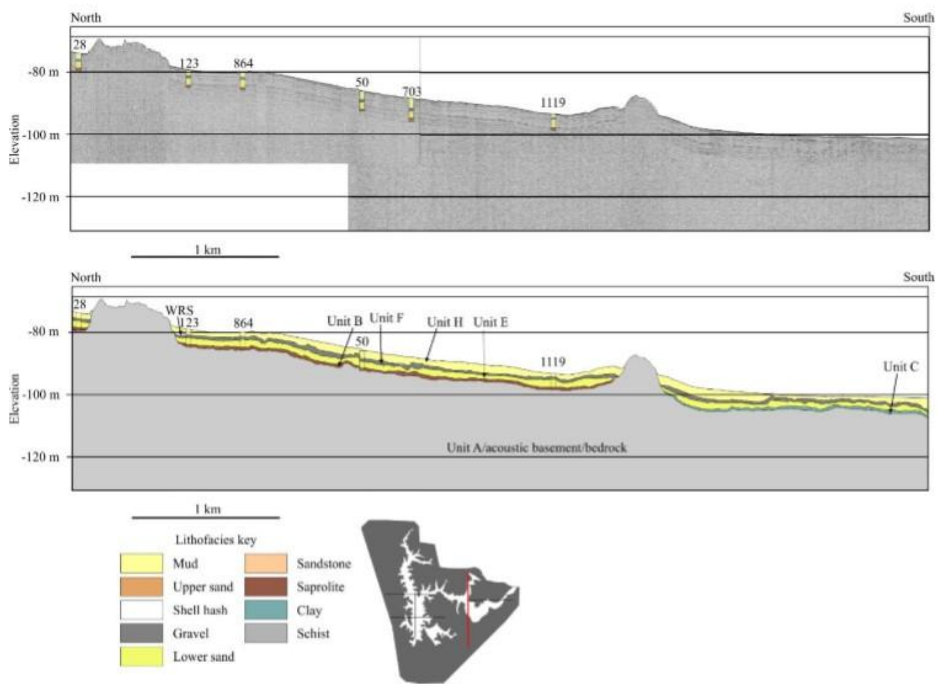

Figure. 9


SCH
a)
cm
QTZITE
SCH
b)
CLY
c)
SPL
d)
CLY
e)
f)
JSP
QTZITE
g)
QTZITE
JSP
CLY
QTZ
h)
i)

Figure. 10

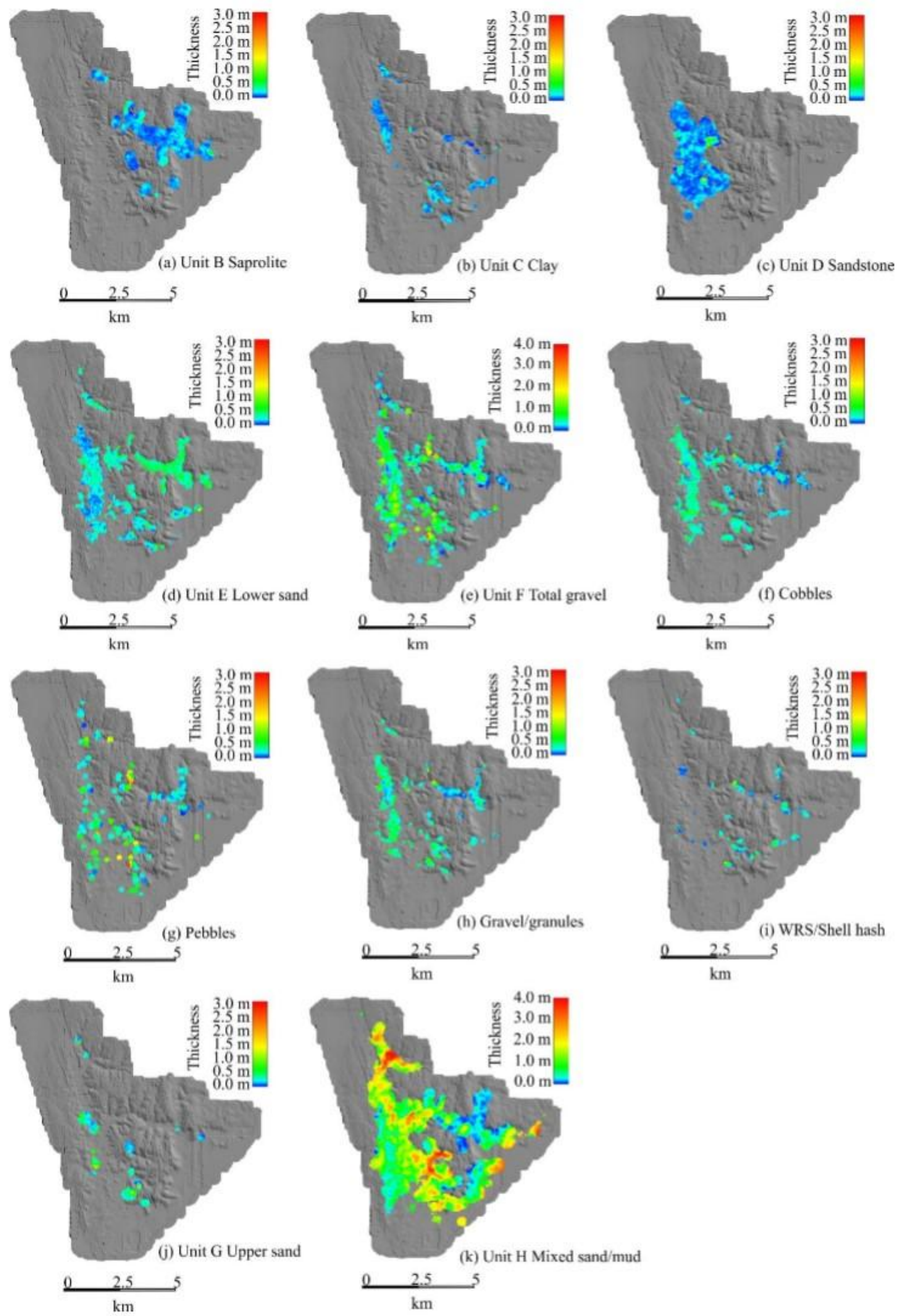

Thickness
3.0 m
2.5 m
2.0 m
1.5 m
1.0 m
0.5 m
0.0 m
4.0 m
(a) Unit B Saprolite
(b) Unit C Clay
(c) Unit D Sandstone
(d) Unit E Lower sand
(e) Unit F Total gravel
(f) Cobbles
(g) Pebbles
(h) Gravel/granules
(i) WRS/Shell hash
(j) Unit G Upper sand
(k) Unit H Mixed sand/mud
0
2.5
5
km

Figure. 11